การเตรียมตัวเร่งปฏิกิริยา Au/TiO_2 และ Ag/TiO_2 ด้วยเทคนิคการเคลือบโดยใช้
คาร์บอนไดออกไซด์วิกฤติยิ่งยวด

นายมนัสชัย เพชรเมือง

PREPARATION OF Au/TiO$_2$ AND Ag/TiO$_2$ CATALYSTS VIA A DEPOSITION
TECHNIQUE USING SUPERCRITICAL CARBON DIOXIDE

Mr. Manatchai Petmuang

A Thesis Submitted in Partial Fulfillment of the Requirements
for the Degree of Master of Engineering Program in Chemical Engineering
Department of Chemical Engineering
Faculty of Engineering
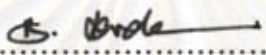Chulalongkorn University
Academic Year 2008

Thesis Title	PREPARATION OF Au/TiO$_2$ AND Ag/TiO$_2$ CATALYSTS VIA A DEPOSITION TECHNIQUE USING SUPERCRITICAL CARBON DIOXIDE
By	Mr. Manatchai Petmuang
Field of Study	Chemical Engineering
Advisor	Akawat Sirisuk, Ph.D.

Accepted by the Faculty of Engineering, Chulalongkorn University in Partial Fulfillment of the Requirements for the Master's Degree

.... Dean of the Faculty of Engineering

(Associate Professor Boonsom Lerdhirunwong, Dr.Ing.)

THESIS COMMITTEE

.... Chairman

(Associate Professor Paisan Kittisupakorn, Ph.D.)

.... Advisor

(Akawat Sirisuk, Ph.D.)

.... Examiner

(Assistant Professor Joongjai Panpranot, Ph.D.)

.... External Examiner

(Kriangsak Kraiwattanawong, D.Eng.)

มนัสชัย   เพชรเมือง : การเตรียมตัวเร่งปฏิกิริยา Au/TiO₂ และ Ag/TiO₂ ด้วยเทคนิค
การเคลือบโดยใช้คาร์บอนไดออกไซด์วิกฤติยิ่งยวด. (PREPARATION OF Au/TiO₂
AND Ag/TiO₂ CATALYSTS VIA A DEPOSITION TECHNIQUE USING
SUPERCRITICAL CARBON DIOXIDE) อ.ที่ปรึกษาวิทยานิพนธ์หลัก:
อ.ดร. อัครวัต   ศิริสุข, 104 หน้า.

งานวิจัยนี้เป็นการศึกษาวิธีการใหม่ในการเตรียมตัวเร่งปฏิกิริยา Au/TiO₂ และ
Ag/TiO₂ ด้วยการใช้คาร์บอนไดออกไซด์วิกฤติยิ่งยวด เป็นตัวทำละลาย และทำการเคลือบโลหะ
บนตัวรองรับไทเทเนียมไดออกไซด์ 2 ชนิด คือ Degussa P-25 และ ไทเทเนียมไดออกไซด์ที่เตรียม
โดยวิธีโซลโวเทอร์มอล ตัวเร่งปฏิกิริยาที่เตรียมได้วิเคราะห์คุณสมบัติของตัวเร่งปฏิกิริยาด้วย
เทคนิค XRD, การดูดซับทางกายภาพของไนโตรเจน, TEM, ICP-OES และ XPS ความว่องไว
ของตัวเร่งปฏิกิริยาทดสอบด้วยปฏิกิริยาออกซิเดชันของคาร์บอนมอนอกไซด์ ตัวเร่งปฏิกิริยา
Au/TiO₂ ได้ศึกษาปัจจัยของตัวทำละลาย ได้แก่ น้ำกลั่น เมธานอล และ อะซิทิลอะซิโตน พบว่า
การใช้ อะซิทิลอะซิโตน เป็นตัวทำละลายให้ความว่องไวสูงที่สุด โดยที่อุณหภูมิ 367 องศา
เซลเซียส มีค่าคอนเวอร์ชันเป็น 50 เปอร์เซ็นต์ สำหรับตัวเร่งปฏิกิริยา Ag/TiO₂ ศึกษาปัจจัย
ต่าง ๆ ได้แก่ ปริมาณโลหะเงิน ความดัน เวลา และชนิดของไทเทเนียมไดออกไซด์ที่ใช้เป็นตัว
รองรับ สภาวะที่ให้ความว่องไวสูงที่สุด คือ ปริมาณเงิน 20 เปอร์เซ็นต์โดยน้ำหนัก ความดัน 20
เมกกะปาสคาล เป็นเวลา 1 ชั่วโมง โดยใช้ตัวรองรับเป็นไทเทเนียมไดออกไซด์ที่เตรียมโดยวิธีโซล
โวเทอร์มอล โดยที่อุณหภูมิ 72 องศาเซลเซียส ให้คอนเวอร์ชันเป็น 50 เปอร์เซ็นต์

ภาควิชา....วิศวกรรมเคมี............ ลายมือชื่อนิสิต.....มนัสชัย เพชรเมือง.......

สาขาวิชา....วิศวกรรมเคมี.......... ลายมือชื่ออ.ที่ปรึกษาวิทยานิพนธ์หลัก...........

ปีการศึกษา...2551.....................

5070405421: MAJOR CHEMICAL ENGINEERING

KEYWORDS: SUPPORTED GOLD CATALYST/ SUPPORTED SILVER CATALYST / CO OXIDATION / TITANIUM DIOXIDE / SUPERCRITICAL CARBON DIOXIDE

MANATCHAI PETMUANG: PREPARATION OF Au/TiO$_2$ AND Ag/TiO$_2$ CATALYSTS VIA A DEPOSITION TECHNIQUE USING SUPERCRITICAL CARBON DIOXIDE.

ADVISOR: AKAWAT SIRISUK, Ph.D., 104 pp.

A novel method for preparation of Au/TiO$_2$ and Ag/TiO$_2$ catalysts via a deposition technique assisted by supercritical carbon dioxide was investigated. Supercritical carbon dioxide was employed as a solvent to dissolve the metal compound and to deposit metal on two type of TiO$_2$ (Degussa P-25 and solvothermal) supports. The catalysts were characterized by XRD, Nitrogen Physisorption, TEM, ICP-OES and XPS. The catalytic activity of the supported metal catalysts was measured for CO oxidation reaction. For Au/TiO$_2$ catalysts, several solvents were employed to dissolve gold precursor including water, methanol, and acetylacetone. The highest catalytic activity was obtained when used acetylacetone as a solvent, producing a light off temperature at 367 $^{\circ}$C. For Ag/TiO$_2$ catalysts, various preparation parameters were investigated, including amount of silver loading, holding time, pressure, and type of TiO$_2$ supports. The highest activity was obtained for the catalyst that was prepared with amount of silver loading of 20 wt%, holding time of one hour, pressure of 20 MPa, and TiO$_2$ support prepared by solvothermal method. The light off temperature for that catalyst was 78 $^{\circ}$C.

Department : Chemical Engineering Student's Signature _____
Field of Study : Chemical Engineering Advisor's Signature _____
Academic Year : 2008

ACKNOWLEDGEMENTS

CONTENTS

LIST OF TABLES

ศูนย์วิทยทรัพยากร
จุฬาลงกรณ์มหาวิทยาลัย

LIST OF FIGURE

Figure **Page**

CHAPTER I

INTRODUCTION

Supported metal catalysts were widely used in chemical industry and environmental protection. The catalytic activity depends on many parameters such as crystallite size of metal, crystal structure, active site, support, pretreatment condition, and preparation method (Qu et al., 2005).

In recent years, there has been an increasing interest in green chemical processes such as supercritical carbon dioxide ($scCO_2$). Supercritical CO_2 is a fluid at a condition above its critical points (T_c = 31.1 ^{o}C and P_c = 7.38 MPa). Supercritical CO_2 is intermediate between gaseous and liquid states. Supercritical CO_2 is the most commonly used because it is inexpensive, nontoxic, nonflammable, and nonpolluting. Supercritical CO_2 can be applied to the production of several materials, including polymer, pharmaceutical, explosive, superconductor, and catalyst (Al-Sayari et al., 2007). Furthermore, supercritical CO_2 has better diffusion inside small pores than water. Therefore, preparation of supported metal catalyst by using supercritical CO_2 appears to be a promising method for preparation of the catalyst that may exhibit high performance in the reactions.

Supported gold catalysts have been of great interest since Haruta discovered its activity for CO oxidation at low temperature when the particle size of gold was smaller than 5 nm (Wong et al., 2007). Supported gold catalysts are more active for CO oxidation than other noble metals at temperatures as low as -73 ^{o}C (Chang et al., 2007). Several metal oxides have been used as supports, including Fe_2O_3 (Moreau and Bond, 2006; Al-Sayari et al., 2007), ZnO (Al-Sayari et al., 2007), Al_2O_3 (Date et al., 2007), CeO_2 (Chang et al., 2007; Tang et al., 2007; Moreau and Bond, 2006), MnO_2 (Chang et al., 2007), TiO_2 (Date and Haruta, 2001; Date et al., 2002; Mallick and Scurrell, 2003; Tai et al., 2004; Moreau and Bond, 2006), SnO_2 (Moreau and Bond, 2006), ZrO_2 (Moreau and Bond, 2007; Zhang et al., 2007), and La_2O_3 (Russo et al., 2006). The Au/TiO_2 catalyst is widely used in various reactions such as oxidation of CO (Date and Haruta, 2001; Date et al., 2002; Mallick and Scurrell, 2003; Tai et al.,

2004; Moreau and Bond, 2006), selective oxidation of hydrocarbon (Stangland et al., 2000; Min et al., 2007), synthesis of hydrogen peroxide (Landon et al., 2002), and water-gas shift (Sakurai et al., 1997; Sandoval et al., 2007). Several studies have shown that the preparation method of supported gold catalysts has an effect on size and dispersion of gold on supports. Deposition precipitation and co-precipitation methods are the most popular ones used for deposition of gold on the supports and give rise to a high activity at low temperature.

Supported silver catalysts have been of increasing interest because having a lower price than noble metal. The benefit of silver metal for CO oxidation reaction is the fact that silver metal can adsorb oxygen on the surface (Qu et al., 2005; Gac et al., 2007). Effects of pretreatment, reaction conditions, crystalline size of silver and type of support were not fully understood yet (Gac et al., 2007). Several materials have been used as supports, including SiO_2 (Qu et al., 2004; Jin et al., 2007), TiO_2 (Frey et al., 2008), CeO_2 (Imamura et al., 2000), Al_2O_3 (Iliopoulou et al., 2004), activated carbon (Chen et al., 2006), MCM-41 (Gac et al., 2007), MnO_2 (Xu et al., 2006), and SBA-15 (Tian et al., 2009). A number of studies have reported many methods to prepare Ag/TiO_2, such as co-precipitation method (Frey et al., 2008), photoreduction process under UV-irradiation (Su et al., 2004; Li et al., 2008), impregnation method (Qu et al., 2005; Xu et al., 2006), and hydrothermal method. The Ag/TiO_2 catalyst is widely used in various reactions such as photodegradation of methyl orange (Ge et al., 2006; Li et al., 2008), photodegradation of sulfur compound (Kato et al., 2005), reduction of nitrobenzene to aniline (Tada et al., 2005), water gas shift reaction (Boccuzzi et al., 2002), and CO oxidation (Frey et al., 2008).

This work can be separated into two parts. In part one supported gold catalysts were studied while silver catalysts were studied in part two. For gold catalyst, effects of pH and solvent on catalytic activity were investigated. For silver catalyst, effects of silver contents, pressure of CO_2 during deposition, holding time and type of titanium dioxide support were investigated. All catalysts were tested for CO oxidation reaction as a probe reaction.

Objectives of the research:

1. To study the deposition of gold and silver on TiO_2 support by means of supercritical carbon dioxide.
2. To investigate the activity of Au/TiO_2 and Ag/TiO_2 catalyst for CO oxidation activity.

The thesis is arranged as follows:

Chapter I is the introduction of this work.

Chapter II presents background information for supported metal catalysts, supercritical CO_2, and CO oxidation reaction.

Chapter III shows the experimental equipment, preparation method for titanium dioxide, methods for metal deposition on supports, and characterization techniques.

Chapter IV presents the results and discussion of the research.

In the last chapter, Chapter V, the overall conclusions and recommendations for the future studies are given.

CHAPTER II

BACKGROUND INFORMATION

2.1 Information on supercritical carbon dioxide

CO_2 is a gas in air or as a solid in dry ice. If both the temperature and pressure are increased, it can adopt properties midway between a gas and a liquid. CO_2 behaves like a supercritical fluid above its critical temperature (31.1 ^{o}C) and pressure (73 atm), expanding to fill its container like a gas, but with a density like that of a liquid. Supercritical CO_2 is becoming an important commercial and industrial solvent due to its role in compound extraction as well as its low cost, low toxicity and low environmental impact. The relatively low temperature of the process and the stability of CO_2 also allow most compounds to be extracted with little damage or denaturing (Wattanamalachai 2006; http://en.wikipedia.org/wiki/Supercritical_carbon_dioxide).

2.1.1 Phase diagram of supercritical carbon dioxide

Two projections of the phase diagram of carbon dioxide are shown in Figures 2.1 and 2.2. In the pressure-temperature phase diagram (see Figure 2.1), one observes the boiling line, which separates the vapor and liquid region and ends at the critical point. At the critical point, the densities of the saturated liquid and vapor phases become equal, resulting in the formation of a single supercritical phase. This phenomenon can be observed in the density-pressure phase diagram for carbon dioxide, as shown in Figure 2.2, where the critical point is located at 31.1 ^{o}C and 73 atm (73.8 bar). With increasing temperature, the liquid-vapor density gap decreases, up to the critical temperature, at which the discontinuity disappears. Thus, above the critical temperature a gas cannot be liquefied by pressure. However, at extremely high pressures the fluid can solidify, as seen at the top of Figure 2.1. By definition, a supercritical fluid is a substance above both its critical temperature and pressure. In a practical sense, the area of interest in supercritical fluids for processing and separation purposes is limited to temperatures in the vicinity of the critical point, where large gradients in the physical properties are observed. The changes near the critical point are not limited to density. Many other physical properties also show large gradients with pressure near the critical point such as viscosity, relative permittivity, and

solvent strength, which are all closely related to the density. At higher temperatures, the fluid starts to behave like a gas, as can be seen in Figure 2.2. For carbon dioxide at 100 ^{o}C, the density increases almost linearly with pressure.
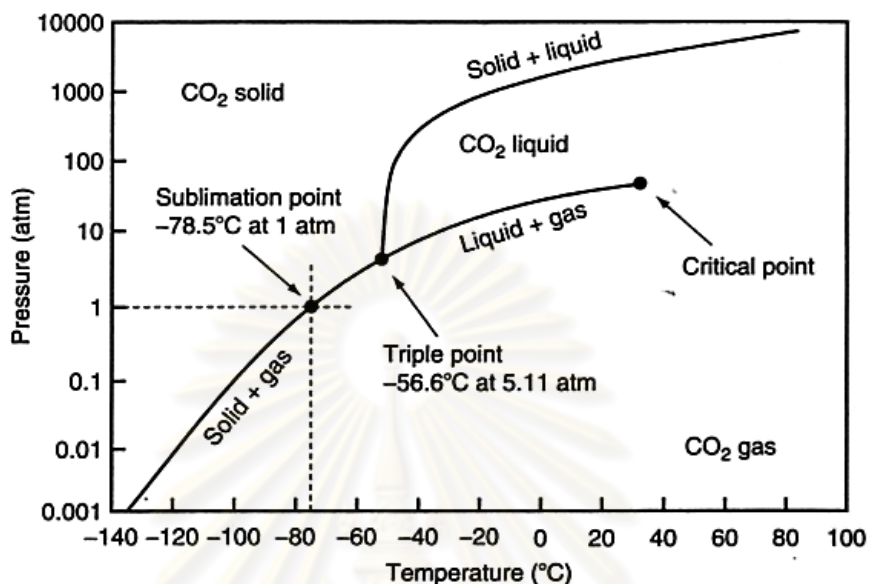
Figure 2.1   Pressure-temperature phase diagram of CO_2 (Grassian, 2005)
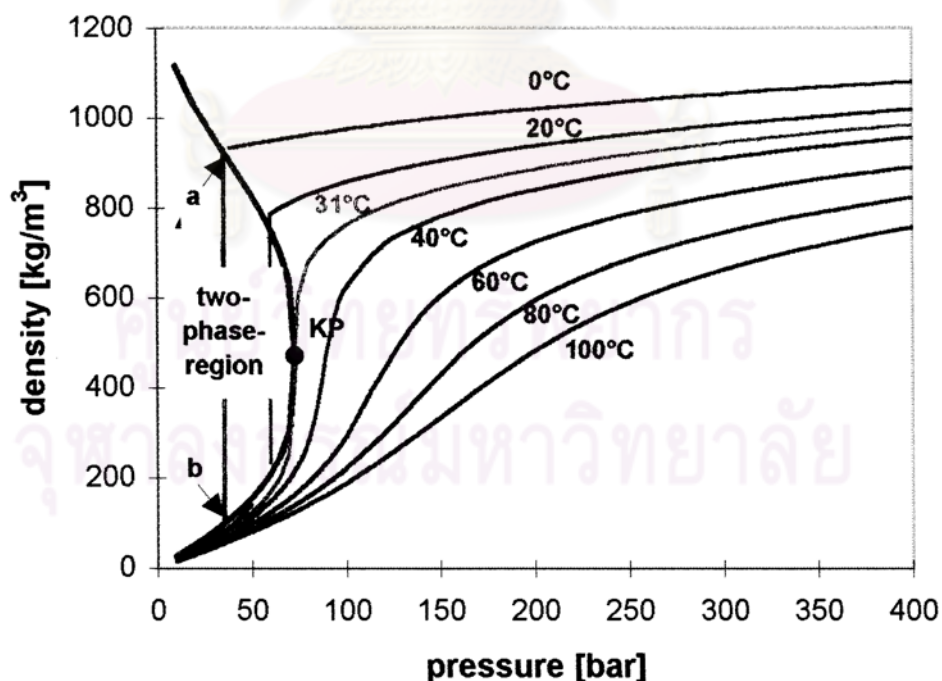
Figure 2.2   Density-pressure phase diagram of CO_2, as calculated by equation of bender (Marr and Gamse, 2000)

2.1.2 Applications of supercritical carbon dioxide

Supercritical CO_2 can be used as a chemical reagent or used as assisted to produce micro and nano scale particles. Chatterjee and coworker (Chatterjee et al., 2006) using a supercritical CO_2 for synthesis gold nanoparticle inside the pore of MCM-48. This work proposed, the particle size of metal is tunable with the pressure of the supercritical CO_2. At the low pressure condition, larger particle sizes were obtained. On the other hand, at high pressure of supercritical CO_2 slow down particle aggregation, resulting in the small particle size, while Jiao and coworkers (Jiao et al., 2007) using a supercritical CO_2 to prepared TiO_2/SiO_2 composite by using PEG as template. The result powder shown a porous titania–silica composites were obtained.

Supercritical CO_2 is also used assisted synthesis nanocomposite on polymers such as the research of Cabanas and coworkers (Cabanas et al., 2004) investigated the deposition method of gold film using supercritical CO_2. Gold films were deposited on several material such as metal, ceramic and polymer substrate. At 60 ^{o}C, the deposition occurred only on metal surfaces or catalytic seed layers. At 125 ^{o}C, gold was deposited readily on all surfaces, including the native oxide of Si wafer and TiN, while Wong and coworkers (Wong et al., 2007) was prepared gold nanoparticle composites using supercritical CO_2 by employing precursor of gold as dimethyl(acetylacetonate)gold(III) and dimethyl(hexafluoroacetylacetonate)gold(III) and using H_2 to reduce gold precursors. Average gold particle sizes in ranged from 3.7 to 6.6 nm. This supercritical fluid processing technique successfully incorporated gold nanoparticles into silica, polyamide, polypropylene and poly(tetrafluoroethylene) (PTFE). Under the conditions employed, dimethyl(acetylacetonate)gold(III) produced samples with sufficiently high metal loadings, allowing in-depth sample analysis. However, the fluorinated analogue, dimethyl(hexafluoroacetylacetonate)gold(III), did not yield samples suitable for characterization.

Many corporations utilize supercritical CO_2 to saturate the polymer with solvent (carbon dioxide). Upon depressurization and heating the carbon dioxide rapidly expands, causing voids within the polymer matrix, i.e. creating foam. Research is also ongoing at many universities in the production of microcellular foams using supercritical CO_2. Supercritical CO_2 is beginning to be used to enhance oil recovery in mature oil fields.

2.2 Information of Au/TiO$_2$ catalysts in CO oxidation reaction

　　　　Although gold has been known to be a very chemically inert material. However, when gold is in very small particles with diameters below 10 nm and is deposited on metal oxides or activated carbon, it becomes surprisingly active, especially at low temperatures, for many reactions such as CO oxidation (Haruta, 2003). The activity of a gold catalyst for CO oxidation is known to depend on various factors, including the particle sizes of gold, the gold precursor, the oxidation state of gold (Au^{+3}, Au^{+1}, Au^0), the preparation methods, the pretreatment conditions, surface areas of support, and the reaction condition. At present, the reaction that has generated the most attention is the oxidation of CO. Several researches were studied on catalytic activity of gold such as Date and Haruta (Date and Haruta, 2001) proposed the effect of moisture on Au/TiO$_2$ catalyst for CO oxidation over a wide range of concentrations from 0.1 to 6000 ppm. The Au/TiO$_2$ was prepared by a deposition precipitation method using HAuCl$_4$ as a gold precursor. Moisture enhanced the reaction by more than 10 times up to 200 ppm. The amount of moisture adsorbed on the catalyst influenced the activity rather than the moisture content in the gas phase, which suggested that the low-temperature CO oxidation over the gold catalyst involved water-derived species on the catalyst surface. The research of Date and coworkers (Date et al., 2002) was studied the catalytic activity and stability of Au/TiO$_2$ catalysts under ambient conditions. The catalysts were prepared by a deposition precipitation method using HAuCl$_4$ as a gold precursor. The best performance was obtained for a catalyst calcined at 200 ^{o}C and left at room temperature for a few days. The activity for CO oxidation was greatly influenced by moisture. The catalyst was successfully regenerated under irradiation with light, while Denkwitz (Denkwitz et al., 2007) was investigated the stability and the deactivation of unconditioned Au/TiO$_2$ catalysts during CO oxidation in a near-stoichiometric and an O$_2$-rich reaction atmosphere. The catalysts were prepared by a deposition-precipitation method, using a HAuCl$_4$·4H$_2$O as a precursor of gold. The average gold particle size was about 1.3 to 2.0 nm. Kinetic and in situ IR spectroscopic measurements revealed a close correlation between the exponentially decreasing formation rate of CO$_2$ and the surface coverage of adsorbed CO (decreasing) and the surface coverage of carbonate (increasing) during deactivation, whereas TEM image revealed no significant change in gold particle size.

　　　　Several studied shown the catalytic activity depend on oxidation state of gold species. For example the research of Chang and coworkers (Chang et al., 2007)

studied CO oxidation over gold catalysts supported on ceria and manganese oxide. The gold catalysts supported on CeO_2 and MnO_2 were prepared by a deposition–precipitation method. The Au/CeO_2 catalyst exhibited higher catalytic activity for CO oxidation than Au/MnO_2 catalyst because of Au/CeO_2 catalyst existence of Au^0 and Au^{3+} states, whereas only Au^0 was detected on Au/MnO_2. The co-existence of Au^0 and Au^{3+} species on Au/CeO_2 appeared to be the main reason for the higher activity of Au/CeO_2.

Moreau and Bond (Moreau and Bond, 2007) studied the influence of the surface area of the support on the activity of gold catalysts for CO oxidation. Au/TiO_2 was prepared by a deposition precipitation method. The gold uptake increased with the surface area of the support and was complete above 200 m^2/g. The adsorption of the gold precursor at pH 9 was equilibrium-limited. The highest activities were found with supports that had surface areas of 50 m^2/g. Catalysts made with anatase supports that had high surface area were that least active but exhibited the least deactivation, while Au/SnO_2 catalysts, gold uptake did not depend on the area of the support and was the maximum at pH 7–8. Very active catalysts (T_{50} = 230–238 K) were obtained using SnO_2 with a surface are of 47 m^2/g. The Au/CeO_2 and Au/ZrO_2 catalysts also confirmed that supports with moderate surface areas produced the most active catalysts, and suggested that surface area was often more important than chemical composition.

Noble metal catalysts are typically prepared by impregnation methods, which, however, cannot produce active gold catalysts. The impregnation method does not lead to high dispersion of gold except for a few cases of very low metal loading because of the lower melting point of Au (1063 ^{o}C), compare to than those of Pd (1550 ^{o}C) and Pt (1769 ^{o}C) (Bond et al., 2006).

The following three methods can deposit gold on a variety of metal oxides as small particles with diameters below 5 nm.

1. Coprecipitation (Haruta, 1997; Bond et al., 2006): Small gold particles supported on various oxide such as Fe_2O_3, NiO and Co_3O_4, were first obtained by this methods in 1987. An Aqueous solution of $HAuCl_4$ and a metal nitrate was poured into an aqueous solution of Na_2CO_3 to obtain a hydroxide or carbonate coprecipitate. The coprecipitates were washed, dried, and calcined in air. This method led to high gold dispersion. This method is a single-step method and easy to carry out. However, some of gold particles could be embedded in the bulk of the support.

2. *Deposition-precipitation* (Haruta, 1997; Bond et al., 2006): After the pH of aqueous solution of $HAuCl_4$ is adjusted to a fixed point in the range of 6 to 10, a metal oxide support in any form (powder, bead, honeycomb, or thin film) is immersed in the solution. Aging for about one hour results in the deposition of $Au(OH)_3$ exclusively on the surface of metal oxide support if concentration and temperature is properly chosen. The remarkable influence of the pH on the particle size of Au is shown in Figure 2.3 for Au/TiO_2. Above pH 6 the main species of Au in solution is transformed from $AuCl_4^-$ to $Au(OH)_nCl_{4-n}$ (n=1-3) and the mean particle diameter of Au in the calcined catalyst becomes smaller than 4 nm.

The above methods can produce hemispherical gold particle, which are strongly attached to metal oxide supports at their flat planes and accordingly thermally more stable than spherical particles. This can be ascribed to the hydroxidic, oxidic, or organic precursor having stronger affinity to metal oxides. It should also be pointed out that the precursors are washed almost completely or prepared without contamination. In this context, some results may not be general because lower activity and deactivation suggest that the sample might be contaminated by Cl^- and Na^+.
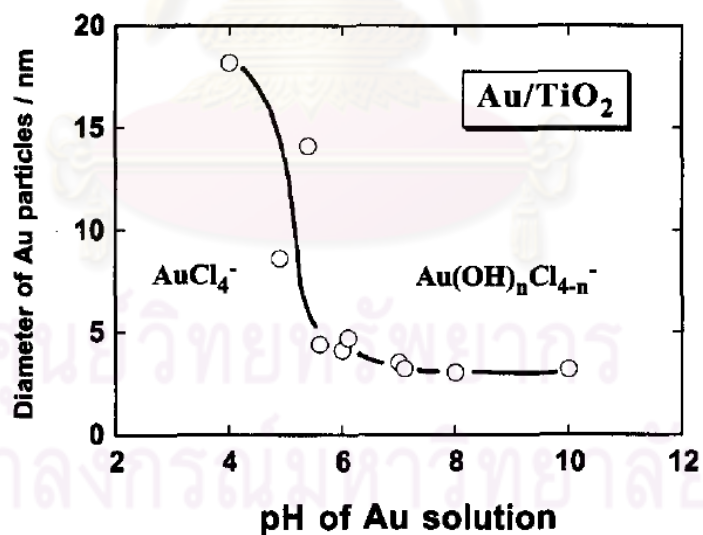
Figure 2.3   The mean particle diameter of Au as a function of the pH of $HAuCl_4$ solution for Au/TiO_2 catalyst prepared by deposition-precipitation method. Au content in the $HAuCl_4$ solution corresponded to 13 wt % with respect to TiO_2. Calcinations were performed in air at 400 $^{\circ}$C (Haruta, 1997)

Supported gold catalysts prepared by the above methods exhibit unique catalytic performances, different from unsupported gold and are often more active than Pd and Pt catalysts at low temperature. The Au/TiO_2 catalysts prepared by deposition-precipitation are active even at temperature below 0 ^{o}C when Au loading are above 1 wt % and have turnover frequencies larger than of Pt/TiO_2 by about one order of magnitude. For CO oxidation, supported gold catalysts should be pretreated in air normally at temperature above 200 ^{o}C. Evacuation at 400 ^{o}C remarkably reduces catalyst activity, which is gradually restored during CO oxidation in the presence of excess oxygen.

2.3 Information of supported silver catalysts

Silver is of particular interest because of distinctive properties, such as good conductivity, chemical stability, antibacterial and catalytic (Sharma et al., 2009). Silver catalyst widely used in oxidation reaction, such as CO oxidation reaction. On the other hand, catalysts prepared by liquid phase reduction turned out to be less active at low temperature but stable above 250 ^{o}C where 100 % CO conversion was observed (Frey et al., 2008). Many researches were studied properties of silver, preparation method and support on catalytic activity. For example, Jin and coworker (Jin et al., 2007) prepared Ag/SiO_2 catalyst by incipient wetness impregnation method using γ-ray irradiation to reduced Ag^+ to anchored on support at room temperature. Existence of excess water during the γ-ray irradiation led to the formation of larger silver nanoparticles. The catalytic activity of Ag/SiO_2 prepared by γ-ray irradiation compare with Ag/SiO_2 prepared by calcinations method, the Ag/SiO_2 prepared by γ-ray irradiation showed an inferior low temperature catalytic activity and a better stability, while Tian and coworker (Tian et al., 2009) prepared the Ag/SBA-15 by in situ reduction method using hexamethylenetetramine and formaldehyde as reducing agent. From the result, the silver particle had a particle size about 6 nm and form inside the channels of SBA-15. The Ag/SBA-15 prepared by using hexamethylenetetramine as reducing agent showed higher catalytic activity than Ag/SBA-15 prepared by using formaldehyde as reducing agent. Sarkany (Sarkany, 2005) prepared Ag/Al_2O_3 catalysts, The catalyst showed the light off temperature (Temperature at conversion equal 50 %, T_{50}) about 250 ^{o}C, while Lippits and coworker (Lippits et al., 2008) comparative studied with group Ib noble metals on

γ-Al$_2$O$_3$, reported rather strongly varying data depending on the method of preparation. Research of Qu and coworker (Qu et al., 2004) studied on silica-supported silver catalysts. The authors claimed pre-treatment procedure of these catalysts seemed to have a strong influence on the low-temperature activity. Unfortunately, no information was provided on the high-temperature stability of these catalysts. Frey and coworker (Frey et al., 2008) studied effect of actual catalysts composition on catalytic activity of CO oxidation reaction. The authors claim the catalytic activity depending on the silver composition in the catalyst.

For photocatalyst, silver particle can act as electron trapper to slow down the rate of electron-hole recombination. Li and coworker (Li et al., 2008) prepared the Ag/TiO$_2$ by photochemical reduction process under ultraviolet irradiation method. The activity of the catalyst was investigated by photodegradation of methyl orange in water. The metallic silver can help the electron-hole separation by attracting photoelectron, while Su and coworker (Su et al., 2004) prepared the Ag/TiO$_2$ by photochemical reduction process under ultraviolet irradiation method. The activity of the catalyst was investigated by photodegradation of methyl iodide.

2.4 Information on oxidation of carbon monoxide

Carbon monoxide (CO) is toxic gas. CO consists of one carbon atom covalently bonded to one oxygen atomand is produced by steam reforming or partial oxidation of carbonaceous materials. It was discovered by Lassonne in 1776 by heating a mixture of charcoal zinc oxide (Wattanamalachai, 2006).

Carbon monoxide burns readily in air or oxygen. Ignition temperature is 644-658 $^{\circ}$C, respectively. Mixtures of carbon monoxide and air are flammable over a wide range of composition at atmospheric pressure. The oxidation of CO, the reaction of carbon monoxide with oxygen to form carbon dioxide, occurs readily at a temperature above 650 $^{\circ}$C. However, gold catalysts are exceptionally active for CO oxidation at low temperature. The activity of gold catalyst for CO oxidation is dependent on various factors, including the nature of the support, the gold precursor, the preparation procedure, the pretreatment condition and the reaction condition. The most probable pathway for CO oxidation over Au/TiO$_2$ catalysts were shown in Figure 2.4.
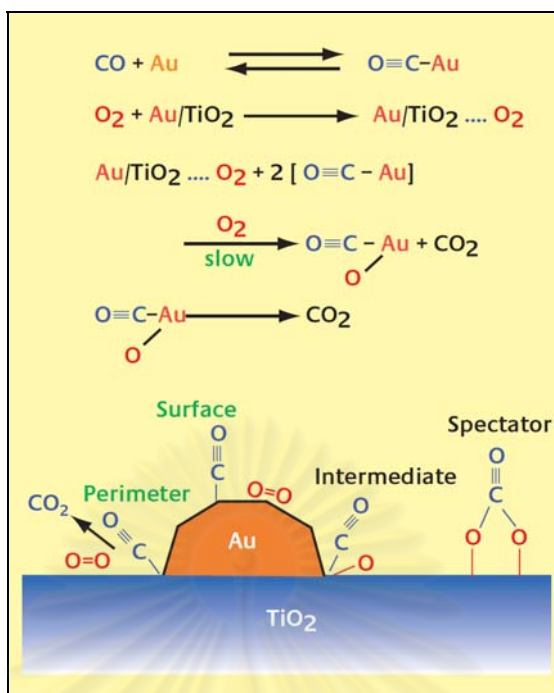
Figure 2.4   Probable pathways for CO oxidation over supported gold catalyst (Haruta, 2004)

ศูนย์วิทยทรัพยากร
จุฬาลงกรณ์มหาวิทยาลัย

CHAPTER III

EXPERIMENTAL

The experimental section in this work is divided into five parts:

- (i) Chemical used in this research
- (ii) Supported gold catalysts preparation method
- (iii) Supported silver catalysts preparation method
- (iv) Catalysts characterization methods
- (v) CO oxidation reaction line

The details of all experiment are described as following:

3.1 Chemicals

The details of chemicals used in this research are listed below.

1. Hydrogen tetrachloroaurate(III) trihydrate ($HAuCl_4 \cdot 3H_2O$), purchased from Aldrich.

2. Titanium dioxide Degussa P25 (TiO_2-P25), purchased from Degussa.

3. Methanol (CH_3OH), purchased from Merck.

4. Acetylacetone ($C_5H_8O_2$), purchased from S.D. Fine Chem.

5. Titanium (IV) butoxide ($Ti[O(CH_2)_3CH_4]_4$), purchased from Sigma-Aldrich.

6. 1,4-butanediol ($HO(CH_2)_4OH$), purchased from Sigma-Aldrich.

7. Silver nitrate ($AgNO_3$), purchased from Asia Pacific Specialty Chemical.

8. Hydrochloric acid (HCl), purchased from J.T. Baker.

9. Nitric acid (HNO_3), purchased from J.T. Baker.

3.2 Preparation method of supported gold catalysts

3.2.1 Deposition of gold by deposition precipitation method

The Au/TiO$_2$ catalysts were prepared via deposition precipitation method described by Buakaew (Buakaew, 2005). First, 0.0818 g (2 wt% of the catalyst prepared) of hydrogen tetrachloroaurate(III) trihydrate was dissolved in 100 cm^3 of distilled water. Then the pH was adjusted to desired value (6, 7, and 8, denoted for

Au/TiO$_2$-pH6, Au/TiO$_2$-pH7, and Au/TiO$_2$-pH8, respectively) using 0.1 M sodium hydroxide solution. When pH reached the desired value, 2 g of titanium dioxide Degussa P25 (TiO$_2$-P25) was added to solution. The pH of the suspension was readjusted to the desired value again. After that, the suspension was heated to temperature of 70 ^{o}C and held at that temperature for one hour. During the process, the pH was maintained by addition of 0.1 M sodium hydroxide solution or 0.1 M hydrochloric acid solution. After one hour, the suspension was cooled and centrifuged five times with distilled water for remove some chloride was remains in the suspension. Then the suspension was dried at 110 ^{o}C for six hours. The notations and preparation conditions were shown in Table 3.1.

Table 3.1 Notations and preparation conditions of catalysts that were prepared by deposition precipitation method

Catalysts	Type of support	Gold contents (wt%)	pH of solution
Au/TiO$_2$-pH6	TiO$_2$-P25	2	6
Au/TiO$_2$-pH7	TiO$_2$-P25	2	7
Au/TiO$_2$-pH8	TiO$_2$-P25	2	8

3.2.2 Deposition of gold on support by using supercritical CO$_2$

The Au/TiO$_2$ catalysts were prepared by using supercritical CO$_2$ method. A hydrogen tetrachloroaurate(III) trihydrate was employed as a precursor for gold. First, 0.0818 g (2 wt% of the catalyst prepared) of HAuCl$_4\cdot$3H$_2$O was dissolved in 3 cm^3 of distilled water (or methanol, or acetylacetone), denoted as Au/TiO$_2$-Water, Au/TiO$_2$-MeOH, and Au/TiO$_2$-Acetyl, respectively. After that, the gold solution was mixed with titanium dioxide powder Degussa P25 (TiO$_2$-P25) in high pressure reactor. The high pressure reactor was connected to the supercritical CO$_2$ equipment (see Figure 3.1). For *in situ* reduction of gold by hydrogen, hydrogen was fed into the high pressure reactor at pressure of 2 MPa and 60 ^{o}C. The reaction was allowed to proceed for 30 minutes. After that, CO$_2$ was fed to the high pressure reactor at 20 MPa and 60°C. The reaction was allowed to proceed for one hour. During the process, auto back-pressure regulator maintained the constant pressure. After the reaction, the reactor was placed in an ice bath and depressurized very slowly and carefully. The

resulting powders were removed from the high pressure reactor and dried at 110 ^{o}C overnight. The notations and preparation conditions were shown in Table 3.2.
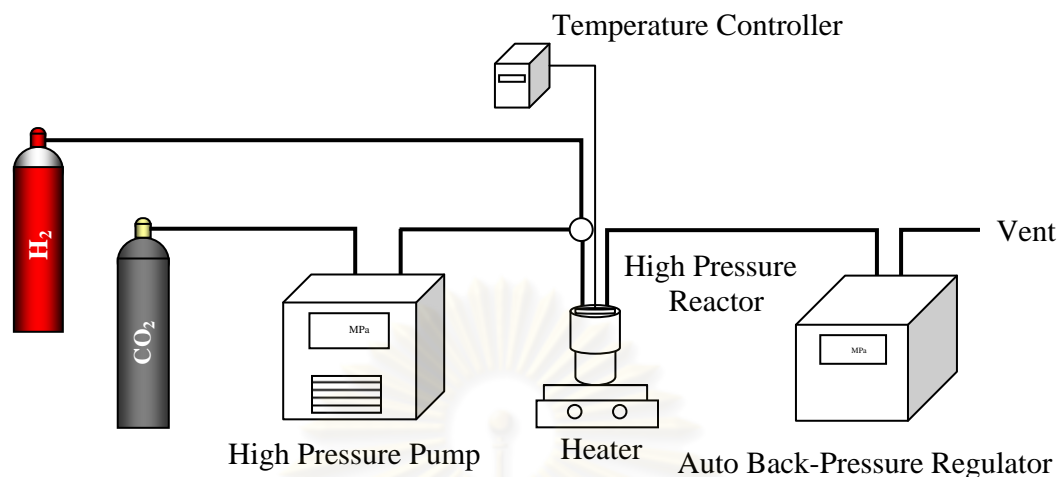
Figure 3.1   Schematic diagram of a system used to deposit gold on the support using supercritical carbon dioxide

3.3 Preparation of supported silver catalysts

3.3.1 Preparation method for TiO$_2$

TiO$_2$ was prepared by a solvothermal method, which is based on the procedure described by Buakaew (Buakaew, 2005). The synthesis was conducted in a 1000 cm^3 stainless steel autoclave, which has a 10 cm inside diameter. First, 15 g of titanium (IV) butoxide was mixed with 100 cm^3 of 1,4-butanediol in the test tube and then placed in the autoclave. In the gap between the test tube and the inside wall of autoclave reactor, 30 cm^3 of 1,4-butanediol was added. After the autoclave was completely purged with nitrogen, it was heated to 300 ^{o}C at the rate of 2.5 ^{o}C/min and held at this temperature for two hours. Autogeneous pressure during the reaction gradually increased as the temperature was raised. After the reaction, the autoclave was cooled to room temperature. The resulting powder collected from the test tube was centrifuged in methanol five times, dried in air at room temperature for six hours, and dried at 110 ^{o}C overnight. The powder was grounded to obtain the final product. The notation for this support is TiO$_2$-ST. Scheme of apparatus is shown in Figure 3.2.
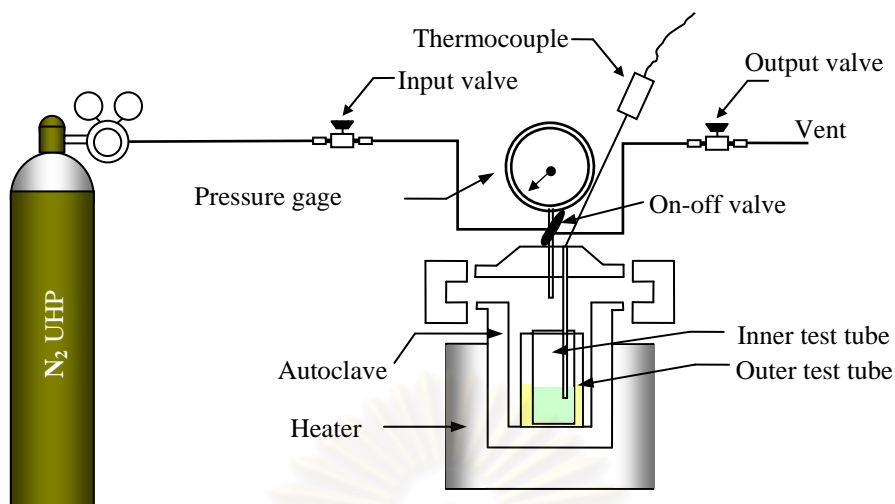
Figure 3.2   Schematic diagram of a system used to synthesize titanium dioxide by a solvothermal method

3.3.2 Deposition of silver by using supercritical CO_2

The Ag/TiO$_2$ catalysts were prepared by using supercritical CO_2 method. First, silver nitrate was dissolved in 3 cm^3 of distilled water and mixed with titanium dioxide powder (TiO$_2$-P25 or TiO$_2$-ST) in high pressure reactor. The high pressure reactor was connected to the supercritical CO_2 equipment (see Figure 3.1). Then pressure of CO_2 was adjusted to desire value (10, 15, and 20 MPa, denoted as Ag/TiO$_2$-10MPa, Ag/TiO$_2$-15MPa, and Ag/TiO$_2$-20MPa, respectively) at a constant temperature of 60 ^{o}C. The reaction was allowed to proceed for 0.5, 1, 2, and 4 hours (denoted as Ag/TiO$_2$-0.5h, Ag/TiO$_2$-1h, Ag/TiO$_2$-2h, and Ag/TiO$_2$-4h, respectively). During the process, auto back-pressure regulator maintained the constant pressure. After the reaction, the reactor was placed in ice bath and depressurized very slowly and carefully. The resulting powders were removed from the high pressure reactor and dried at 110 ^{o}C overnight. The notations of 2 wt% Ag/TiO$_2$, 10 wt% Ag/TiO$_2$, 20 wt% Ag/TiO$_2$ referred to silver contents of 2 wt%, 10 wt%, and 20 wt%, respectively. The notations and preparation conditions were listed in Table 3.2.

Table 3.2 Notations and preparation conditions of catalysts that were prepared by using supercritical CO_2

Catalysts	Type of support	Type of solvent	Metal catalyst	Metal content (wt %)	Pressure of CO_2 (MPa)	Holding time (h)
Au/TiO$_2$-Water	TiO$_2$-P25	Water	Gold	2	20	1
Au/TiO$_2$-MeOH	TiO$_2$-P25	Methanol	Gold	2	20	1
Au/TiO$_2$-Acetyl	TiO$_2$-P25	Acetylacetone	Gold	2	20	1
2 wt% Ag/TiO$_2$	TiO$_2$-P25	Water	Silver	2	20	1
10 wt% Ag/TiO$_2$	TiO$_2$-P25	Water	Silver	10	20	1
20 wt% Ag/TiO$_2$	TiO$_2$-P25	Water	Silver	20	20	1
Ag/TiO$_2$-10MPa	TiO$_2$-P25	Water	Silver	20	10	1
Ag/TiO$_2$-15MPa	TiO$_2$-P25	Water	Silver	20	15	1
Ag/TiO$_2$-20MPa	TiO$_2$-P25	Water	Silver	20	20	1
Ag/TiO$_2$-0.5h	TiO$_2$-P25	Water	Silver	20	20	0.5
Ag/TiO$_2$-1h	TiO$_2$-P25	Water	Silver	20	20	1
Ag/TiO$_2$-2h	TiO$_2$-P25	Water	Silver	20	20	2
Ag/TiO$_2$-4h	TiO$_2$-P25	Water	Silver	20	20	4
Ag/TiO$_2$-P25	TiO$_2$-P25	Water	Silver	20	20	1
Ag/TiO$_2$-ST	TiO$_2$-ST	Water	Silver	20	20	1

3.4 Catalysts characterizations

3.4.1 X-ray diffraction (XRD)

The crystalline structure and X-ray diffraction (XRD) patterns of all catalysts were determined by the SIEMENS D5000 X-ray diffractometer connected with a personal computer using Diffract AT version 3.3 for a full control of the XRD analyzer. The measurements were carried out by using Cu Kα radiation with Ni filter. A scanned range of 2θ from 20° to 80° and resolution was 0.04^o. Average crystallite sizes of catalysts were calculated from Scherrer equation using the full width at half maximum of intensity of diffraction pattern.

3.4.2 Surface area measurement

The single point BET surface area of all catalysts samples were measured by the Micromeritrics ChemiSorb 2750 using nitrogen as the adsorbate. Approximately 0.2 g of the catalysts was placed on glass wool inside the U-tube and the sample was degassed at 200 ^{o}C for one hour.

3.4.3 Transmission electron microscopy (TEM)

The morphology and crystallite size of all catalysts were measured by the JEOL 2010 Transmission Electron Microscope (TEM) operated at 100 kV. The average crystallite sizes were measured by SemAfore program version 5.00.

3.4.4 Inductively-coupled plasma optical emission spectroscopy (ICP-OES)

The metal content in catalysts was measured by inductively-coupled plasma optical emission spectroscopy using the Optima 2100 DV spectrometer. For Au/TiO$_2$ catalysts, approximately 0.0125 g of sample was dissolved in aqua regia solution (6 cm^3 of concentrated hydrochloric acid mixed with 2 cm^3 of concentrated nitric acid). The solution was stirred for four hours to digest the metal and the support. After that, the solution was diluted to 50 cm^3. The calibration standards were prepared from 1,000 ppm standard gold solution available from Sigma-Aldrich. The calibration standards contained 2 ppm, 5 ppm, 8 ppm, and 10 ppm of gold. For Ag/TiO$_2$ catalysts, approximately 0.01 g of sample was dissolved in 8 cm^3 of concentrated nitric acid. The solution was stirred for four hours to digest the metal and the support. After that, the solution was diluted to 50 cm^3. The calibration standards were prepared from

1,000 ppm standard silver solution available from PerkinElmer. The calibration standards contained 20 ppm, 30 ppm, 40 ppm, and 50 ppm of silver. For the blank sample, a mixture of concentrated hydrochloric acid and concentrated nitric acid were mixed together (similar to the one used to digest the sample).

3.4.5 X-ray photoelectron spectroscopy (XPS)

The X-ray photoelectron spectroscopy (XPS) was performed using the AMICUS / ESCA 3400 X-ray photoelectron spectrometer. X-ray photoelectron spectra were recorded under a vacuum exceeding 5×10^{-6} Pa using Mg Kα radiation. For analysis, the C 1s peak was used as reference by adjusted the binding energy to 285.0 eV. Deconvolution of complex spectra were done by fitting with Gaussian (70%)-Lorentzian (30%) shapes using version 2 software equipped with the XPS system.

3.5 Measurement of catalytic activity of supported metal catalysts

Catalytic activity measurement for CO oxidation was carried out in a fixed-bed reactor consisting of a pyrex tube (5 mm ID) and a coaxially-centered thermocouple with its tip located in the middle of the bed (see Figure 3.3). Approximately 0.1 g of the catalyst was placed between two quartz wool plugs inside the reactor. The reactor was then placed in a furnace. The temperature of the reaction was controlled by a temperature controller, which was connected to the furnace.

Prior to the experiment involving the supported silver catalyst, the catalyst was reduced in situ at 400 $^{\circ}$C in a stream of 10% H_2/He at flow rate 50 cm^3/min for one hour. After that, hydrogen was removed by purging with helium for another hour before the activity measurements. Two reactant gases, 1% CO/He and 2% O_2/He, were mixed and fed to the reactor. The composition of effluent gas was analyzed by a Shimadzu gas chromatograph with a TC detector. Helium was used as the carrier gas and the column used was a molecular sieves 5A column (3 m × 3 mmØ). Molecular sieves 5A were used to analyze N_2, CO, O_2, H_2, and other hydrocarbons.

The CO conversion is calculated based on CO consumption as follows:

$$\text{CO conversion} (\%) = \frac{[\text{CO}]_{\text{inlet}} - [\text{CO}]_{\text{outlet}}}{[\text{CO}]_{\text{inlet}}} \times 100 \qquad (3.1)$$
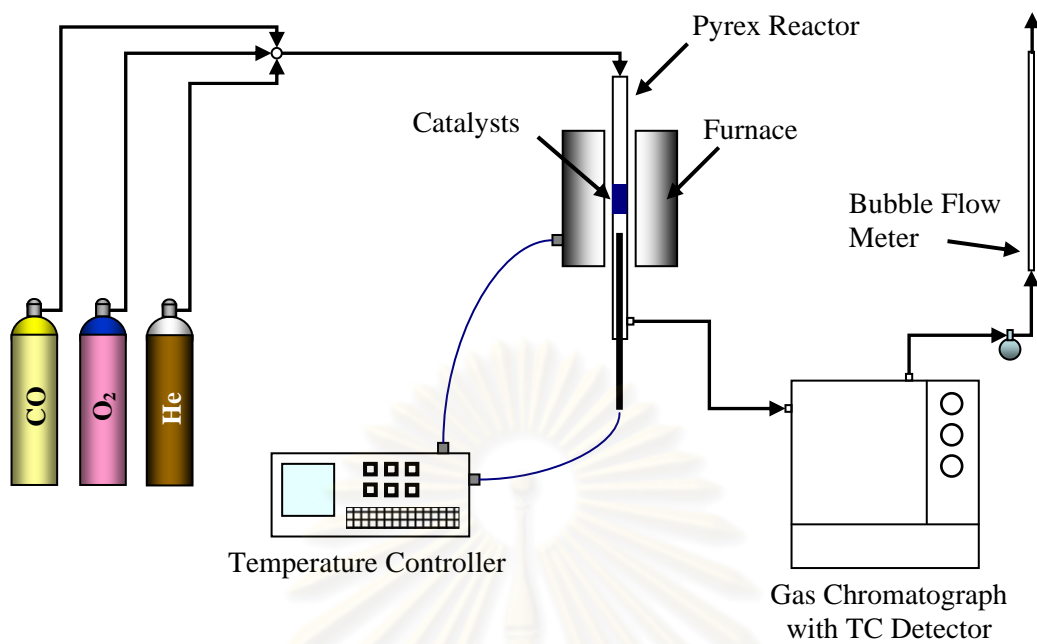
Figure 3.3   Schematic diagram of a reactor system employed for oxidation of CO experiment

CHAPTER IV

RESULTS AND DISCUSSION

In this chapter, results involving supported gold catalysts are presented and discussed in sections 4.1 and 4.2. The results and discussion involving supported silver catalysts are in sections 4.3 to 4.6.

4.1 Supported gold catalysts that were prepared by deposition precipitation method

4.1.1 The phase structure and specific surface area

The phase structure of catalysts was determined using XRD technique. The XRD patterns of supported gold catalysts are shown in Figure 4.1. The XRD diffraction pattern possessed diffraction peaks at 2θ of 25.3^{o}, 37.8^{o}, 48.1^{o}, 54.0^{o}, 55.2^{o}, 62.8^{o}, 68.0^{o}, 72.0^{o}, and 76.1^{o}, corresponding to titanium dioxide anatase phase and diffraction peaks at 2θ of 27.5^{o}, 36.1^{o}, and 41.4^{o}, corresponding to titanium dioxide rutile phase. However, the diffraction pattern of gold was not observed probably because the particle size of gold was too small or the dispersion of metal on the support was high (Ho and Yeung, 2006). The crystallite sizes of TiO_2 anatase phase was 22.3 nm (Calculated from the Scherrer equation). Example of crystallite sizes calculation using the Scherrer equation is illustrated in Appendix A. Specific surface areas of the TiO_2-P25 support was 41 m^2/g. Supported gold catalysts has specific surface areas between 41 - 42 m^2/g.
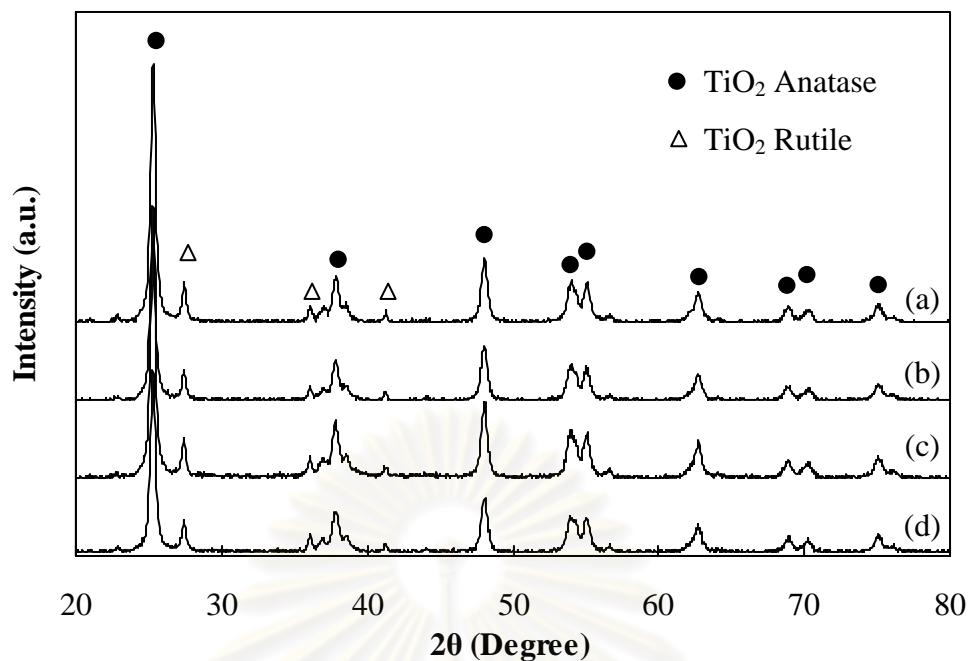
Figure 4.1   XRD patterns of (a) TiO$_2$-P25 support and Au/TiO$_2$ catalysts prepared by deposition precipitation method at (b) pH 6, (c) pH 7, and (d) pH 8.

4.1.2 Transmission electron microscopy (TEM)

The transmission electron microscopy (TEM) was employed to determine the particles size distribution of gold on TiO$_2$-P25. From the TEM images of TiO$_2$-P25, Au/TiO$_2$-pH6, Au/TiO$_2$-pH7, and Au/TiO$_2$-pH8 were shown in Figures 4.2, 4.3, 4.4, and 4.5, respectively. Gold nanoparticles were well dispersed on the TiO$_2$-P25 support were reasonably uniform in size for all samples. The gold particle sizes were 7.6, 3.3, and 11.6 nm for Au/TiO$_2$-pH6, Au/TiO$_2$-pH7, and Au/TiO$_2$-pH8, respectively. For Au/TiO$_2$-pH7 catalyst, narrow the gold nanoparticles were the smallest in size and the standard deviation was narrow, indicating uniform gold particle size. The standard deviation values were listed in Table 4.1. Particle size distributions were show in Appendix B.
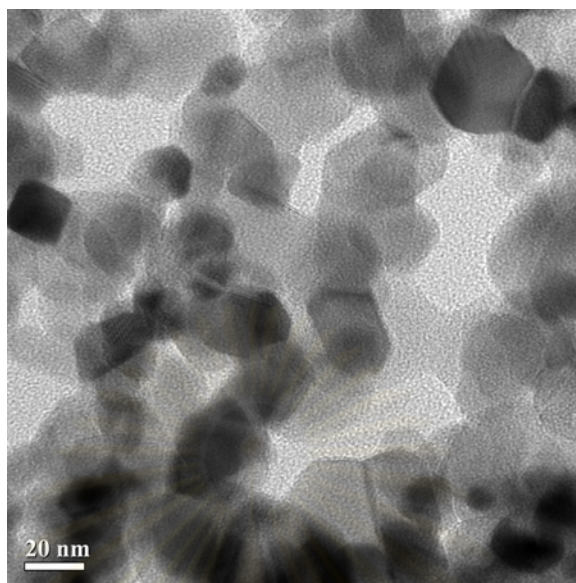
Figure 4.2   TEM image of TiO$_2$-P25 support. The scale bar is 20 nm.
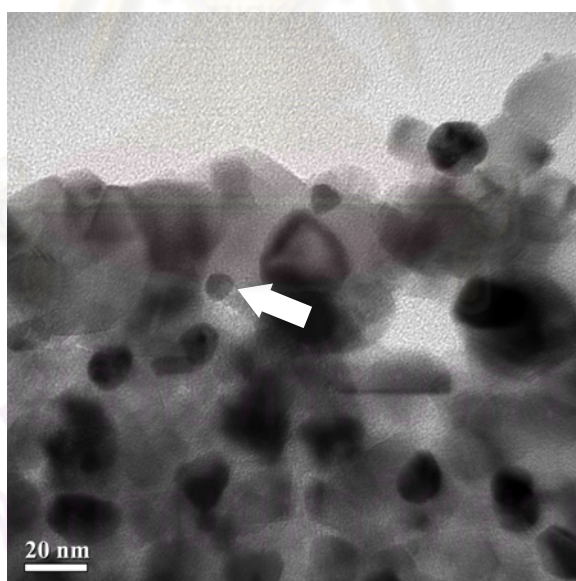
Figure 4.3   TEM image of Au/TiO$_2$ catalyst that was prepared at pH 6. The scale bar is 20 nm.
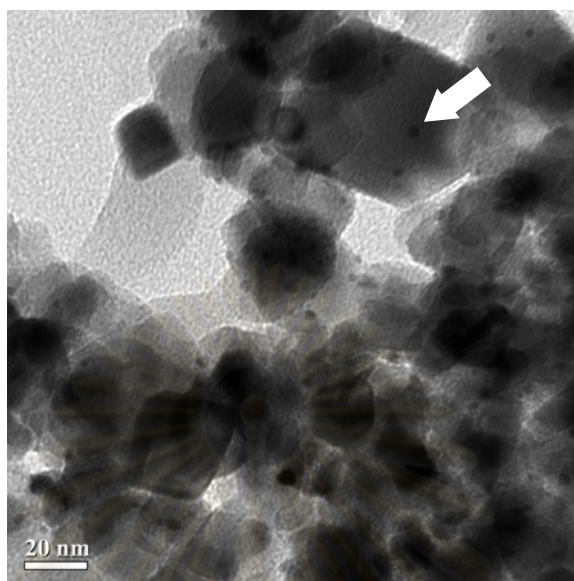
Figure 4.4   TEM image of Au/TiO$_2$ catalyst that was prepared at pH 7. The scale
bar is 20 nm.
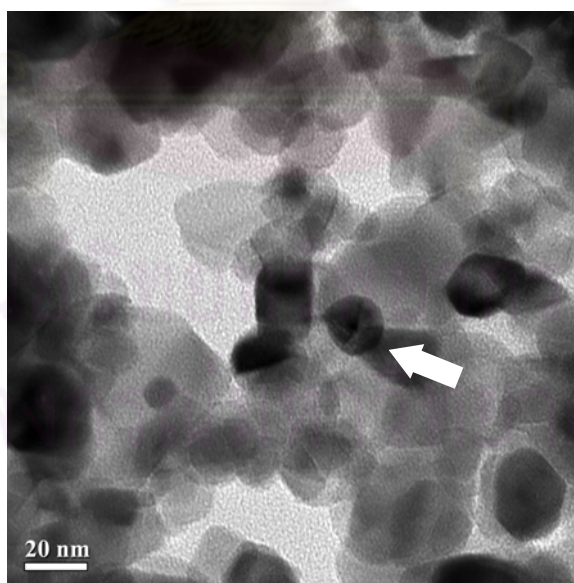
Figure 4.5   TEM image of Au/TiO$_2$ catalyst that was prepared at pH 8. The scale
bar is 20 nm.

Table 4.1 Average particle size, standard deviation of gold and gold content on the supported gold catalysts that were prepared by deposition precipitation method

Catalysts	Average gold particle size (nm)[*]	Standard deviation of gold particle size (nm)	Actual gold content (%) [**]
Au/TiO$_2$-pH6	7.6	2.6	1.4
Au/TiO$_2$-pH7	3.3	1.0	1.1
Au/TiO$_2$-pH8	11.6	3.8	0.9

*Estimated by TEM images

** Measurement by ICP-OES

4.1.3 Gold content in the supported gold catalysts

The amount of gold deposited on the TiO$_2$-P25 support was measured by inductively-coupled plasma optical emission spectroscopy (ICP-OES). The results are listed in Table 4.1. The gold uptakes were the highest at pH 6 and decreased when pH rose. The actual gold contents were 1.4, 1.1, and 0.9 % for Au/TiO$_2$-pH6, Au/TiO$_2$-pH7, and Au/TiO$_2$-pH8, respectively. The gold species in HAuCl$_4$ solutions changed according to the pH. As the pH value increased, hydrolysis of gold species and chlorine loss occurred. The higher the pH value, the higher the hydrolysis extension of the gold complex. This led to a higher Cl$^-$ concentration in solution (see Figure 4.6). Therefore, higher pH value gave rise to lower gold content due to the competition between Cl$^-$ and gold complex for the same site on TiO$_2$ surface (Souza et al., 2008). Moreover, the charge on TiO$_2$ surface also affected the amount of gold deposited on the support. Moreau and Bond (Moreau and Bond, 2007) claimed that the charge on TiO$_2$ surface depended on pH. Below the isoelectric point positive due to protonation of the surface hydroxyls, while above the isoelectric point the charge is negative due to removal of protons from the surface hydroxyls. The isoelectric point value for TiO$_2$-P25 is pH~6 (Moreau and Bond, 2007).
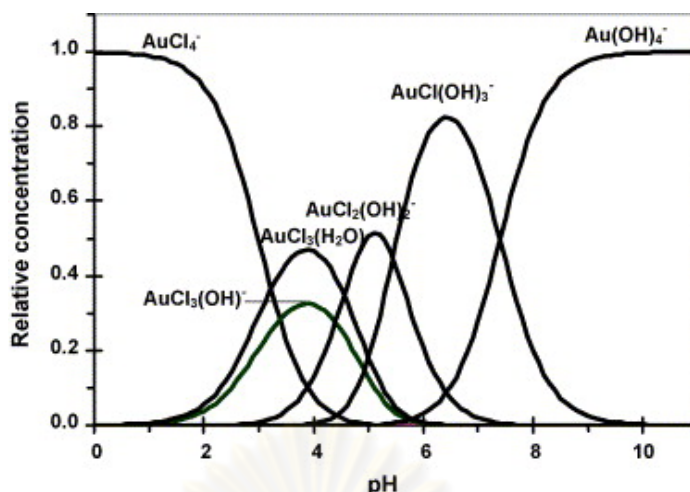
Figure 4.6 Relative concentration of anionic gold species as a function of pH derived from $AuCl_4^-$ by hydrolysis. Total $[Au] = 4 \times 10^{-3}$ M (Moreau and Bond, 2007)

4.1.4 X-ray photoelectron spectroscopy (XPS)

X-ray photoelectron spectroscopy (XPS) was performed to determine the oxidation state of gold species. The Au 4f emission spectra for Au/TiO_2 catalysts were shown in Figure 4.7, 4.8, and 4.9 for the catalysts prepared at pH 6, 7, and 8, respectively. The major XPS peaks shown binding energies of 4f level at 83.2 eV (Au $4f_{7/2}$) and 86.7 eV (Au $4f_{5/2}$). The binding energies reported were indicative of zero oxidation state for gold (Au^0) (Pillai and Deevi, 2006; Zhang et al., 2007).
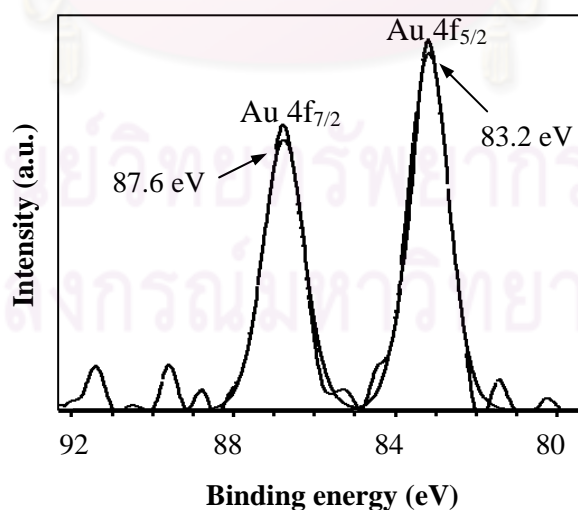
Figure 4.7 XPS spectra of Au 4f level of Au/TiO_2 catalysts prepared by deposition precipitation method at pH6
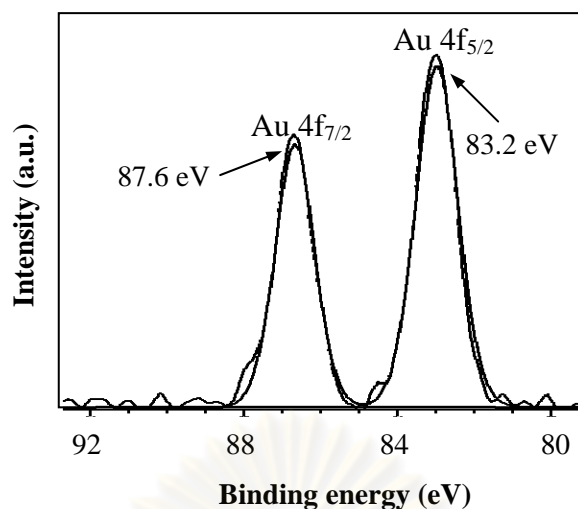
Figure 4.8   XPS spectra of Au 4f level of Au/TiO$_2$ catalysts prepared by deposition precipitation method at pH7
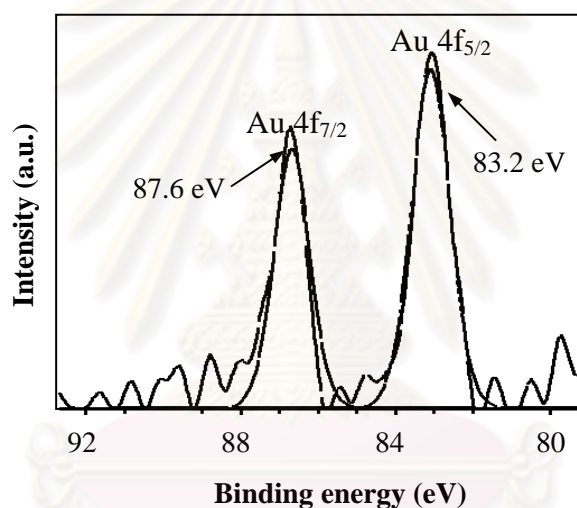
Figure 4.9   XPS spectra of Au 4f level of Au/TiO$_2$ catalysts prepared by deposition precipitation method at pH8

4.1.5 Catalytic activities of Au/TiO$_2$ catalysts

The catalytic activities of Au/TiO$_2$ catalysts were measured at a temperature ranging from 30 ^{o}C to 150 ^{o}C. Figure 4.10 displays CO conversions as a function of a reaction temperature for Au/TiO$_2$ catalysts prepared by deposition precipitation method. The lights off temperature (a temperature which 50 % conversion was achieved, T$_{50}$) were 55°C, 42°C, and 74°C for Au/TiO$_2$-pH6, Au/TiO$_2$-pH7, and Au/TiO$_2$-pH8, respectively. The activities of the catalysts were in the following order Au/TiO$_2$-pH7 > Au/TiO$_2$-pH6 > Au/TiO$_2$-pH8. The catalytic activities appeared to be dependent on the gold particle size, where small gold particle size gave rise to a higher catalytic activity than large one.
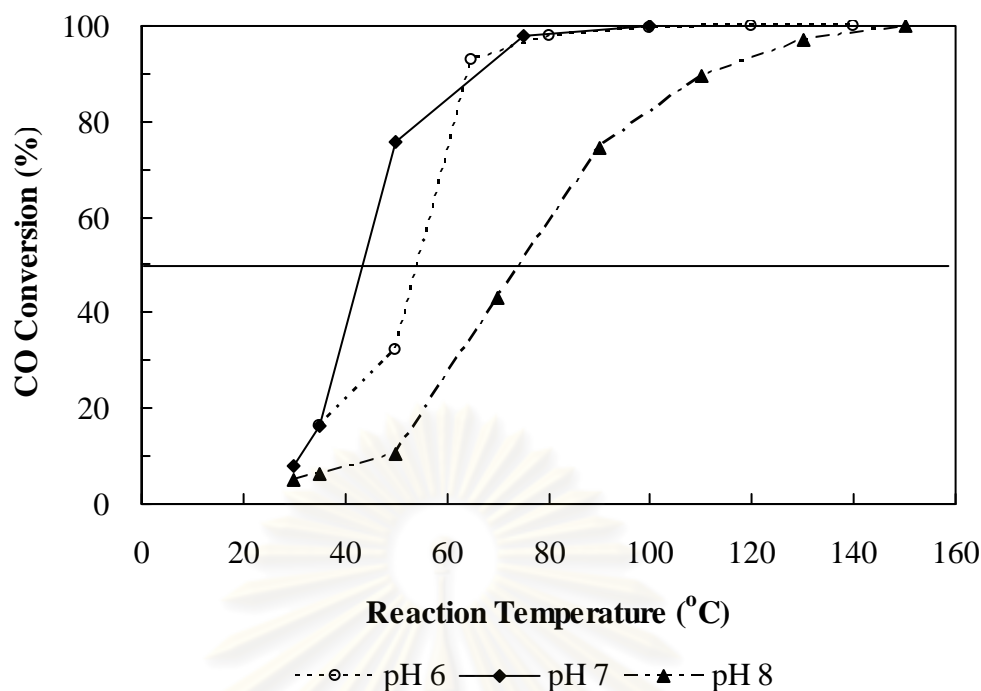
Figure 4.10   CO conversion as a function of a reaction temperature for Au/TiO$_2$ catalysts prepared by deposition precipitation method

4.2 Supported gold catalysts that were prepared using supercritical CO$_2$ technique

4.2.1 The phase structure and specific surface area

The phase structure of catalysts was determined using XRD technique. The XRD patterns of supported gold catalysts are shown in Figure 4.11. The XRD diffraction pattern possessed diffraction peaks at 2θ of 25.3^o, 37.8^o, 48.1^o, 54.0^o, 55.2^o, 62.8^o, 68.0^o, 72.0^o, and 76.1^o, corresponding to titanium dioxide anatase phase and diffraction peaks at 2θ of 27.5^o, 36.1^o, and 41.4^o, corresponding to titanium dioxide rutile phase, while diffraction peak at 2θ of 38.0^o and 44.4^o, corresponding to gold metal. The diffraction peak at 2θ about 38°, peak were overlap between anatase and gold metal. The crystallite sizes of gold metal were calculated using the Scherrer equation at diffraction peak at 2θ is 44.4^o (200). The crystallite sizes of gold are listed in Table 4.2. Specific surface areas of the TiO$_2$-P25 support was 41 m^2/g. Supported gold catalysts had specific surface areas between 40 - 42 m^2/g.
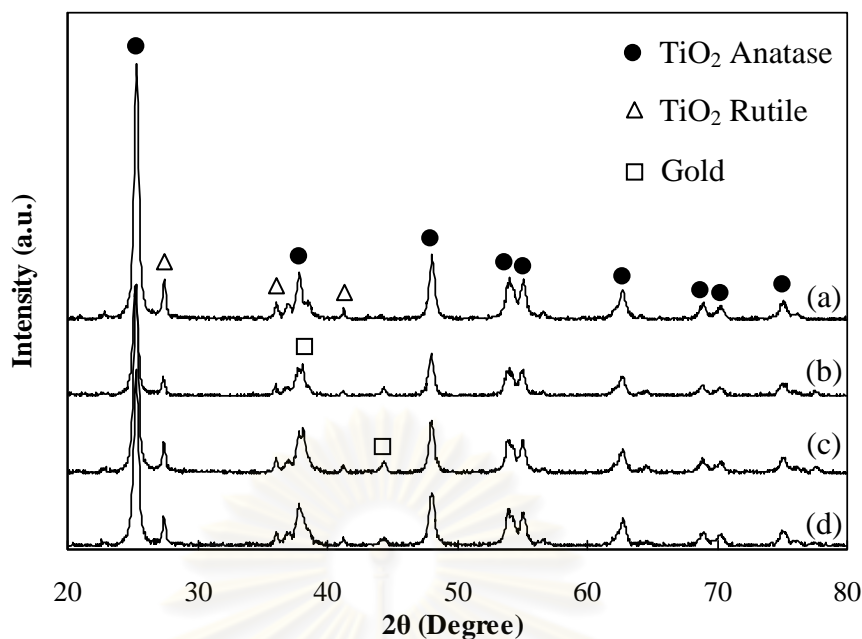
Figure 4.11 XRD patterns of (a) TiO$_2$-P25 support and Au/TiO$_2$ catalysts prepared with (b) Water, (c) MeOH, and (d) Acetylacetone as a solvent

Table 4.2 Crystallite size of gold and gold contents in catalyst

Samples	Crystallite size of gold (nm)*	Gold content (%)**
Au/TiO$_2$-Water	68.1	1.5
Au/TiO$_2$-MeOH	31.9	1.6
Au/TiO$_2$-Acetyl	19.4	1.9

*Calculated by Scherrer equation at diffraction peak 2θ is 44.4^o (200)

**Measurement by ICP-OES

4.2.2 Transmission electron microscopy (TEM)

The transmission electron microscopy (TEM) was employed to determine the particles size distribution of gold on TiO$_2$-P25. The TEM image of TiO$_2$-P25 was shown in Figure 4.2. Figures 4.12, 4.13, and 4.14 were the TEM images of Au/TiO$_2$-Water, Au/TiO$_2$-MeOH, and Au/TiO$_2$-Acetyl, respectively. From the TEM images were not observed gold particles dispersed on the TiO$_2$-P25 support.
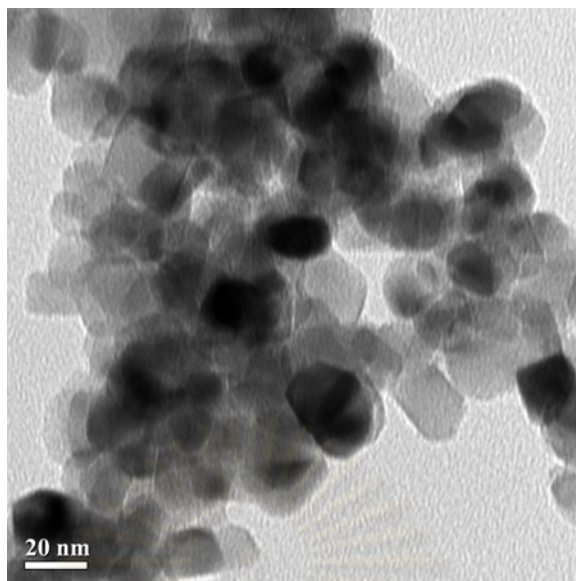
Figure 4.12   TEM image of Au/TiO$_2$-Water catalyst. The scale bar is 20 nm.
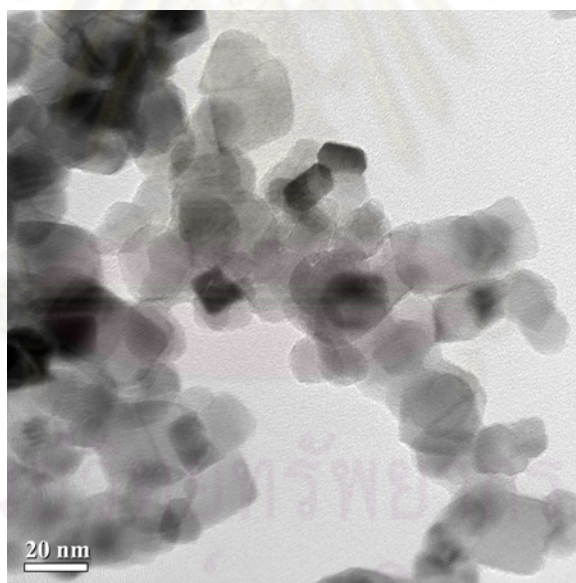
Figure 4.13   TEM image of Au/TiO$_2$-MeOH catalyst. The scale bar is 20 nm.
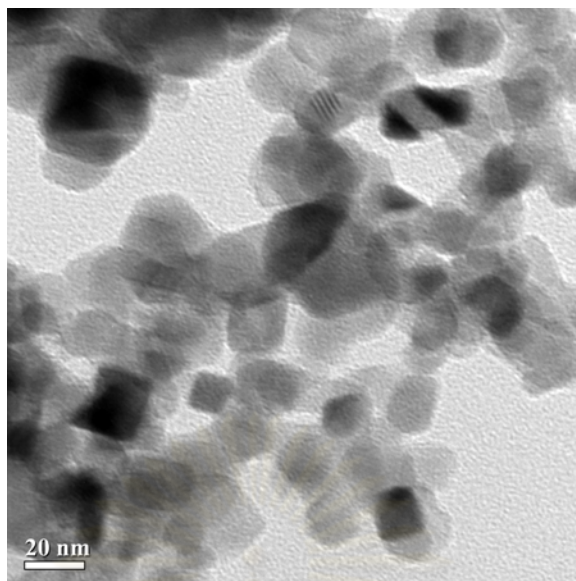
Figure 4.14 TEM image of Au/TiO$_2$-Acetyl catalyst. The scale bar is 20 nm.

4.2.3 Gold content in the supported gold catalysts

The amount of gold deposited on the TiO$_2$-P25 support was measured by inductively-coupled plasma optical emission spectroscopy (ICP-OES). The results are listed in Table 4.2. The Au/TiO$_2$-Acetyl was shown highest gold content. The actual gold contents were 1.5, 1.6, and 1.9 % for Au/TiO$_2$-Water, Au/TiO$_2$-MeOH, and Au/TiO$_2$-Acetyl, respectively. The amount of gold was lower than nominal value probably because some gold was dissolved in supercritical CO$_2$, thus it was removed with CO$_2$ from the reactor (Wattanamalachai, 2006).

4.2.4 X-ray photoelectron spectroscopy (XPS)

X-ray photoelectron spectroscopy (XPS) was performed to determine the oxidation state of gold species. The Au 4f emission spectra for Au/TiO$_2$ catalysts were shown in Figure 4.15 (a), (b), and (c) for Au/TiO$_2$-Water, Au/TiO$_2$-MeOH, and Au/TiO$_2$-Acetyl, respectively. For all catalysts were not observed the XPS peak of Au 4f level.
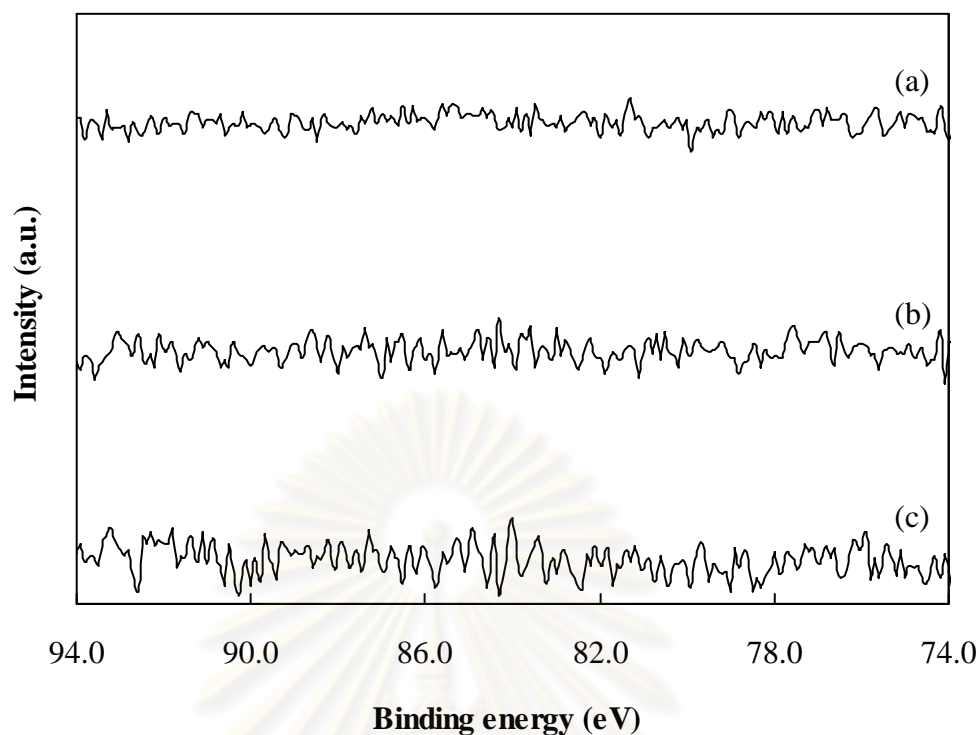
Figure 4.15 XPS spectra of Au 4f level of Au/TiO_2 catalysts prepared with (b) Water, (c) MeOH, and (d) Acetylacetone as a solvent

4.2.5 Catalytic activities of Au/TiO_2 catalysts

The catalytic activities of Au/TiO_2 catalysts were measured at a temperature ranging from 200^oC to 475^oC. Figure 4.16 displays CO conversions as a function of a reaction temperature for Au/TiO_2 catalysts were prepared using supercritical CO_2 technique. The T_{50} were 418^oC, 390^oC, and 367^oC for Au/TiO_2-Water, Au/TiO_2-MeOH, and Au/TiO_2-Acetyl, respectively. The activities of the catalysts were in the following order Au/TiO_2-Acetyl > Au/TiO_2-MeOH > Au/TiO_2-Water. The catalytic activity appeared to be dependent on the gold particle size, where small gold particle size gave rise to a higher catalytic activity than large one.

Figure 4.16 CO conversions as a function of a reaction temperature for Au/TiO$_2$ catalysts prepared using supercritical CO$_2$ technique

4.3 Comparative study effect of amount of silver on catalytic activity

4.3.1 The phase structure and specific surface area

The phase structure of catalysts was determined using XRD technique. Figure 4.17 displays XRD patterns of supported silver catalysts with different amount of silver. For 2 wt% Ag/TiO$_2$ catalyst (see Figure 4.17 (b)), the diffraction peak was be observed at 2θ of 25.3^o, 37.8^o, 48.1^o, 54.0^o, 55.2^o, 62.8^o, 68.0^o, 72.0^o, and 76.1^o, corresponding to titanium dioxide anatase phase and diffraction peaks at 2θ of 27.5^o, 36.1^o, and 41.4^o, corresponding to titanium dioxide rutile phase. However, the diffraction peak of silver was not observed probably because the low amount of silver or dispersion of metal on the support was high (Ho and Yeung, 2006). For 10 wt% Ag/TiO$_2$ and 20 wt% Ag/TiO$_2$ catalysts (see Figure 4.17 (c) and (d)), the XRD patterns possessed the diffraction peaks at 2θ of 25.3^o, 37.8^o, 48.1^o, 54.0^o, 55.2^o, 62.8^o, 68.0^o, 72.0^o, and 76.1^o, corresponding to titanium dioxide anatase phase, diffraction peaks at 2θ of 27.5^o, 36.1^o, and 41.4^o, corresponding to titanium dioxide

rutile phase, diffraction peak at 2θ of 24.3°, corresponding to Ag_2O, diffraction peak at 2θ of 43.4°, corresponding to Ag, and diffraction peaks at 2θ of 21.6°, 29.6°, 31.9°, and 32.8°, corresponding to Ag_2CO_3. Specific surface areas of the TiO_2-P25 support was 41 m^2/g. Supported silver catalysts had specific surface areas were 42, 30, and 18 m^2/g for 2 wt% Ag/TiO_2, 10 wt% Ag/TiO_2, and 20 wt% Ag/TiO_2, respectively. The supported silver catalysts had a smaller specific surface area than TiO_2-P25 support probably because the silver particle deposited inside the pore of support.

Figure 4.17 XRD patterns of (a) TiO_2-P25 support and Ag/TiO_2 catalysts prepared using supercritical CO_2 technique with different of amount of silver, (b) 2 wt%, (c) 10 wt%, and (d) 20 wt%

4.3.2 Transmission electron microscopy (TEM)

The transmission electron microscopy (TEM) was employed to determine the particle sizes distribution of silver on TiO_2-P25. TEM image of TiO_2-P25 was shown in Figure 4.2. Figures 4.18, 4.19, and 4.20 were TEM images of 2 wt% Ag/TiO_2, 10 wt% Ag/TiO_2, and 20 wt% Ag/TiO_2, respectively. Silver nanoparticles were uniform and well dispersed on TiO_2-P25 support. The silver particle sizes of were 2.8, 3.0, and 2.8 nm for 2 wt% Ag/TiO_2, 10 wt% Ag/TiO_2, and 20 wt% Ag/TiO_2, respectively (see Table 4.3). The silver particles size distributions are listed in Appendix B.
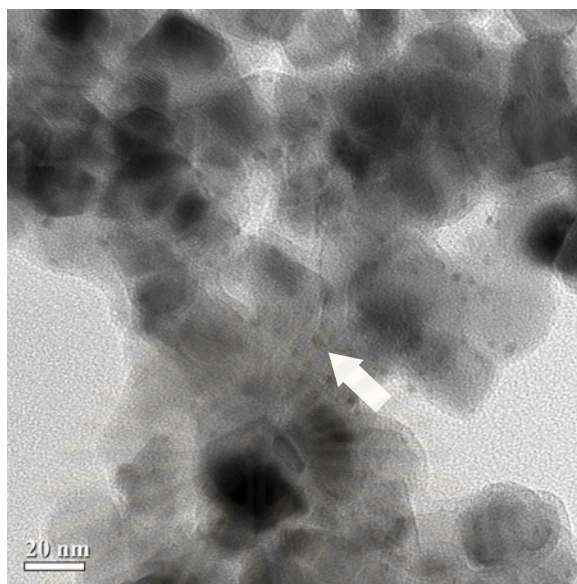
Figure 4.18 TEM image of 2 wt% Ag/TiO$_2$ catalyst. The scale bar is 20 nm.
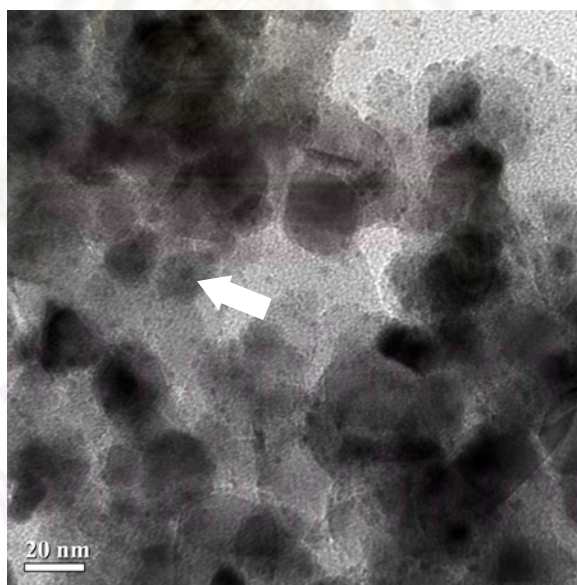
Figure 4.19 TEM image of 10 wt% Ag/TiO$_2$ catalyst. The scale bar is 20 nm.
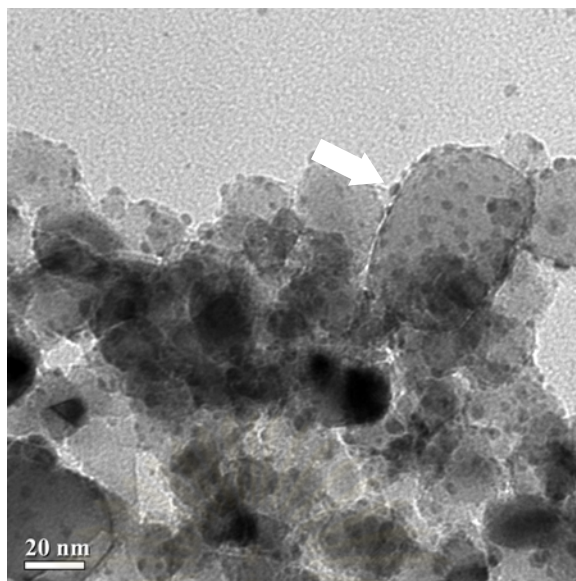
Figure 4.20   TEM image of 20 wt% Ag/TiO$_2$ catalyst. The scale bar is 20 nm.

Table 4.3   Average particle size, standard deviation of silver and silver content on the supported silver catalysts that were prepared with different amount of silver

Catalysts	Average silver particle size (nm)*	Standard deviation of gold particle size (nm)	Actual silver content (%)**
2 wt% Ag/TiO$_2$	2.8	0.8	0.8
10 wt% Ag/TiO$_2$	3.0	0.9	6.0
20 wt% Ag/TiO$_2$	2.8	0.8	13.2

*Estimated by TEM images

**Measurement by ICP-OES

4.3.3 Silver content in the supported silver catalysts

The amount of silver deposited on the TiO$_2$-P25 support was measured by inductively-coupled plasma optical emission spectroscopy (ICP-OES). The results are listed in Table 4.3. The actual silver contents were 0.8, 6.0, and 13.2 % for 2 wt% Ag/TiO$_2$, 10 wt% Ag/TiO$_2$, and 20 wt% Ag/TiO$_2$, respectively. The amount of silver was lower than nominal value probably because some silver was dissolved in supercritical CO$_2$, thus it was removed with CO$_2$ from the reactor (Wattanamalachai, 2006).

4.3.4 X-ray photoelectron spectroscopy (XPS)

X-ray photoelectron spectroscopy (XPS) was performed to determine the oxidation state of silver species. The Ag 3d emission spectra for Ag/TiO$_2$ catalysts were shown in Figures 4.21, 4.22, and 4.23 for 2 wt% Ag/TiO$_2$, 10 wt% Ag/TiO$_2$, and 20 wt% Ag/TiO$_2$, respectively. Figure 4.21 displays XPS Ag 3d spectra of 2 wt% Ag/TiO$_2$ catalyst. The XPS spectra possessed binding energies of Ag 3d level at 368.1 eV (Ag 3d$_{5/2}$) and 374.2 eV (Ag 3d$_{3/2}$). The binding energies were indicative silver form in Ag^0. Figure 4.22 displays XPS Ag 3d spectra of 10 wt% Ag/TiO$_2$ catalyst. The XPS spectra possessed binding energies of Ag 3d level at 366.2 eV (Ag 3d$_{5/2}$), 368.1 eV (Ag 3d$_{5/2}$), and 374.2 eV (Ag 3d$_{3/2}$). The binding energies were indicative silver form in Ag^0 and Ag$^+$. Usually, the elements in the positive ionic state show a shift of core-level binding energy towards higher energies with respect to the neutral state due to the initial state effect. However, silver is one of the exceptions. A large contribution from the extra-atomic relaxation energy counteracts the effects caused by the initial state, and the binding energy of Ag 3d tends to shift towards lower energy in the oxidized states (Jin et al., 2007). Figure 4.23 displays XPS Ag 3d spectra of 20 wt% Ag/TiO$_2$ catalyst. The XPS spectra possessed binding energies of Ag 3d level at 366.6 eV (Ag 3d$_{5/2}$), 368.5 eV (Ag 3d$_{5/2}$), and 374.5 eV (Ag 3d$_{3/2}$). The binding energies were indicative silver form in Ag^0 and Ag$^+$.
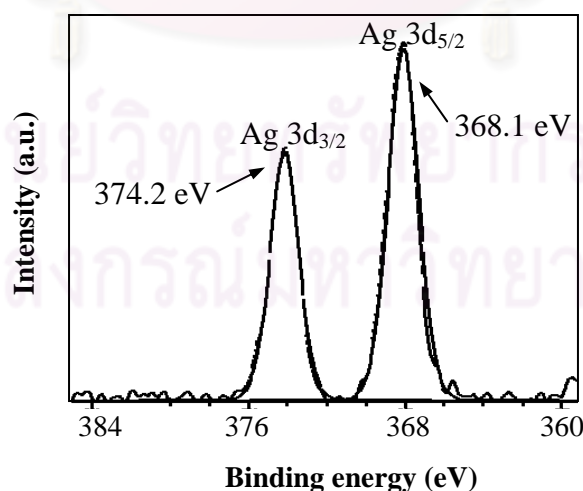
Figure 4.21   XPS spectra of Ag 3d level of 2 wt% Ag/TiO$_2$ catalyst
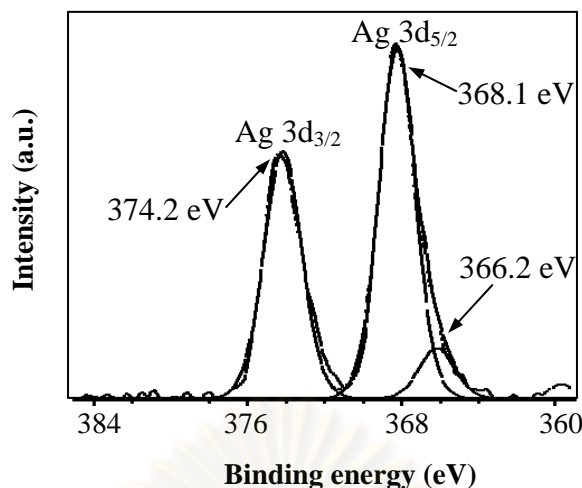
Figure 4.22 XPS spectra of Ag 3d level of 10 wt% Ag/TiO$_2$ catalyst
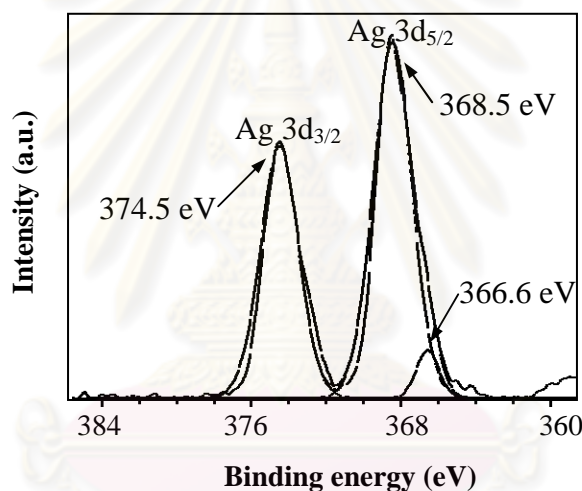
Figure 4.23 XPS spectra of Ag 3d level of 20 wt% Ag/TiO$_2$ catalyst

4.3.5 Catalytic activities of Ag/TiO$_2$ catalysts

The activities of Ag/TiO$_2$ catalysts were measured at a temperature ranging from 30 °C to 475 °C. The catalytic activities of catalysts as a function of temperature were shown in Figure 4.24. The T$_{50}$ were 345°C, 102°C, and 80°C for 2 wt% Ag/TiO$_2$, 10 wt% Ag/TiO$_2$, and 20 wt% Ag/TiO$_2$, respectively. The activities of the catalysts were in the following order 20 wt% Ag/TiO$_2$ > 10 wt% Ag/TiO$_2$ > 2 wt% Ag/TiO$_2$. The catalytic activity appeared to be dependent on silver content on the catalysts. The catalytic activities are good agreement with Frey and coworker (Frey et al., 2008).
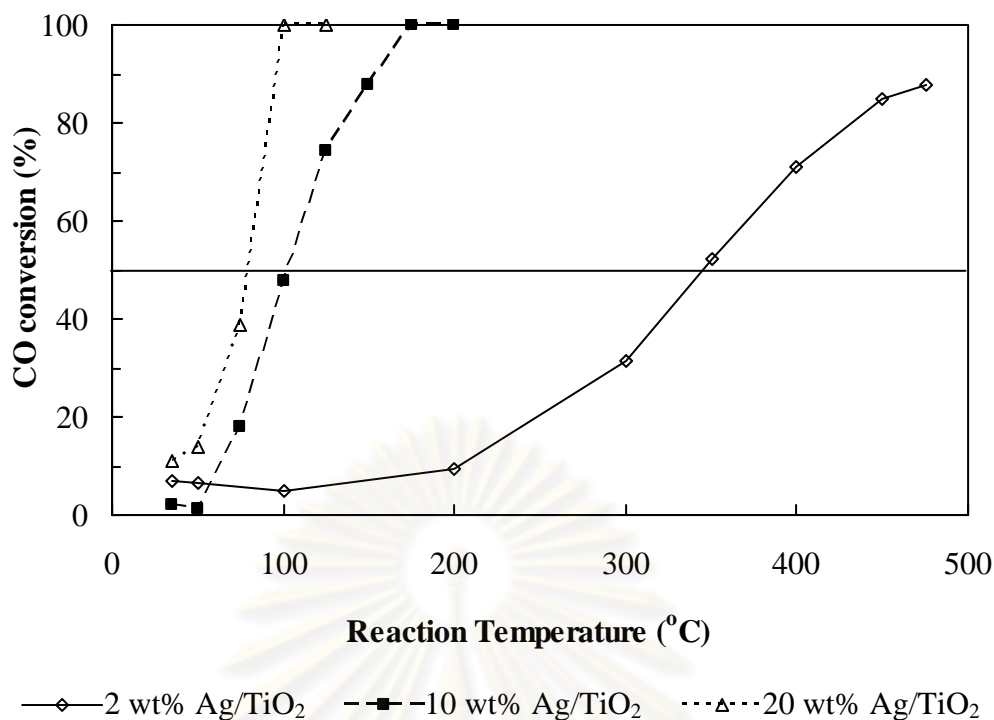
Figure 4.24 CO conversions as a function of a reaction temperature for Ag/TiO_2 catalysts prepared using supercritical CO_2 technique with different amount of silver

4.4 Comparative study effect of pressure of CO_2 on catalytic activity

4.4.1 The phase structure and specific surface area

The phase structure of catalysts was determined using XRD technique. Figure 4.25 displays XRD patterns of supported silver catalysts with different pressure of CO_2. For all catalysts were shown XRD diffraction peaks at 2θ of 25.3^o, 37.8^o, 48.1^o, 54.0^o, 55.2^o, 62.8^o, 68.0^o, 72.0^o, and 76.1^o, corresponding to titanium dioxide anatase phase and diffraction peaks at 2θ of 27.5^o, 36.1^o, and 41.4^o, corresponding to titanium dioxide rutile phase, while diffraction peak at 2θ of 24.3^o, corresponding to Ag_2O, diffraction peak at 2θ of 43.4^o, corresponding to Ag, and diffraction peaks at 2θ of 21.6^o, 29.6^o, 31.9^o, and 32.8^o, corresponding to Ag_2CO_3. Supported silver catalysts had specific surface areas between 15 - 18 m^2/g.
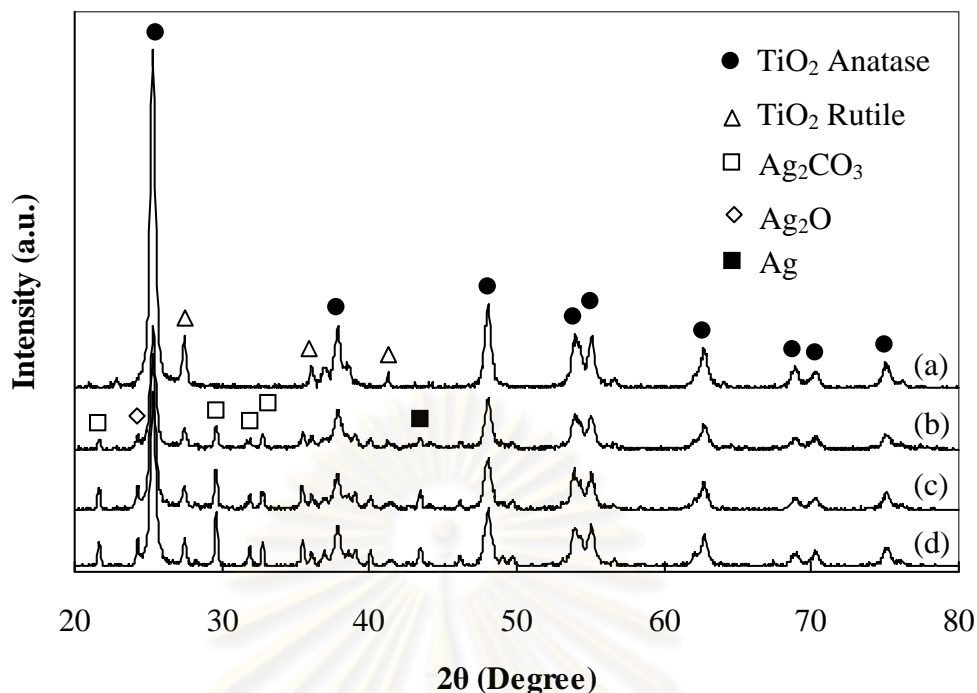
Figure 4.25   XRD patterns of (a) TiO_2-P25 support and Ag/TiO_2 catalysts prepared using supercritical CO_2 technique with different pressure of CO_2 (b) 10 MPa, (c) 15 MPa, and (d) 20 MPa

4.4.2 Transmission electron microscopy (TEM)

The transmission electron microscopy (TEM) was employed to determine the particle sizes distribution of silver on TiO_2-P25. The TEM image of TiO_2-P25 was shown in Figure 4.2. Figures 4.26, 4.27, and 4.28 were the TEM images of Ag/TiO_2-10MPa, Ag/TiO_2-15MPa, and Ag/TiO_2-20MPa, respectively. Silver nanoparticles were uniform and well dispersed on TiO_2-P25 support. The silver particle sizes were 3.1, 3.0, and 2.8 nm for Ag/TiO_2-10MPa, Ag/TiO_2-15MPa, and Ag/TiO_2-20MPa, respectively (see Table 4.4).

Figure 4.26 TEM image of Ag/TiO$_2$-10MPa catalyst. The scale bar is 20 nm.

Figure 4.27 TEM image of Ag/TiO$_2$-15MPa catalyst. The scale bar is 20 nm.

Figure 4.28 TEM image of Ag/TiO$_2$-20MPa catalyst. The scale bar is 20 nm.

Table 4.4 Average particle size, standard deviation of silver and silver content on the supported silver catalysts that were prepared with different pressure of CO$_2$

Catalysts	Average silver particle size (nm)*	Standard deviation of silver particle size (nm)	Actual silver content (%) **
Ag/TiO$_2$-10MPa	3.1	1.5	12.3
Ag/TiO$_2$-15MPa	3.0	1.1	12.7
Ag/TiO$_2$-20MPa	2.8	0.8	13.2

*Estimated by TEM images

**Measurement by ICP-OES

4.4.3 Silver content in the supported silver catalysts

The amount of silver deposited on TiO$_2$-P25 support was measured by inductively-coupled plasma optical emission spectroscopy (ICP- OES). The results were listed in Table 4.4. The actual silver contents were 12.3, 12.7, and 13.2 % for Ag/TiO$_2$-10MPa, Ag/TiO$_2$-15MPa, and Ag/TiO$_2$-20MPa, respectively.

4.4.4 X-ray photoelectron spectroscopy (XPS)

X-ray photoelectron spectroscopy (XPS) was performed to determine the oxidation state of silver species. The Ag 3d emission spectra for Ag/TiO$_2$ catalysts were shown in Figures 4.29, 4.30, and 4.31 for Ag/TiO$_2$-10MPa, Ag/TiO$_2$-15MPa, and Ag/TiO$_2$-20MPa, respectively. Figure 4.29 displays XPS Ag 3d spectra of Ag/TiO$_2$-10MPa catalyst. The XPS spectra possessed binding energies of Ag 3d level at 367.1 eV (Ag 3d$_{5/2}$), 369.2 eV (Ag 3d$_{5/2}$), and 375.2 eV (Ag 3d$_{3/2}$). Figure 4.30 displays XPS Ag 3d spectra of Ag/TiO$_2$-15MPa catalyst. The XPS spectra possessed binding energies of Ag 3d level at 366.7 eV (Ag 3d$_{5/2}$), 368.4 eV (Ag 3d$_{5/2}$), and 374.4 eV (Ag 3d$_{3/2}$). Figure 4.31 displays XPS Ag 3d spectra of Ag/TiO$_2$-20MPa catalyst. The XPS spectra possessed binding energies of Ag 3d level at 366.6 eV (Ag 3d$_{5/2}$), 368.5 eV (Ag 3d$_{5/2}$), and 374.5 eV (Ag 3d$_{3/2}$). The binding energies were indicated silver form in Ag^0 and Ag$^+$.

Figure 4.29   XPS spectra of Ag 3d level of Ag/TiO$_2$-10MPa catalyst
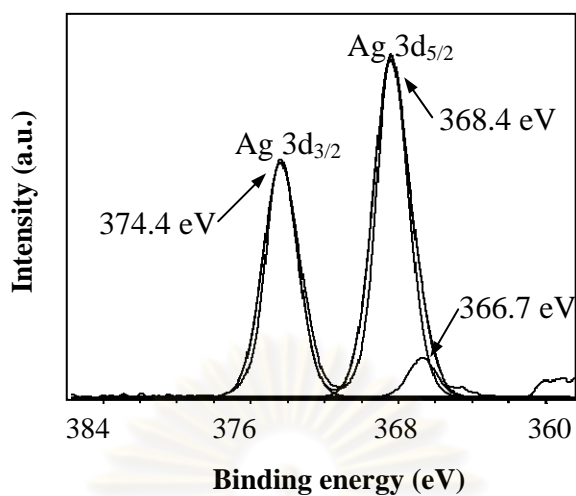
Figure 4.30 XPS spectra of Ag 3d level of Ag/TiO$_2$-15MPa catalyst
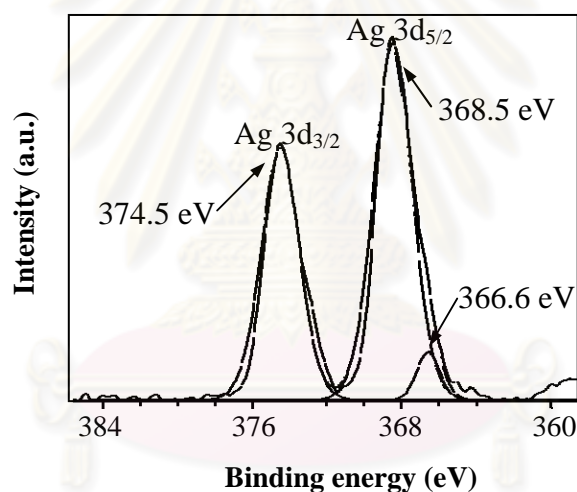
Figure 4.31 XPS spectra of Ag 3d level of Ag/TiO$_2$-20MPa catalyst

4.4.5 Catalytic activities of Ag/TiO$_2$ catalysts

The activities of Ag/TiO$_2$ catalysts were measured at a temperature ranging from 30 ^{o}C to 180 ^{o}C. The catalytic activities of catalysts as a function of a temperature displays in Figure 4.32. The T$_{50}$ were 90°C, 90°C, and 80°C for for Ag/TiO$_2$-10MPa, Ag/TiO$_2$-15MPa, and Ag/TiO$_2$-20MPa, respectively. The activities of the catalysts were in the following order Ag/TiO$_2$-20MPa > Ag/TiO$_2$-15MPa $\cong$ Ag/TiO$_2$-10MPa.
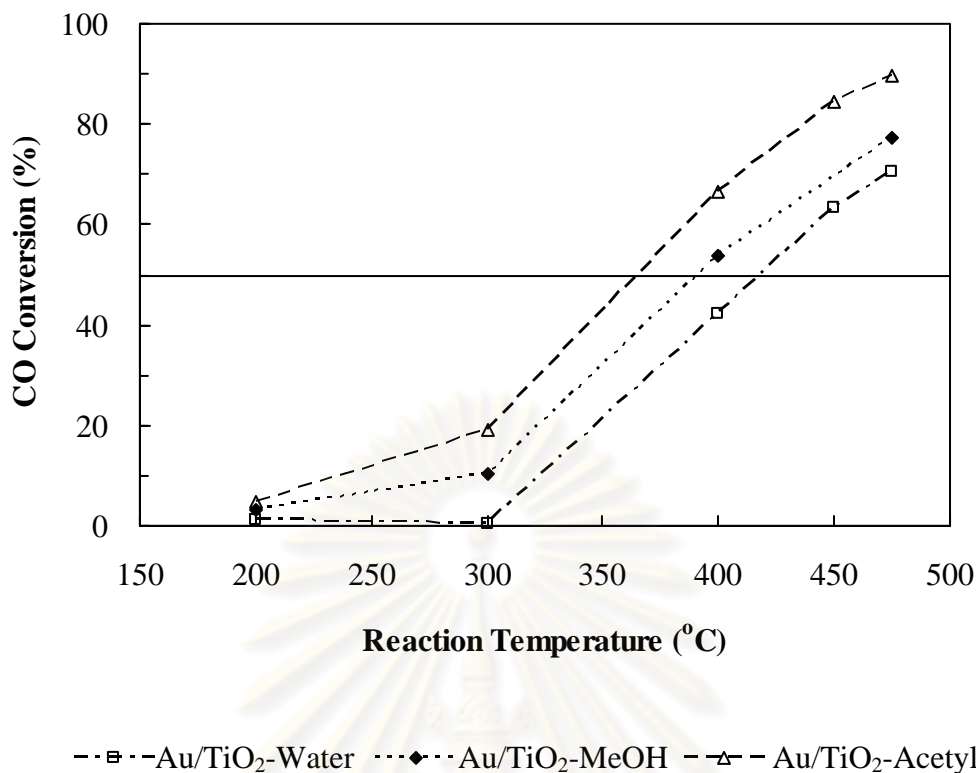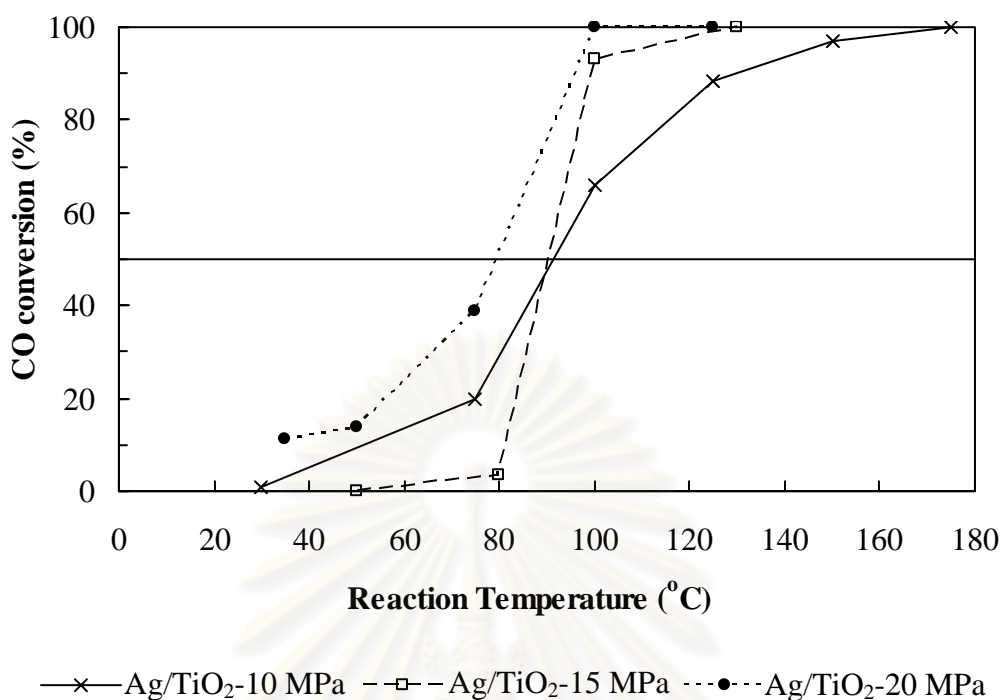
Figure 4.32 CO conversions as a function of a reaction temperature for Ag/TiO$_2$ catalysts were prepared using supercritical CO$_2$ technique with different pressure of CO$_2$

4.5 Comparative study effect of holding time on catalytic activity

4.5.1 The phase structure and specific surface area

The phase structure of catalysts was determined using XRD technique. Figure 4.33 (b), (c), (d), and (e) displays XRD patterns of supported silver catalysts with different holding time. For all catalysts were shown XRD diffraction peaks at 2θ of 25.3^o, 37.8^o, 48.1^o, 54.0^o, 55.2^o, 62.8^o, 68.0^o, 72.0^o, and 76.1^o, corresponding to titanium dioxide anatase phase and diffraction peaks at 2θ of 27.5^o, 36.1^o, and 41.4^o, corresponding to titanium dioxide rutile phase, while diffraction peak at 2θ of 24.3^o, corresponding to Ag$_2$O, diffraction peak at 2θ of 43.4^o, corresponding to Ag, and diffraction peaks at 2θ of 21.6^o, 29.6^o, 31.9^o, and 32.8^o, corresponding to Ag$_2$CO$_3$. Supported silver catalysts had specific surface areas between 15 – 21 m^2/g.
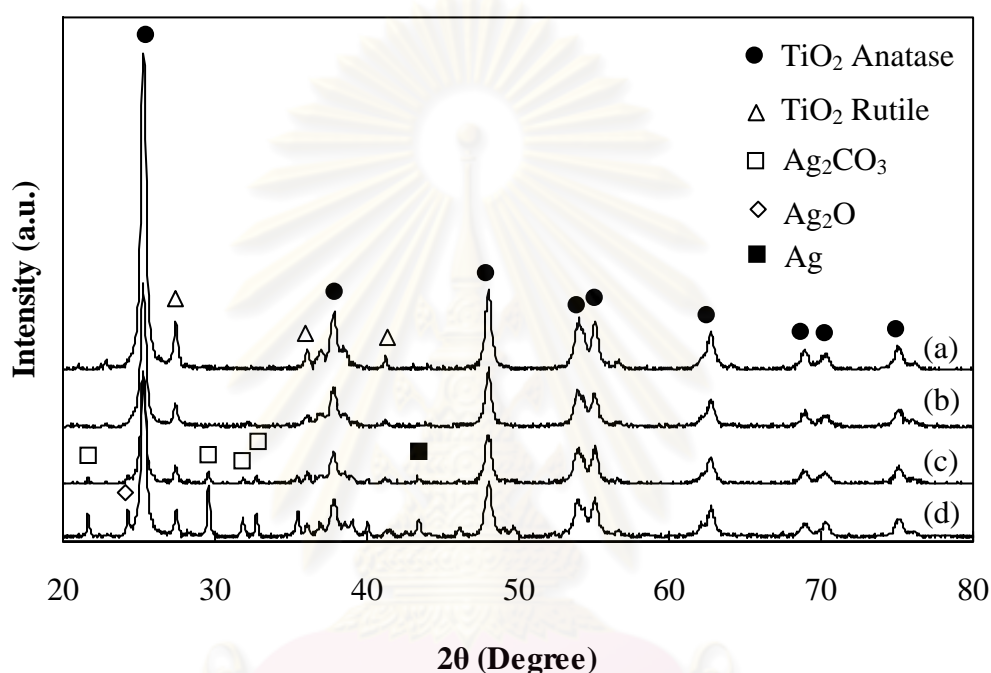
Figure 4.33 XRD patterns of (a) TiO_2-P25 support and Ag/TiO_2 catalysts prepared using supercritical CO_2 technique with different holding time (b) 0.5 hour, (c) 1 hour, (d) 2 hour, and (e) 4 hour

4.5.2 Transmission electron microscopy (TEM)

The transmission electron microscopy (TEM) was employed to determine the particle sizes distribution of silver on TiO_2-P25 support. The TEM image of TiO_2-P25 was shown in Figure 4.2. Figures 4.34, 4.35, 4.36, and 4.37 were shown TEM images of Ag/TiO_2-0.5h, Ag/TiO_2-1h, Ag/TiO_2-2h, and Ag/TiO_2-4h, respectively. Silver nanoparticles were uniform and well dispersed on TiO_2-P25 support. The silver particle size were 5.8, 2.8, 3.9 and 2.7 nm for Ag/TiO_2-0.5h, Ag/TiO_2-1h, Ag/TiO_2-2h, and Ag/TiO_2-4h, respectively (see Table 4.5). For the Ag/TiO_2-0.5h catalyst, silver particle was large size probably because a short of time to reaction occurring for deposited silver on TiO_2-P25 support.
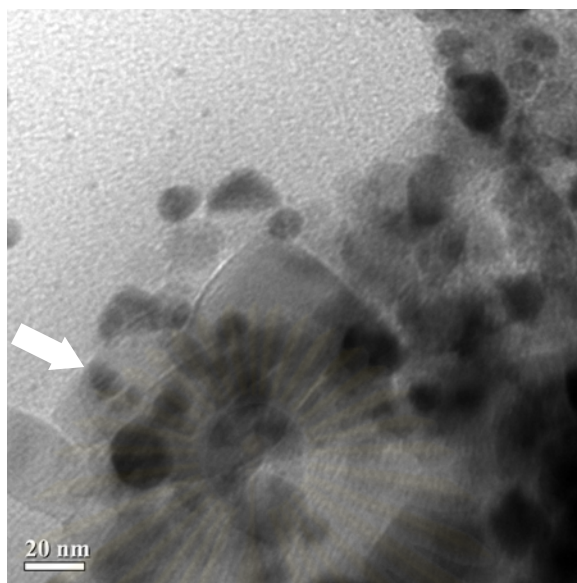
Figure 4.34 TEM image of Ag/TiO$_2$-0.5h catalyst. The scale bar is 20 nm.
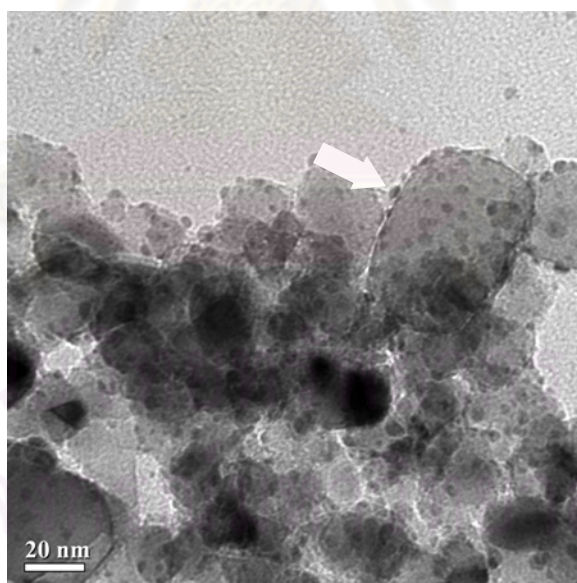
Figure 4.35 TEM image of Ag/TiO$_2$-1h catalyst. The scale bar is 20 nm.
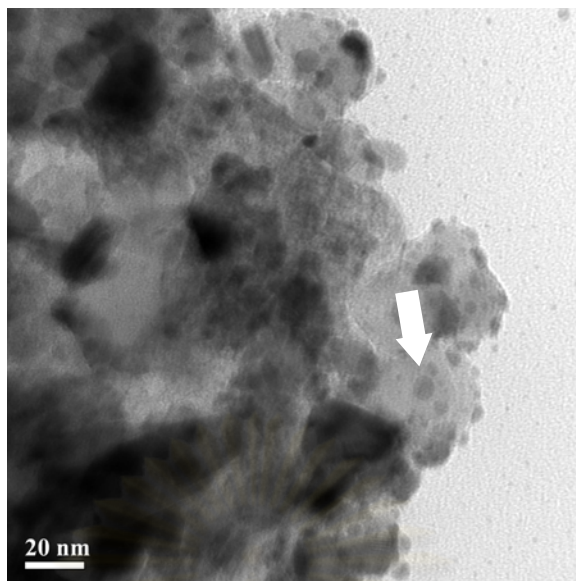
Figure 4.36   TEM image of Ag/TiO$_2$-2h catalyst. The scale bar is 20 nm.
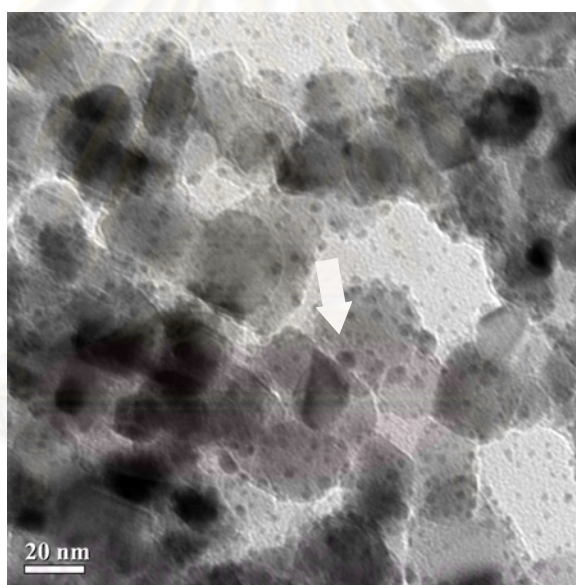
Figure 4.37   TEM image of Ag/TiO$_2$-4h catalyst. The scale bar is 20 nm.

4.5.3 Silver content in the supported silver catalysts

The amount of silver deposited on TiO$_2$-P25 support was measured by inductively-coupled plasma optical emission spectroscopy (ICP-OES). The results are listed in Table 4.5. The actual silver contents were 13.2, 13.2, 13.2, and 12.9 % for Ag/TiO$_2$-0.5h, Ag/TiO$_2$-1h, Ag/TiO$_2$-2h, and Ag/TiO$_2$-4h, respectively.

Table 4.5 Average particle size, standard deviation of silver and silver content on the supported silver catalysts that were prepared with different holding time

Catalysts	Average silver particle size (nm)*	Standard deviation of silver particle size (nm)	Actual silver content (%)**
Ag/TiO$_2$-0.5 h	5.8	2.3	13.2
Ag/TiO$_2$-1 h	2.8	0.8	13.2
Ag/TiO$_2$-2 h	3.9	1.2	13.2
Ag/TiO$_2$-4 h	2.7	0.9	12.9

*Estimated by TEM images

**Measurement by ICP-OES

4.5.4 X-ray photoelectron spectroscopy (XPS)

X-ray photoelectron spectroscopy (XPS) was performed to determine the oxidation state of silver species. The Ag 3d emission spectra for Ag/TiO$_2$ catalysts were shown in Figures 4.38, 4.39, 4.40, and 4.41 for Ag/TiO$_2$-0.5h, Ag/TiO$_2$-1h, Ag/TiO$_2$-2h, and Ag/TiO$_2$-4h, respectively. Figure 4.38 displays XPS Ag 3d spectra of Ag/TiO$_2$-0.5h catalyst. The XPS spectra possessed binding energies of Ag 3d level at 367.4 eV (Ag 3d$_{5/2}$), 368.7 eV (Ag 3d$_{5/2}$), and 374.8 eV (Ag 3d$_{3/2}$). Figure 4.39 displays XPS Ag 3d spectra of Ag/TiO$_2$-1h catalyst. The XPS spectra possessed binding energies of Ag 3d level at 366.6 eV (Ag 3d$_{5/2}$), 368.5 eV (Ag 3d$_{5/2}$), and 374.5 eV (Ag 3d$_{3/2}$). Figure 4.40 displays XPS Ag 3d spectra of Ag/TiO$_2$-2h catalyst. The XPS spectra possessed binding energies of Ag 3d level at 366.1 eV (Ag 3d$_{5/2}$), 368.9 eV (Ag 3d$_{5/2}$), and 374.9 eV (Ag 3d$_{3/2}$). Figure 4.41 displays XPS Ag 3d spectra of Ag/TiO$_2$-4h catalyst. The XPS spectra possessed binding energies of Ag 3d level at 367.0 eV (Ag 3d$_{5/2}$), 368.7 eV (Ag 3d$_{5/2}$), and 374.8 eV (Ag 3d$_{3/2}$). The binding energies were indicative silver form in Ag^0 and Ag$^+$.
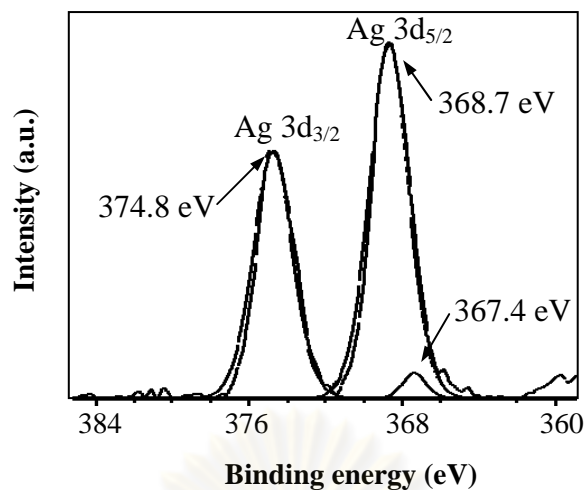
Figure 4.38 XPS spectra of Ag 3d level of Ag/TiO$_2$-0.5h catalyst
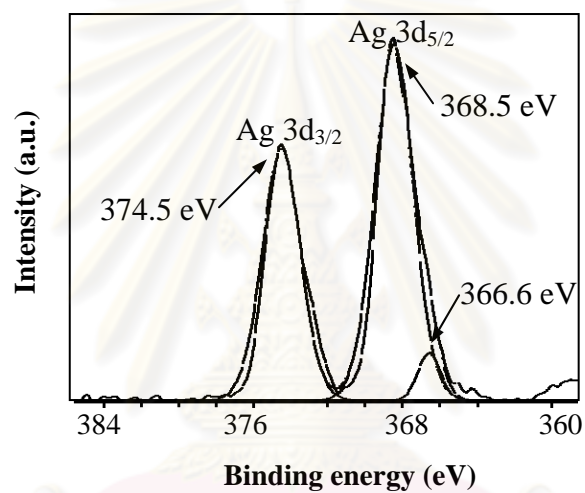
Figure 4.39 XPS spectra of Ag 3d level of Ag/TiO$_2$-1h catalyst
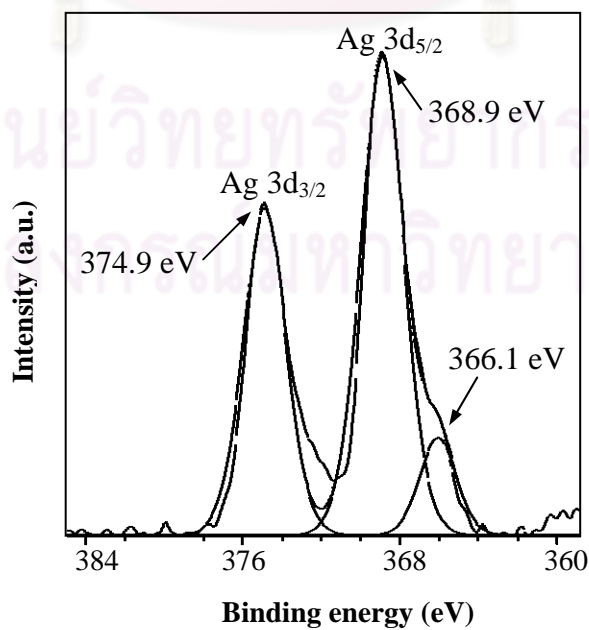
Figure 4.40 XPS spectra of Ag 3d level of Ag/TiO$_2$-2h catalyst
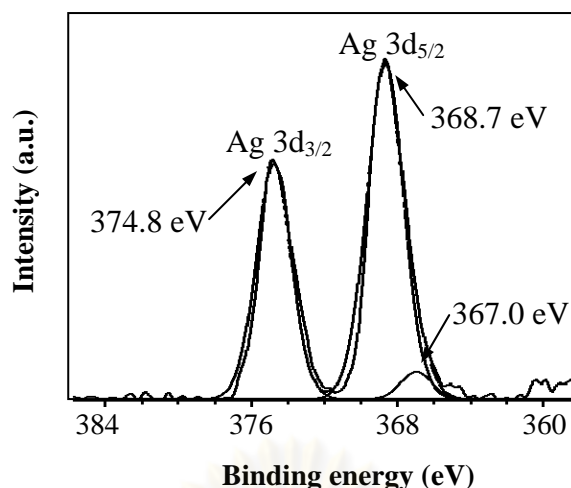
Figure 4.41 XPS spectra of Ag 3d level of Ag/TiO$_2$-4h catalyst

4.5.5 Catalytic activities of Ag/TiO$_2$ catalysts

The activities of Ag/TiO$_2$ catalysts were measured at a temperature ranging from 30°C to 140°C. The catalytic activities of catalysts as a function of a temperature displays in Figure 4.42. The T$_{50}$ were 96°C, 80°C, 90°C, and 87°C for Ag/TiO$_2$-0.5h, Ag/TiO$_2$-1h, Ag/TiO$_2$-2h, and Ag/TiO$_2$-4h, respectively. The activities of the catalysts were in the following order Ag/TiO$_2$-1 h > Ag/TiO$_2$-4 h $\cong$ Ag/TiO$_2$-2 h > Ag/TiO$_2$-0.5h. The catalytic activity appeared to be dependent on silver content.
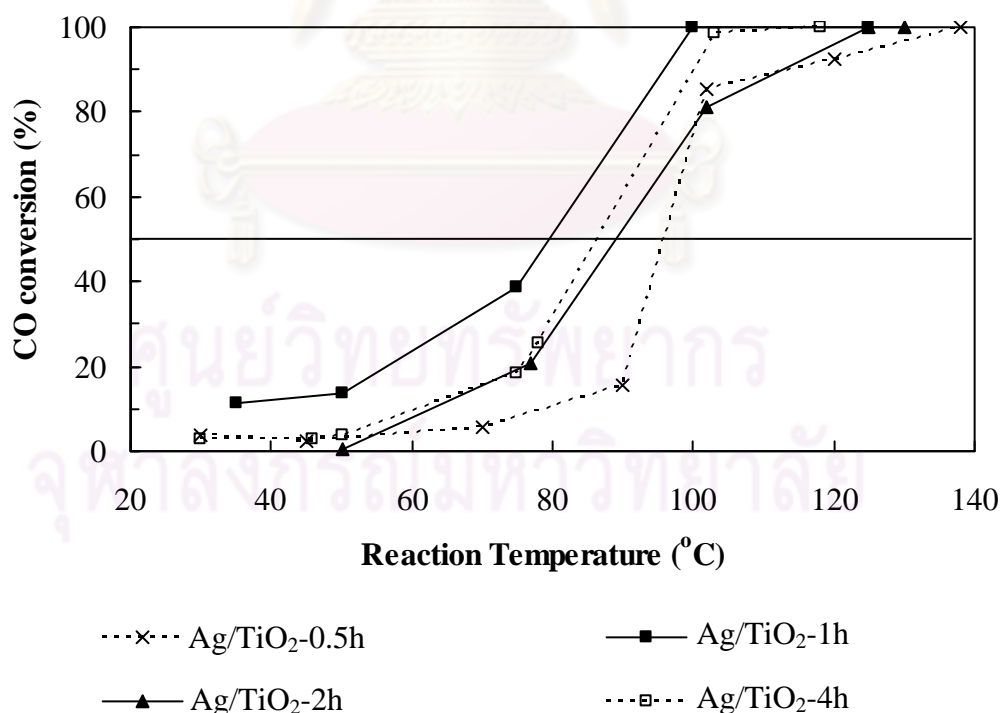
Figure 4.42 CO conversions as a function of a reaction temperature for Ag/TiO$_2$ catalysts that were prepared using supercritical CO$_2$ technique with different holding time

4.6 Comparative study on support to catalytic activity

4.6.1 The phase structure and specific surface area

The phase structure of catalysts was determined using XRD technique. The XRD patterns of supported silver catalysts with different TiO_2 support were shown in Figure 4.43 (a) and (c) for TiO_2-P25 and TiO_2-ST, respectively. For TiO_2-P25 support were shown XRD diffraction peaks at 2θ of 25.3°, 37.8°, 48.1°, 54.0°, 55.2°, 62.8°, 68.0°, 72.0°, and 76.1°, corresponding to titanium dioxide anatase phase and diffraction peaks at 2θ of 27.5°, 36.1°, and 41.4°, corresponding to titanium dioxide rutile phase. However, TiO_2-ST support (see Figure 4.43 (c)) was shown only anatase phase. Figure 4.43 (b) displays XRD patterns of Ag/TiO_2-P25 catalyst, the XRD patterns possessed diffraction peaks at 2θ of 25.3°, 37.8°, 48.1°, 54.0°, 55.2°, 62.8°, 68.0°, 72.0°, and 76.1°, corresponding to titanium dioxide anatase phase, diffraction peaks at 2θ of 27.5°, 36.1°, and 41.4°, corresponding to titanium dioxide rutile phase. The diffraction peak at 2θ of 24.3°, corresponding to Ag_2O, diffraction peak at 2θ of 43.4°, corresponding to Ag, and diffraction peaks at 2θ of 21.6°, 29.6°, 31.9°, and 32.8°, corresponding to Ag_2CO_3. For Ag/TiO_2-ST catalyst, XRD diffraction pattern was shown in Figure 4.43 (d). The XRD patterns possessed the diffraction peaks at 2θ of 25.3°, 37.8°, 48.1°, 54.0°, 55.2°, 62.8°, 68.0°, 72.0°, and 76.1°, corresponding to titanium dioxide anatase phase, while the diffraction peak of Ag_2O was shown at 2θ of 24.3°, diffraction peak at 2θ of 43.4°, corresponding to Ag, and diffraction peaks at 2θ of 21.6°, 29.6°, 31.9°, and 32.8°, corresponding to Ag_2CO_3. The crystallite sizes of TiO_2 anatase phase of TiO_2-ST support was 11.8 nm (Calculated from the Scherrer equation). Specific surface areas of the TiO_2-P25 and TiO_2-ST support were 41 and 72 m^2/g, respectively. The Ag/TiO_2-P25 and Ag/TiO_2-ST catalysts had specific surface areas were 18 and 51 m^2/g, respectively.
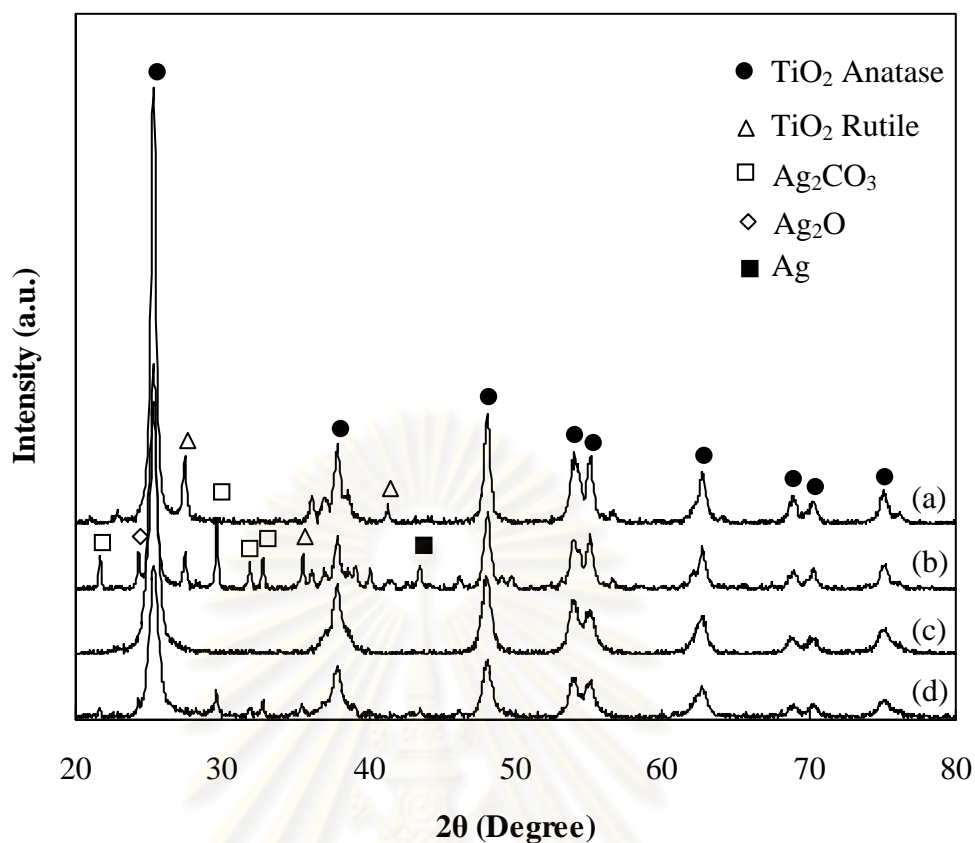
Figure 4.43   XRD patterns of (a) TiO_2-P25 and (c) TiO_2-ST support and Ag/TiO_2 catalysts prepared using supercritical CO_2 technique with different type of TiO_2 support (b) Ag/TiO_2-P25 and (d) Ag/TiO_2-ST catalyst

4.6.2 Transmission electron microscopy (TEM)

The transmission electron microscopy (TEM) was employed to determine the particle sizes distribution of silver on TiO_2. The TEM image of TiO_2-P25 was shown in Figure 4.2. Figures 4.44 and 4.45, and 4.46 were TEM images of TiO_2-ST, Ag/TiO_2-ST, and Ag/TiO_2-P25, respectively. From the TEM image of TiO_2-ST support (see Figure 4.44) was the average TiO_2 particles size about 11.7 nm. (see Appendix B). The TEM images of Ag/TiO_2-ST and Ag/TiO_2-P25 catalysts were shown in Figures 4.45 and 4.46. TEM images shown silver particle sizes were uniform and well dispersed on TiO_2 support. The silver particles size were 3.0 and 2.8 nm for Ag/TiO_2-ST and Ag/TiO_2-P25, respectively (see Table 4.6).
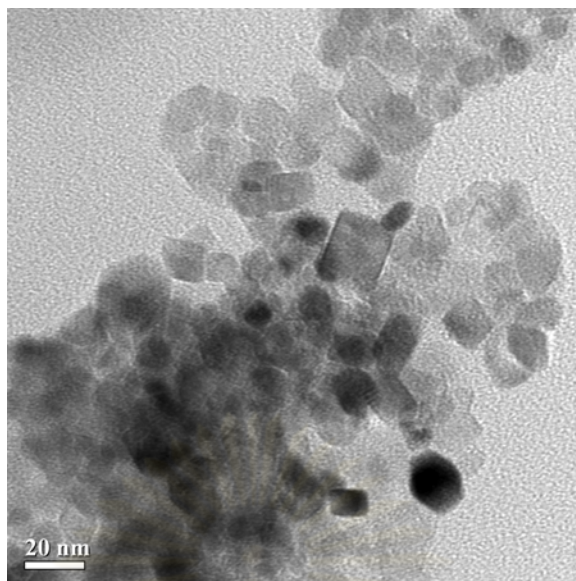
Figure 4.44 TEM image of TiO$_2$-ST support. The scale bar is 20 nm.
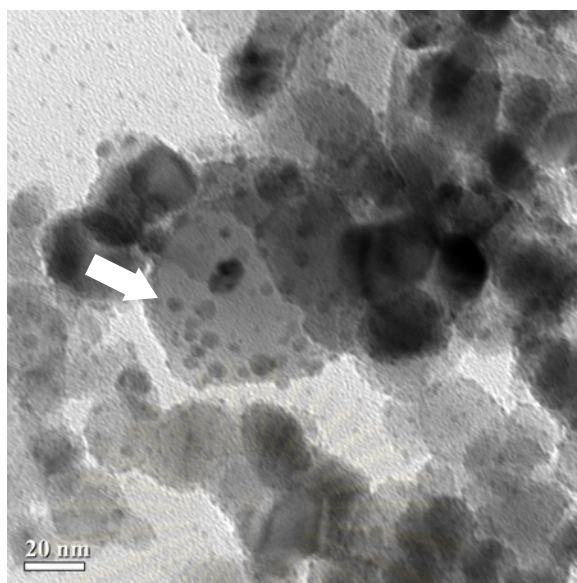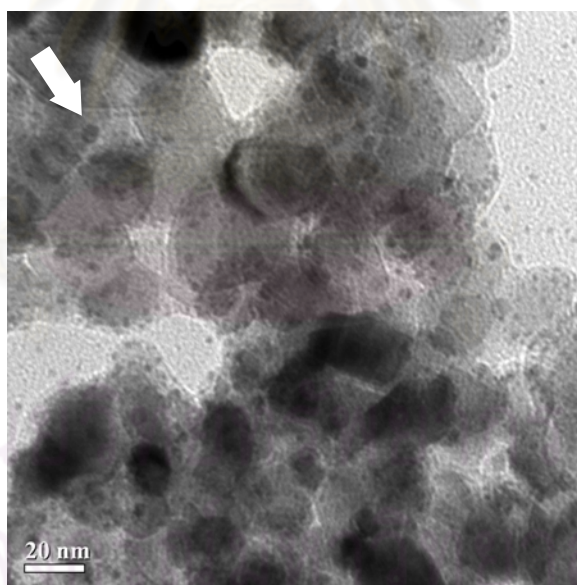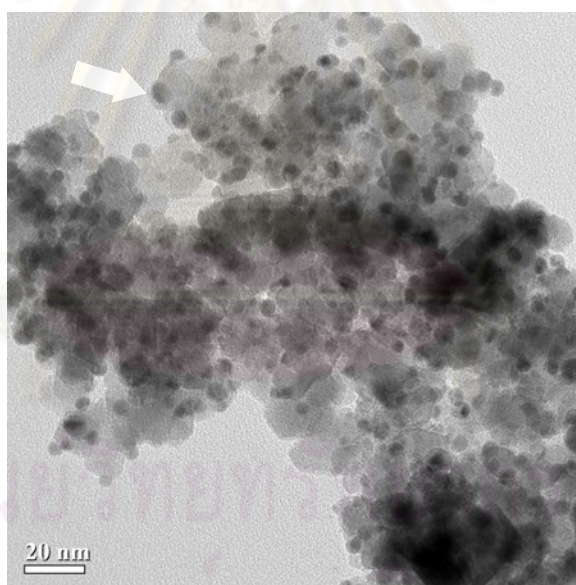

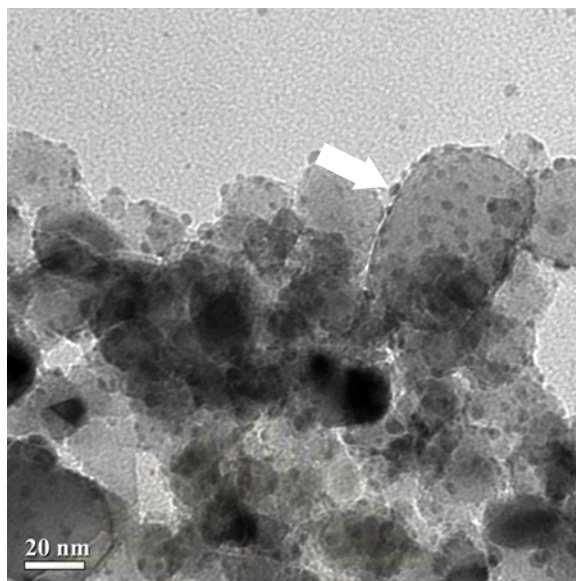**Figure 4.45** TEM image of Ag/TiO$_2$-ST catalyst. The scale bar is 20 nm.
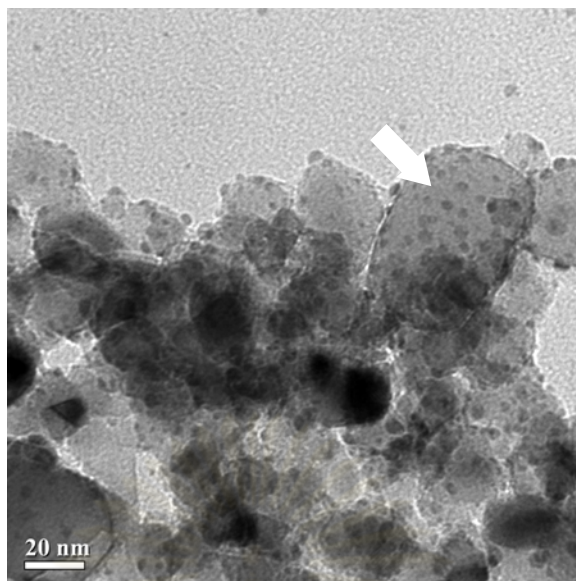
Figure 4.46   TEM image of Ag/TiO$_2$-P25 catalyst. The scale bar is 20 nm.

Table 4.6   Average particle size, standard deviation of silver and silver content on the supported silver catalysts that were prepared with different type of TiO$_2$ support

Catalysts	Average silver particle size (nm)*	Standard deviation of silver particle size (nm)	Actual silver content (%) **
Ag/TiO$_2$-ST	3.0	0.9	13.4
Ag/TiO$_2$-P25	2.8	0.8	13.2

*Estimated by TEM images

**Measurement by ICP-OES

4.6.3 Silver content in the supported silver catalysts

The amount of silver deposited on the TiO$_2$ support was measured by inductively-coupled plasma optical emission spectroscopy (ICP-OES). The results were listed in Table 4.6. The actual silver contents were 13.4 and 13.2 % for Ag/TiO$_2$-ST and Ag/TiO$_2$-P25, respectively.

4.6.4 X-ray photoelectron spectroscopy (XPS)

X-ray photoelectron spectroscopy (XPS) was performed to determine the oxidation state of silver species. The Ag 3d emission spectra for Ag/TiO$_2$-ST and Ag/TiO$_2$-P25 catalysts were shown in Figures 4.47 and 4.48, respectively. Figure 4.47 displays XPS Ag 3d spectra of Ag/TiO$_2$-ST catalyst. The XPS spectra possessed binding energies of Ag 3d level at 366.4 eV (Ag 3d$_{5/2}$), 368.9 eV (Ag 3d$_{5/2}$), and 374.8 eV (Ag 3d$_{3/2}$). Figure 4.48 displays XPS Ag 3d spectra of Ag/TiO$_2$-P25 catalyst. The XPS spectra possessed binding energies of Ag 3d level at 366.6 eV (Ag 3d$_{5/2}$), 368.5 eV (Ag 3d$_{5/2}$), and 374.5 eV (Ag 3d$_{3/2}$). The binding energies were indicative silver form in Ag^0 and Ag$^+$.
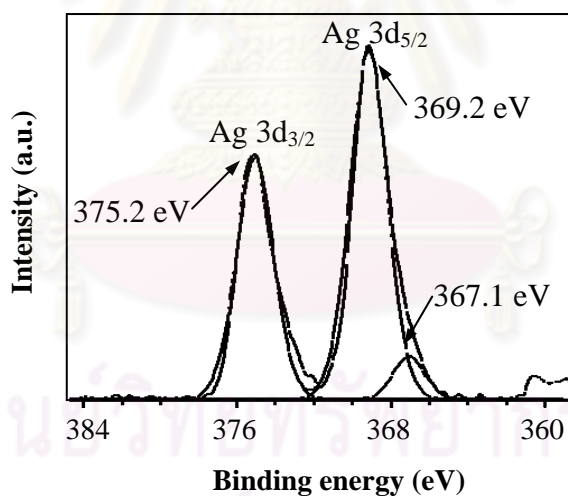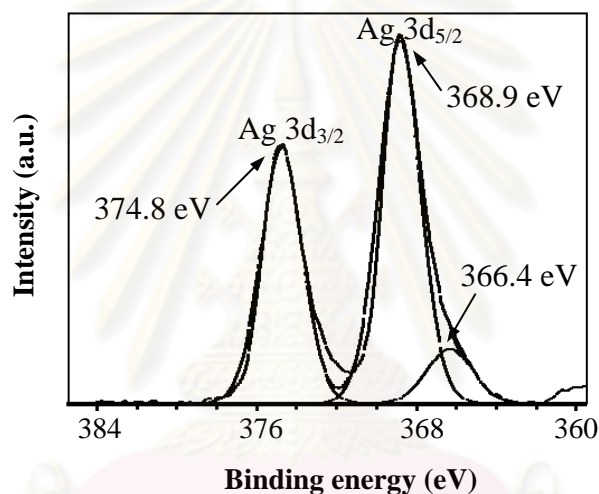

Figure 4.47 XPS spectra of Ag 3d level of Ag/TiO$_2$-ST catalyst
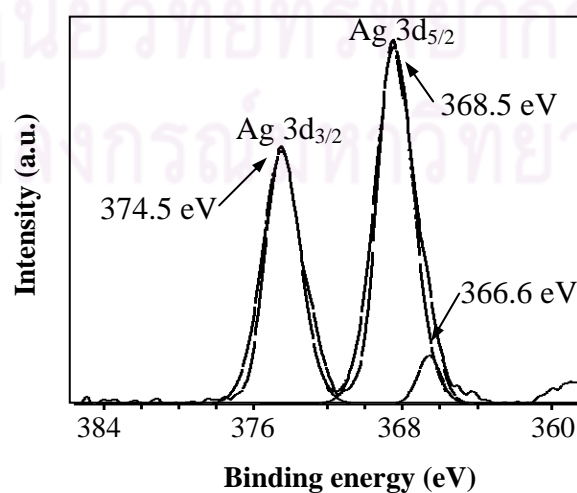
Figure 4.48 XPS spectra of Ag 3d level of Ag/TiO$_2$-P25 catalyst

4.6.5 Catalytic activities of Ag/TiO$_2$ catalysts

The activities of Ag/TiO$_2$ catalysts were measured at a temperature ranging from 30 ^{o}C to 150 ^{o}C. The catalytic activities of catalysts as a function of a temperature displays in Figure 4.49. The T$_{50}$ were 72°C and 80°C for Ag/TiO$_2$-ST and Ag/TiO$_2$-P25, respectively. The Ag/TiO$_2$-ST catalyst was more active than Ag/TiO$_2$-P25 catalyst. The catalytic activities appeared to be dependent on particle silver size or phase of titanium dioxide or specific surface area.
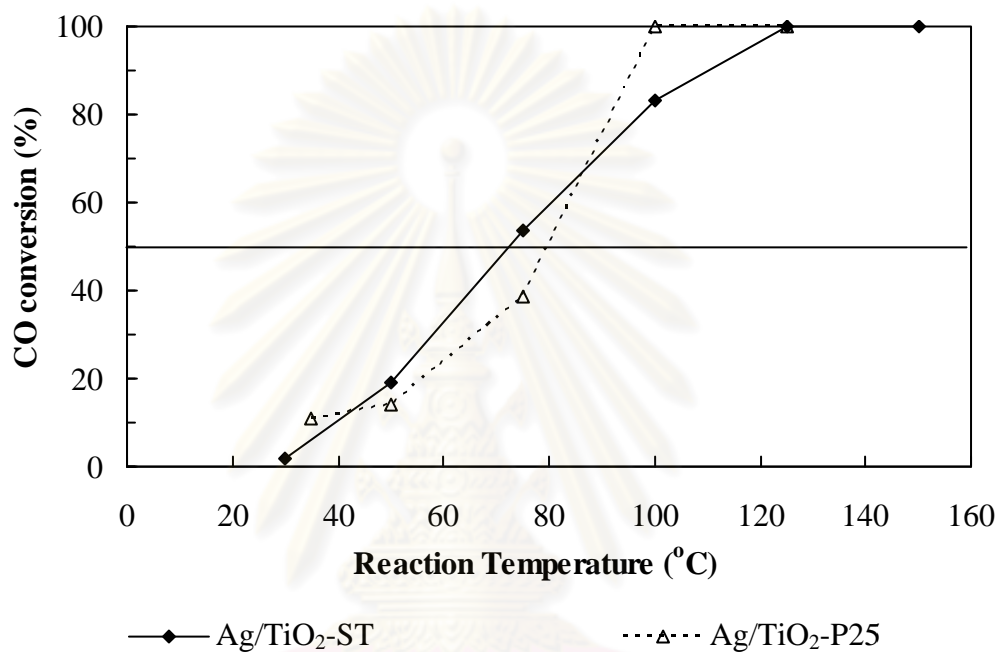
Figure 4.49 CO conversions as a function of a reaction temperature for Ag/TiO$_2$-ST and Ag/TiO$_2$-P25 catalyst

CHAPTER V

CONCLUSIONS AND RECOMMENDATIONS

5.1 Conclusions

5.1.1 Supported gold catalysts

In this part study, properties of Au/TiO_2 catalyst prepared by the deposition precipitation method and the deposition using supercritical CO_2 technique were investigated. The conclusions of the study are summarized as followed:

1. Au/TiO_2 catalysts that were prepared by the deposition precipitation method exhibited higher activities for CO oxidation than the catalyst prepared by the deposition using supercritical CO_2 due to smaller particle size of gold on support.

2. Catalytic activities for CO oxidation were dependent on gold particle size and gold content in catalyst.

5.1.2 Supported silver catalysts

In this part study, properties of Ag/TiO_2 catalysts prepared by the deposition using supercritical CO_2 technique were investigated. The conclusions of the study are summarized as followed:

1. The deposition of silver nanoparticles on titanium dioxide by using supercritical CO_2 as solvent had silver particles size ranging of 2 to 6 nm.

2. Catalytic activities for CO oxidation depended on silver particle size and silver content in catalyst.

3. The lowest light off temperature was obtained for the catalyst that was prepared with a 20 wt% of silver, pressure CO_2 was 20 MPa, holding time of 1 hour, and TiO_2 support prepared by solvothermal method.

5.2 Recommendation for future studies

1. Employ Ag/TiO_2 catalyst in other reactions such as selective oxidation of CO in excess hydrogen or CO hydrogenation.

2. Investigate the deposition of other metal on the support by using supercritical CO_2.

REFERENCES

Al-Sayari, S., Carley, A. F., Taylor, S. H., and Hutching, G. J. Au/ZnO and Au/Fe$_2$O$_3$ Catalysts for CO Oxidation at Ambient Temperature: Comments on the Effect of Synthesis Conditions on the Preparation of High Activity Catalysts Prepared by Coprecipitation. Topic in Catalysis 44, 1-2 (2007): 123-128.

Boccuzzi, F., Chiorino, A., Manzoli, M., Andreeva, D., Tabakova, T., Ilieva, L., and Iadakiev, V. Gold, Silver, and Copper Catalysts Supported on TiO$_2$ for Pure Hydrogen Production. Catalysis Today 75 (2002): 169-175.

Bond, G. C., Louis, C., and Thomson, D. T. Catalysis by Gold 1st ed. Singapore: Imperial College Press, 2006.

Buakaew, P. Photooxidation of Ethylene over Gold Deposited Titanium Dioxide. Master's Thesis, Department of Chemical Engineering, Faculty of Engineering, Chulalongkorn University, 2005.

Cabanas, A., Long, D. P., and Watkins, J. J. Deposition of Gold Film and Nanostructures from Supercritical Carbon Dioxide. Chemistry of Materials 16 (2004): 2028-2033.

Chang, L., Sasirekha, N., Rajesh, B., and Chen, Y. CO Oxidation on Ceria- and Manganese Oxide-Supported Gold Catalysts. Separation and Purification Technology 58 (2007): 211-218.

Chatterjee, M., Ikushima, Y., Hakuta, Y., and Kawanami, H. In Situ Synthesis of Gold Nanoparticles Inside the Pores of MCM-48 in Supercritical Carbon Dioxide and Its Catalytic Application. Advanced Synthesis and Catalysis 348 (2006): 1580-1590.

Chen, L., Ma, D., Li, X., and Bao, X. Silver Catalysts Supported over Activated Carbons for the Selective Oxidation of CO in Excess Hydrogen: Effects of Different Treatments on the Supports. Catalysis Letters 111, 3-4 (2006): 133-139.

Date, M. and Haruta, M. Moisture Effect on CO Oxidation over Au/TiO$_2$ Catalyst. Journal of Catalysis 201 (2001): 221-224.

Date, M., Ichihashi, Y., Chiorino, A., Boccuzzi, F., and Haruta, M. Performance of Au/TiO$_2$ Catalyst under Ambient Conditions. Catalysis Today 72 (2002): 89-94.

Date, M., Imai H., Tsubota S., and Haruta, M. *In situ* Measurements under Flow Condition of the CO Oxidation over Supported Gold Nanoparticles. Catalysis Today 122 (2007): 222-225.

Denkwitz, Y., Zhao, Z., Hormann, U., Kaiser, U., Plzak, V., and Behm, R. J. Stability and Deactivation of Unconditioned Au/TiO_2 Catalyst during CO Oxidation in a Near-Stoichiometric and O_2-Rich Reaction Atmosphere. Journal of Catalysis 251 (2007): 363-373.

Frey, K., Iablokov, V., Melaet, G., Guczi, L., and Kruse, N. CO Oxidation Activity of Ag/TiO_2 Catalysts Prepared via Oxalate Co-Precipitation. Catalysis Letters 124 (2008): 74-79.

Gac, W., Derylo-Marczewska, A., Pasieczna-Patkowska, S., Popivnyak, N., and Zukocinski, G. The Influence of the Preparation Methods and Pretreatment Conditions on the Properties of Ag-MCM-41 Catalysts. Journal of Molecular Catalysis A: Chemical 268 (2007): 15-23.

Ge, L., Xu, M., and Fang, H. Preparation and Characterization of Silver and Indium Vanadate Co-Doped TiO_2 Thin Films as Visible-Light-Activated Photocatalyst. Journal of Sol-Gel Science and Technology 40 (2006): 65-73.

Grassian, V. H. Environmental Catalysis. 1st ed. Florida: Taylor and Francis CRC Press, 2005: 613-618.

Haruta, M. Size- and Support-Dependency in the Catalysis of Gold. Catalysis Today 36 (1997): 153-166.

Haruta, M. When Gold is not Noble: Catalysis by Nanoparticles. Chemical Record 3 (2003): 75-87.

Haruta, M. Gold as a Novel Catalyst in the 21st Century: Preparation, Working Mechanism and Applications. Gold Bulletin 37, 1-2 (2004): 27-36.

Ho, K.Y. and Yeung, K.L. Effects of Ozone Pretreatment on the Performance of Au/TiO_2 Catalyst for CO Oxidation Reaction. Journal of Catalysis 242 (2006): 131-141.

Iliopoulou, E.F., Evdou, A.P., Lemonidou, A.A., and Vasalos, I.A. Ag/Alumina Catalysts for the Selective Catalytic Reduction of NOx using Various Reductants. Applied Catalysis A: General 274 (2004): 179-189.

Imamura, S., Yamada, H., and Utani, K. Combustion Activity of Ag/CeO_2 Composite Catalyst. Applied Catalysis A: General 192 (2000): 221-226.

Jiao, J., Xu, Q., and Li, L. Porous TiO_2/SiO_2 Composite Prepared using PEG as Template Direction Reagent with Assistance of Supercritical CO_2. Journal of Colloid and Interface Science 316 (2007): 596-603.

Jin, L., Qian, K., Jiang, Z., and Huang, W. Ag/SiO_2 Catalysts Prepared via γ-Ray Irradiation and their Catalytic Activities in CO Oxidation. Journal of Molecular Catalysis A: Chemical 274 (2007): 95-100.

Kato, S., Hirano, Y., Iwata, M., Sano, T., Takeuchib, K., and Matsuzawa, S. Photocatalytic Degradation of Gaseous Sulfur Compounds by Silver-Deposited Titanium Dioxide. Applied Catalysis B: Environmental 57 (2005): 109-115.

Kubacka, A., Ferrer, M., Martínez-Arias, A., and Fernández-Gacía, M., Ag Promotion of TiO_2-Anatase Disinfection Capability: Study of *Escherichia Coli* Inactivation. Applied Catalysis B: Environmental 84 (2008): 87-93.

Landon, P., Collier, P.J., Papworth, A.J., Kiely, C.J., and Hutchings G.J. Direct Formation of Hydrogen Peroxide from H_2/O_2 using a Gold Catalyst. Chemical Communications (2002): 2058-2059.

Li, H., Duan, X., Liu, G., and Liu, X. Photochemical Synthesis and Characterization of Ag/TiO_2 Nanotube Composites. Journal of Materials Science 43 (2008): 1669-1676.

Lippits, M.J., Gluhoi, A.C., and Nieuwenhuys, B.E. A Comparative Study of the Effect of Addition of CeO_x and Li_2O on γ-Al_2O_3 Supported Copper, Silver, and Gold Catalysts in the Preferential Oxidation of CO. Topic in Catalysis 44, 1-2 (2007): 159-165.

Mallick, K. and Scurrell, M. S. CO Oxidation over Gold Nanoparticles Supported on TiO_2 and TiO_2-ZnO: Catalytic Activity Effects due to Surface Modification of TiO_2 with ZnO. Applied Catalysis A: General 253 (2003): 527-536.

Marr, R. and Gamse, T. Use of Supercritical Fluids for Different Processes Including New Developments: a Review. Chemical Engineering and Processing 39 (2000): 19-28.

Min, B. K. and Friend, C. M. Heterogeneous Gold-Based Catalysis for Green Chemistry: Low-Temperature CO Oxidation and Propene Oxidation. Chemical Reviews 107 (2007): 2709-2724.

Moreau, F. and Bond, G.C. CO Oxidation Activity of Gold Catalysts Supported on Various Oxides and their Improvement by Inclusion of an Iron Component. Catalysis Today 114 (2006): 362-368.

Moreau, F. and Bond, G.C. Influence of the Surface Area of the Support on the Activity of Gold Catalysts for CO oxidation. Catalysis Today 122 (2007): 215-221.

Moreau, F. and Bond, G.C. Preparation and Reactivation of Au/TiO_2 Catalysts. Catalysis Today 122 (2007): 260-265.

Pillai, U.R. and Deevi, S. Highly Active Gold-Ceria Catalyst for the Room Temperature Oxidation of Carbon Monoxide. Applied Catalysis A: General 299 (2006): 266-273.

Qu, Z., Huang, W., Cheng, M., Dong, X., and Bao, X. CO Selective Oxidation in H_2-Rich Gas over Ag Nanoparticles-Effect of Oxygen Treatment Temperature on the Activity of Silver Particles Mechanically Mixed with SiO_2. Catalysis Today 93–95 (2004): 247-255.

Qu, Z., Huang, W., Cheng, M., Shi, C., and Bao, X. Low-temperature Selective Oxidation of CO in H_2-Rich Gases over Ag/SiO_2 Catalysts. Journal of Molecular Catalysis A: Chemical 239 (2005): 22-31.

Qu, Z., Huang, W., Zhou, S., Zheng, H., Liu, X., Cheng, M., and Bao, X. Enhancement of the Catalytic Performance of Supported-metal Catalysts by Pretreatment of the Support. Journal of Catalysis 234 (2005): 33-36.

Russo, N., Fino, D., Saracco, G., and Specchia, V. Supported Gold Catalysts for CO Oxidation. Catalysis Today 117 (2006):214-219.

Sakurai, H., Ueda, A., Kobayashi, T., and M. Haruta. Low-Temperature Water–Gas Shift Reaction over Gold Deposited on TiO_2. Chemical Communications (1997): 271-272.

Sandoval, A., Gomez-Cortes, A., Zanella, R., Diaz, G., and Saniger, J.M. Gold Nanoparticles: Supported effects for the WGS reaction. Journal of Molecular Catalysis A: Chemical 278 (2007): 200-208.

Sarkany, A. Electroless Deposition of Au on Ag Sol: Oxidation of Carbon Monoxide and Methanol. Colloids and Surfaces A: Physicochem. Eng. Aspects 269 (2005): 67–71.

Sharma, V.K., Yngard, R.A., and Lin, Y. Silver Nanoparticles: Green Synthesis and their Antimicrobial Activities. Advances in Colloid and Interface Science 145, 1-2 (2009): 83-96.

Souza, K.R., Lima, A.F., Sousa, F.F., and Appel, L.G. Preparing Au/ZnO by Precipitation-Deposition Technique. Applied Catalysis A: General 340 (2008): 133-139.

Stangland, E. E., Stavens, K. B., Andres, R. P., and Delgass, W. N. Characterization of Gold–Titania Catalysts via Oxidation of Propylene to Propylene Oxide. Journal of Catalysis 191 (2000): 332-347.

Tada, H., Ishida, T., Takao, A., Ito, S., Mukhopadhyay, S., Akita, T., Tanaka, K., and Kobayashi, H. Kinetic and DFT Studies on the Ag/TiO_2-Photocatalyzed Selective Reduction of Nitrobenzene to Aniline. ChemPhysChem 6 (2005): 1537-1543.

Tai, Y., Murakami, J., Tajiri, K., Ohashi, F., Date, M., and Tsubota, S. Oxidation of Carbon Monoxide on Au Nanoparticles in Titania and Titania-Coated Silica Aerogel. Applied Catalysis A: General 268 (2004): 183-187.

Tang, Z., Edwards, J. K., Bartley, J. K., Taylor, S. H., Carley, A. F., Herzing, A. A., Kiely, C. J., and Hutchings, G. J. Nanocrystalline Cerium Oxide Produced by Supercritical Antisolvent Precipitation as a Support for High-Activity Gold Catalysts. Journal of Catalysis 249 (2007): 208-219.

Tian, D., Yong, G., Dai, Y., Yan, X., and Liu, X. CO Oxidation Catalyzed by Ag/SBA-15 Catalysts Prepared via *In situ* Reduction: The Influence of Reducing Agents. Catalysis Letter (2009): Article in Press.

Wattanamalachai, S. Preparation of Cu/ZnO and Cu/TiO_2 Catalysts via Deposition Technique using Supercritical Carbon Dioxide. Master's Thesis, Department of Chemical Engineering, Faculty of Engineering, Chulalongkorn University, 2006.

Wong, B., Yoda, S., and Howdle, S. M. The Preparation of Gold Nanoparticle Composites using Supercritical Carbon Dioxide. Journal of Supercritical Fluid 42 (2007): 282-287.

Yoda, S., Ohtake, K., Takebayashi, Y., Sugeta, T., and Sako, T. Preparation of SiO_2-TiO_2 Aerogels using Supercritical Impregnation. Journal of Sol-Gel Science and Technology 19 (2000): 719-723.

Xu, R., Wang, X., Wang, D., Zhou, K., and Li, Y. Surface Structure Effects in Nanocrystal MnO_2 and Ag/MnO_2 Catalytic Oxidation of CO. <u>Journal of Catalysis</u> 237 (2006): 426-430.

Zhang, X., Shi, H., and Xu, B-Q. Comparative Study of Au/ZrO_2 Catalysts in CO Oxidation and 1,3-Butadiene Hydrogenation. <u>Catalysis Today</u> 122 (2007): 330-337.

APPENDICES

APPENDIX A

CALCULATION OF THE CRYSTALLITE SIZE

Calculation of the crystallite size by Debye-Scherrer equation

The crystallite size was calculated from the width at half-height of the diffraction peak of XRD pattern using the Debye-Scherrer equation.

From Scherrer equation:

$$D = \frac{K\lambda}{\beta \cos \theta} \qquad (A1)$$

where D = Crystallite size, Å

K = Crystallite-shape factor = 0.9

λ = X-ray wavelength, 1.5418 Å for CuKα

θ =   Observed peak angle, degree

β = X-ray diffraction broadening, radian

The X-ray diffraction broadening (β) is the corrected width of powder diffraction free from all broadening due to the instrument. The α-Alumina was used as a standard sample to provide instrumental broadening data (see Figure A.2). The most common correction for the X-ray diffraction broadening (β) can be obtained by using the Warren formula.

From Warren's formula:

$$\beta = \sqrt{B_M^2 - B_S^2} \qquad (A2)$$

Where B_M = The measured peak width in radians at half peak height.

B_S =   The corresponding width of a standard material.

Example: Calculation of the crystallite size of gold of Au/TiO$_2$-Water catalyst
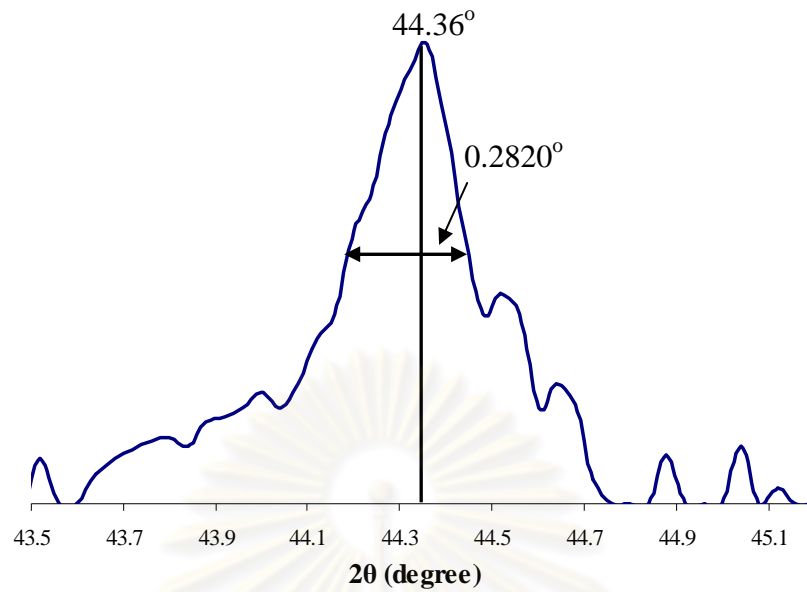
Figure A.1 The 200 diffraction peak of gold for calculation of the crystalline size

An interesting diffraction peak is the (200) plane occurred at the 2θ of 44.36^o

The half-height width of (200) diffraction peak $\quad= 0.2820^o$

$\qquad\qquad\qquad\qquad\qquad\qquad\qquad\qquad = (2\pi \times 0.2820)/360$

$\qquad\qquad\qquad\qquad\qquad\qquad\qquad\qquad = 0.0049 \quad \text{radian}$

The corresponding half-height width of peak of α-alumina $\quad = 0.0044$ radian

The broadening, $\beta = \sqrt{B_M^2 - B_S^2}$

$\qquad\qquad = \sqrt{0.0049^2 - 0.0044^2}$

$\qquad\qquad = 0.0022$ radian

$\beta \quad = \quad 0.0022$ radian

$2\theta \quad = \quad 44.36^o$

$\theta \quad = \quad 22.18^o$

$\lambda \quad = \quad 1.5418$ Å

The crystallite size $\quad = \quad \dfrac{0.9 \times 1.5418}{0.0022 \times \cos 22.18} \quad = \quad 681.1$ Å

$\qquad\qquad\qquad\qquad = \quad 68.11$ nm

The plot shows the x-axis labeled "2θ (degree)" and y-axis labeled "Bs (radian)". The fitted curve equation:

$$y = 6E\text{-}07x^2 - 1E\text{-}05x + 0.0037$$
$$R^2 = 0.9989$$
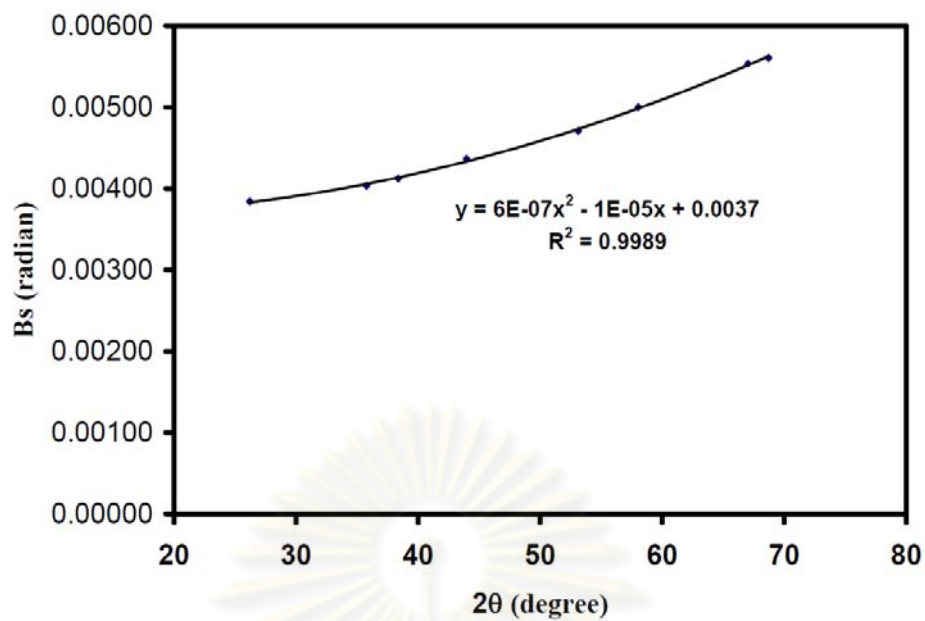
Figure A.2   The plot indicating the value of line broadening due to the equipment. The data were obtained by using α-alumina as a standard

APPENDIX B

PARTICLE SIZES DISTRIBUTION
AND CALCULATION OF TEM RESULTS

Particle sizes distribution of titanium dioxide

The particle sizes distribution of TiO_2-ST was shown in Table B1.

Table B1   Particle sizes of TiO_2-ST

No.	Particle sizes (nm)	No.	Particle sizes (nm)	No.	Particle sizes (nm)
1	8.15	26	10.26	51	11.17
2	8.45	27	10.26	52	11.18
3	8.69	28	10.34	53	11.24
4	9.02	29	10.34	54	11.26
5	9.06	30	10.34	55	11.27
6	9.07	31	10.34	56	11.33
7	9.07	32	10.38	57	11.35
8	9.07	33	10.38	58	11.37
9	9.09	34	10.41	59	11.39
10	9.18	35	10.47	60	11.39
11	9.25	36	10.54	61	11.46
12	9.32	37	10.55	62	11.53
13	9.41	38	10.57	63	11.61
14	9.41	39	10.59	64	11.69
15	9.57	40	10.62	65	11.74
16	9.66	41	10.63	66	11.77
17	9.75	42	10.70	67	11.80
18	9.75	43	10.73	68	11.80
19	9.86	44	10.78	69	11.82
20	9.97	45	10.81	70	11.92
21	9.99	46	10.88	71	11.95
22	10.01	47	10.96	72	12.05
23	10.01	48	10.96	73	12.06
24	10.10	49	11.09	74	12.15
25	10.22	50	11.14	75	12.16

Table B1   Particle sizes of TiO_2-ST (Cont.)

No.	Particle sizes (nm)	No.	Particle sizes (nm)	No.	Particle sizes (nm)
76	12.16	90	13.20	104	14.60
77	12.16	91	13.23	105	15.05
78	12.23	92	13.30	106	15.14
79	12.33	93	13.31	107	15.15
80	12.35	94	13.47	108	15.30
81	12.44	95	13.49	109	15.91
82	12.54	96	13.59	110	16.30
83	12.58	97	13.59	111	16.32
84	12.63	98	13.65	112	16.42
85	12.73	99	13.71	113	16.55
86	12.97	100	13.74	114	16.78
87	13.14	101	13.80	115	16.95
88	13.14	102	14.25		
89	13.14	103	14.35		

Average particle sizes = 11.7 nm

Standard deviation   = 2.0   nm
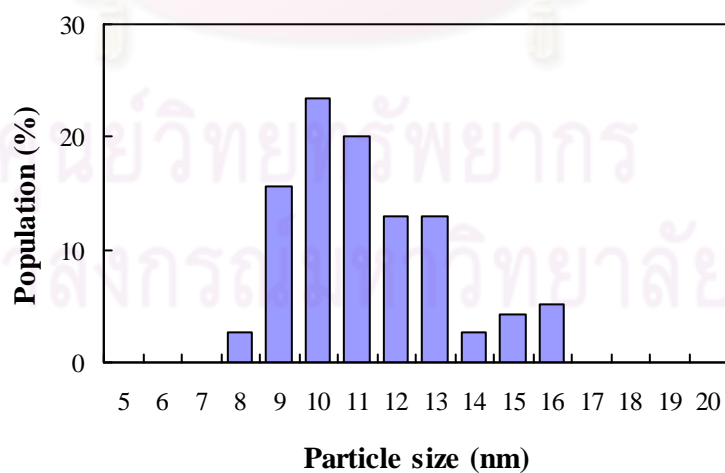
Figure B.1   Particle sizes distribution of TiO_2-ST

Particle sizes distribution of gold nanoparticles of Au/TiO$_2$ catalysts that were prepared by deposition precipitation method

The particle sizes distributions of gold nanoparticles are shown in Table B2 to B4 for Au/TiO$_2$-pH6, Au/TiO$_2$-pH7, and Au/TiO$_2$-pH8, respectively.

Table B2 Gold particle sizes of Au/TiO$_2$-pH6 catalyst

No.	Particle sizes (nm)	No.	Particle sizes (nm)	No.	Particle sizes (nm)
1	2.84	31	6.14	61	7.63
2	3.29	32	6.23	62	7.64
3	3.57	33	6.46	63	7.72
4	3.67	34	6.49	64	7.74
5	4.01	35	6.52	65	7.77
6	4.06	36	6.59	66	7.77
7	4.22	37	6.59	67	7.90
8	4.49	38	6.61	68	8.07
9	4.58	39	6.62	69	8.20
10	4.61	40	6.67	70	8.24
11	4.65	41	6.69	71	8.32
12	4.87	42	6.78	72	8.38
13	5.00	43	6.84	73	8.38
14	5.02	44	6.84	74	8.47
15	5.08	45	6.88	75	8.49
16	5.10	46	6.89	76	8.51
17	5.18	47	6.92	77	8.68
18	5.20	48	6.95	78	8.79
19	5.21	49	7.02	79	8.92
20	5.31	50	7.09	80	9.15
21	5.46	51	7.09	81	9.37
22	5.68	52	7.10	82	9.41
23	5.88	53	7.26	83	9.53
24	5.88	54	7.46	84	9.66
25	5.93	55	7.49	85	9.75
26	6.01	56	7.52	86	10.47
27	6.06	57	7.54	87	11.43
28	6.07	58	7.55	88	11.59
29	6.11	59	7.59	89	11.64
30	6.11	60	7.59	90	11.66

Table B2 Gold particle sizes of Au/TiO$_2$-pH6 catalyst (Cont.)

No.	Particle sizes (nm)	No.	Particle sizes (nm)	No.	Particle sizes (nm)
91	11.87	95	12.70	99	13.38
92	12.03	96	12.75	100	13.66
93	12.33	97	12.77	101	14.26
94	12.37	98	13.04		

Average particle sizes = 7.6 nm

Standard deviation   = 2.6 nm
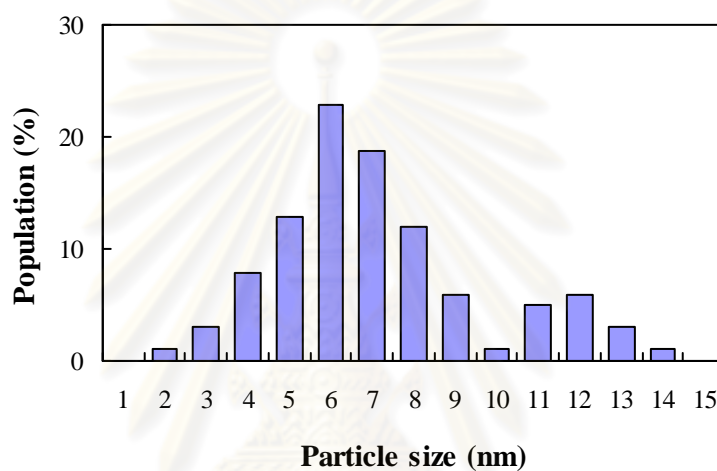
Figure B.2 Gold particles sizes distribution of Au/TiO$_2$-pH6 catalyst

Table B3 Gold particle sizes of Au/TiO$_2$-pH7 catalyst

No.	Particle sizes (nm)	No.	Particle sizes (nm)	No.	Particle sizes (nm)
1	1.20	14	2.38	27	2.61
2	1.65	15	2.38	28	2.61
3	1.72	16	2.40	29	2.61
4	1.82	17	2.40	30	2.64
5	1.82	18	2.41	31	2.66
6	1.97	19	2.42	32	2.68
7	1.99	20	2.42	33	2.72
8	2.15	21	2.54	34	2.81
9	2.20	22	2.55	35	2.85
10	2.24	23	2.56	36	2.88
11	2.24	24	2.59	37	2.89
12	2.34	25	2.60	38	2.89
13	2.37	26	2.60	39	2.91

Table B3 Gold particle sizes of Au/TiO$_2$-pH7 catalyst (Cont.)

No.	Particle sizes (nm)	No.	Particle sizes (nm)	No.	Particle sizes (nm)
40	2.92	64	3.23	88	3.93
41	2.93	65	3.24	89	3.94
42	2.95	66	3.24	90	3.98
43	2.96	67	3.28	91	3.99
44	2.96	68	3.28	92	4.02
45	2.96	69	3.30	93	4.15
46	2.97	70	3.30	94	4.17
47	2.99	71	3.31	95	4.24
48	3.00	72	3.44	96	4.38
49	3.08	73	3.45	97	4.44
50	3.09	74	3.54	98	4.49
51	3.09	75	3.57	99	4.51
52	3.10	76	3.63	100	4.72
53	3.13	77	3.64	101	4.81
54	3.13	78	3.68	102	4.86
55	3.13	79	3.69	103	4.89
56	3.13	80	3.76	104	5.12
57	3.17	81	3.78	105	5.22
58	3.17	82	3.81	106	5.31
59	3.17	83	3.83	107	5.34
60	3.22	84	3.84	108	5.41
61	3.22	85	3.84	109	5.44
62	3.22	86	3.92	110	7.59
63	3.22	87	3.92		

Average particle sizes = 3.3 nm

Standard deviation = 1.0 nm
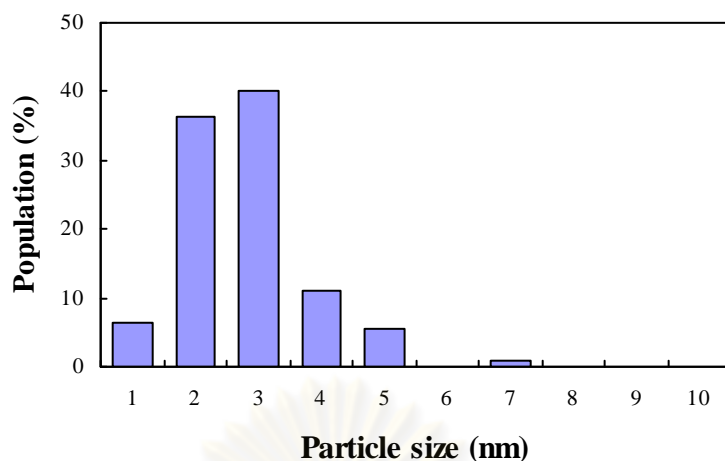
Figure B.3 Gold particle sizes distribution of Au/TiO$_2$-pH7 catalyst

Table B4 Gold particle sizes of Au/TiO$_2$-pH8 catalyst

No.	Particle sizes (nm)	No.	Particle sizes (nm)	No.	Particle sizes (nm)
1	5.15	21	7.21	41	10.85
2	5.84	22	7.30	42	10.90
3	5.89	23	7.35	43	10.96
4	5.89	24	7.43	44	10.97
5	6.30	25	7.59	45	11.06
6	6.36	26	7.81	46	11.10
7	6.40	27	7.92	47	11.10
8	6.43	28	8.06	48	11.20
9	6.44	29	8.98	49	11.31
10	6.50	30	9.05	50	11.62
11	6.54	31	9.23	51	11.84
12	6.65	32	9.35	52	12.00
13	6.65	33	9.44	53	12.14
14	6.72	34	9.70	54	12.16
15	6.83	35	9.72	55	12.19
16	6.88	36	9.94	56	12.59
17	7.02	37	10.13	57	12.89
18	7.14	38	10.14	58	12.89
19	7.14	39	10.41	59	12.90
20	7.16	40	10.71	60	13.01

Table B4 Gold particle sizes of Au/TiO$_2$-pH8 catalyst (Cont.)

No.	Particle sizes (nm)	No.	Particle sizes (nm)	No.	Particle sizes (nm)
61	13.08	75	14.08	89	16.31
62	13.10	76	14.13	90	16.71
63	13.15	77	14.30	91	16.77
64	13.23	78	14.47	92	16.82
65	13.25	79	14.53	93	17.08
66	13.34	80	14.57	94	17.10
67	13.52	81	14.81	95	17.45
68	13.57	82	14.94	96	17.82
69	13.58	83	14.98	97	18.41
70	13.70	84	15.28	98	18.57
71	13.80	85	15.87	99	18.66
72	13.88	86	15.90	100	19.66
73	13.88	87	15.93	101	19.75
74	14.07	88	16.21		

Average particle sizes = 11.6 nm

Standard deviation   = 3.8   nm
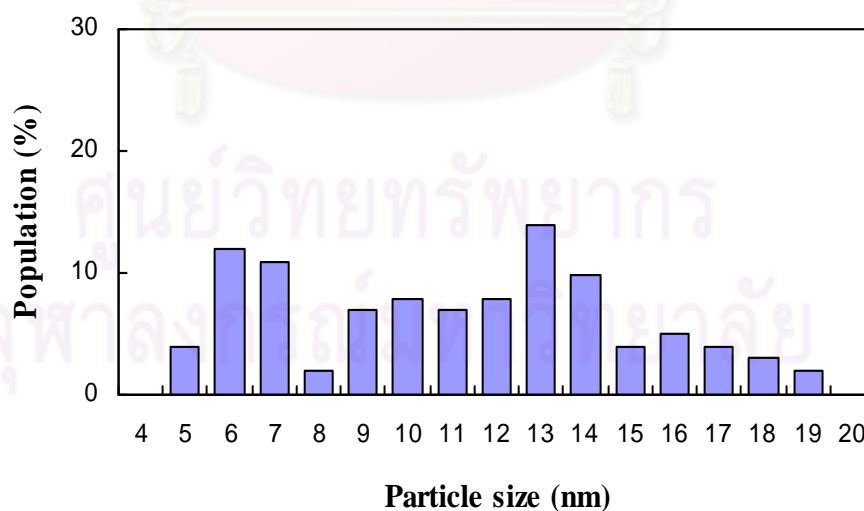
Figure B.4 Gold particle sizes distribution of Au/TiO$_2$-pH8 catalyst

Particle sizes distribution of silver nanoparticles of Ag/TiO$_2$ catalysts

The particle sizes distribution of silver nanoparticles are shown in Table B5 to B7 for 2 wt% Ag/TiO$_2$, 10 wt% Ag/TiO$_2$, and 20 wt% Ag/TiO$_2$, respectively.

Table B5   Silver particle sizes of 2 wt% Ag/TiO$_2$ catalyst

No.	Particles sizes (nm)	No.	Particles sizes (nm)	No.	Particles sizes (nm)
1	1.27	32	2.25	63	2.89
2	1.34	33	2.27	64	2.89
3	1.36	34	2.34	65	2.94
4	1.62	35	2.35	66	3.02
5	1.74	36	2.35	67	3.05
6	1.77	37	2.36	68	3.05
7	1.78	38	2.43	69	3.06
8	1.79	39	2.46	70	3.08
9	1.81	40	2.47	71	3.10
10	1.82	41	2.49	72	3.12
11	1.87	42	2.50	73	3.13
12	1.88	43	2.50	74	3.13
13	1.90	44	2.50	75	3.13
14	1.90	45	2.56	76	3.14
15	1.94	46	2.57	77	3.15
16	1.95	47	2.58	78	3.18
17	2.00	48	2.63	79	3.19
18	2.01	49	2.64	80	3.27
19	2.01	50	2.65	81	3.31
20	2.03	51	2.67	82	3.32
21	2.04	52	2.69	83	3.36
22	2.08	53	2.71	84	3.36
23	2.08	54	2.72	85	3.38
24	2.15	55	2.72	86	3.42
25	2.17	56	2.73	87	3.43
26	2.18	57	2.74	88	3.43
27	2.18	58	2.75	89	3.47
28	2.18	59	2.76	90	3.48
39	2.21	60	2.77	91	3.49
30	2.24	61	2.80	92	3.52
31	2.24	62	2.87	93	3.57

Table B5 Silver particle sizes of 2 wt% Ag/TiO$_2$ catalyst (Cont.)

No.	Particle sizes (nm)	No.	Particle sizes (nm)	No.	Particle sizes (nm)
94	3.77	98	4.08	102	4.63
95	3.80	99	4.30	103	5.39
96	3.81	100	4.34	104	5.62
97	3.83	101	4.59	105	5.70

Average particle sizes = 2.8 nm

Standard deviation   = 0.8 nm
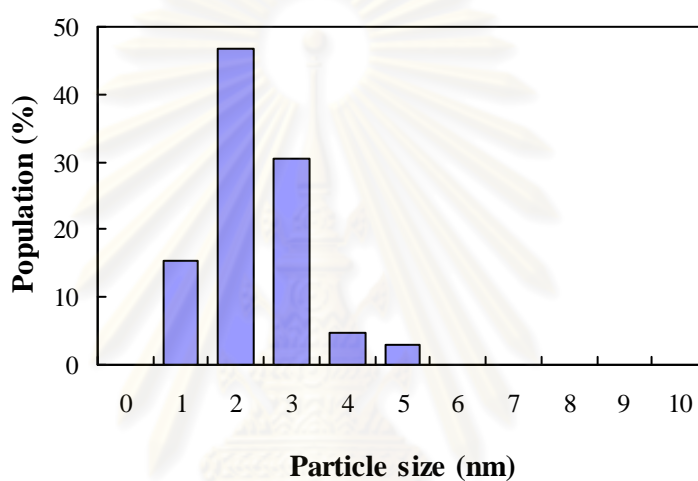
Figure B.5   Silver particle sizes distribution of 2 wt% Ag/TiO$_2$ catalyst

Table B6   Silver particle sizes of 10 wt% Ag/TiO$_2$ catalyst

No.	Particle sizes (nm)	No.	Particle sizes (nm)	No.	Particle sizes (nm)
1	1.15	13	2.16	25	2.39
2	1.47	14	2.16	26	2.43
3	1.67	15	2.17	27	2.45
4	1.69	16	2.19	28	2.46
5	1.77	17	2.24	39	2.49
6	1.85	18	2.27	30	2.49
7	1.88	19	2.29	31	2.49
8	1.88	20	2.30	32	2.51
9	1.88	21	2.32	33	2.54
10	1.89	22	2.33	34	2.55
11	2.03	23	2.34	35	2.57
12	2.12	24	2.37	36	2.61

Table B6 Silver particle sizes of 10 wt% Ag/TiO$_2$ catalyst (Cont.)

No.	Particle sizes (nm)	No.	Particle sizes (nm)	No.	Particle sizes (nm)
37	2.62	59	2.98	81	3.68
38	2.62	60	3.07	82	3.78
39	2.63	61	3.08	83	3.78
40	2.74	62	3.10	84	3.83
41	2.74	63	3.10	85	3.87
42	2.74	64	3.13	86	4.05
43	2.75	65	3.13	87	4.08
44	2.82	66	3.16	88	4.22
45	2.82	67	3.19	89	4.34
46	2.82	68	3.19	90	4.36
47	2.82	69	3.33	91	4.39
48	2.82	70	3.35	92	4.41
49	2.82	71	3.37	93	4.46
50	2.82	72	3.38	94	4.60
51	2.82	73	3.38	95	4.74
52	2.82	74	3.39	96	4.92
53	2.86	75	3.39	97	4.98
54	2.90	76	3.43	98	5.34
55	2.91	77	3.49	99	5.45
56	2.92	78	3.55	100	5.46
57	2.92	79	3.57	101	5.94
58	2.97	80	3.67		

Average particle sizes = 3.0 nm

Standard deviation   = 0.9 nm
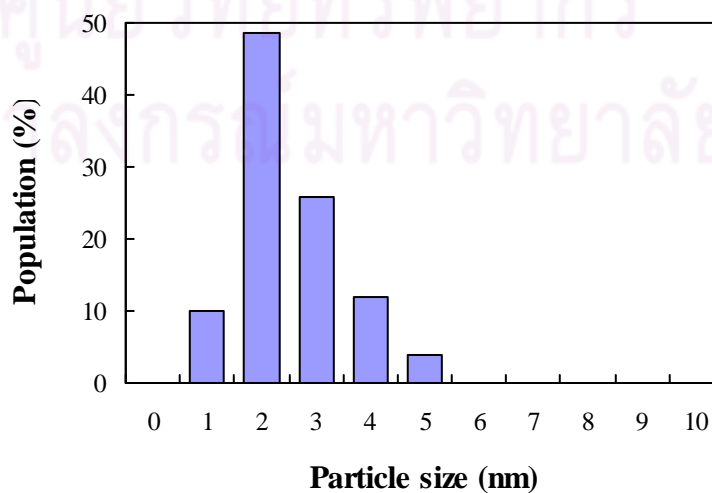
Figure B.6 Silver particle sizes distribution of 10 wt% Ag/TiO$_2$ catalyst

Table B7 Silver particle sizes of 20 wt% Ag/TiO$_2$ catalyst

No.	Particle sizes (nm)	No.	Particle sizes (nm)	No.	Particle sizes (nm)
1	1.18	36	2.18	71	2.60
2	1.28	37	2.18	72	2.60
3	1.37	38	2.19	73	2.60
4	1.44	39	2.20	74	2.65
5	1.48	40	2.20	75	2.67
6	1.51	41	2.21	76	2.67
7	1.52	42	2.22	77	2.67
8	1.52	43	2.22	78	2.67
9	1.52	44	2.22	79	2.69
10	1.55	45	2.24	80	2.69
11	1.64	46	2.26	81	2.69
12	1.67	47	2.26	82	2.69
13	1.69	48	2.28	83	2.71
14	1.74	49	2.34	84	2.72
15	1.76	50	2.38	85	2.72
16	1.76	51	2.38	86	2.75
17	1.76	52	2.39	87	2.78
18	1.87	53	2.43	88	2.78
19	1.90	54	2.45	89	2.80
20	1.91	55	2.45	90	2.82
21	1.93	56	2.46	91	2.83
22	1.95	57	2.46	92	2.83
23	1.95	58	2.46	93	2.84
24	2.02	59	2.46	94	2.85
25	2.03	60	2.48	95	2.86
26	2.07	61	2.48	96	2.86
27	2.11	62	2.49	97	2.86
28	2.15	63	2.51	98	2.90
29	2.15	64	2.52	99	2.93
30	2.15	65	2.52	100	3.03
31	2.15	66	2.53	101	3.04
32	2.15	67	2.54	102	3.04
33	2.15	68	2.55	103	3.06
34	2.17	69	2.56	104	3.08
35	2.18	70	2.59	105	3.09

Table B7 Silver particle sizes of 2 wt% Ag/TiO$_2$ catalyst (Cont.)

No.	Particle sizes (nm)	No.	Particle sizes (nm)	No.	Particle sizes (nm)
106	3.10	126	3.29	146	3.66
107	3.10	127	3.32	147	3.70
108	3.10	128	3.32	148	3.74
109	3.11	129	3.33	149	3.76
110	3.13	130	3.33	150	3.76
111	3.14	131	3.34	151	4.02
112	3.14	132	3.35	152	4.04
113	3.14	133	3.35	153	4.06
114	3.14	134	3.35	154	4.09
115	3.15	135	3.36	155	4.10
116	3.16	136	3.42	156	4.12
117	3.17	137	3.42	157	4.30
118	3.18	138	3.45	158	4.36
119	3.20	139	3.46	159	4.37
120	3.20	140	3.48	160	4.39
121	3.22	141	3.51	161	4.65
122	3.28	142	3.64	162	4.76
123	3.28	143	3.65	163	4.96
124	3.28	144	3.65	164	5.21
125	3.29	145	3.65		

Average particle sizes = 2.8 nm

Standard deviation   = 0.8 nm

Figure B.7 Silver particle sizes distribution of 20 wt% Ag/TiO$_2$ catalyst

The particle sizes distributions of silver nanoparticles are shown in Table B8 to B10 for Ag/TiO$_2$-10MPa, Ag/TiO$_2$-15MPa, and Ag/TiO$_2$-20MPa, respectively.

Table B8 Silver particle sizes of Ag/TiO$_2$-10MPa catalyst

No.	Particle sizes (nm)	No.	Particle sizes (nm)	No.	Particle sizes (nm)
1	1.22	36	2.15	65	2.83
2	1.25	37	2.15	66	2.87
3	1.27	38	2.15	67	2.88
4	1.50	36	2.15	68	2.88
5	1.53	37	2.17	69	2.90
6	1.59	38	2.21	70	2.92
7	1.61	39	2.25	71	2.93
8	1.72	40	2.31	72	2.96
9	1.78	41	2.39	73	2.99
10	1.78	42	2.43	74	3.01
11	1.78	43	2.43	75	3.01
12	1.78	44	2.43	76	3.08
13	1.81	45	2.44	77	3.11
14	1.86	46	2.44	78	3.15
15	1.87	47	2.45	79	3.24
16	1.87	48	2.45	80	3.36
17	1.87	49	2.45	81	3.36
18	1.87	50	2.45	82	3.38
19	1.87	51	2.47	83	3.38
20	1.87	52	2.47	84	3.38
21	1.89	53	2.52	85	3.53
22	1.94	54	2.52	86	3.53
23	1.94	55	2.60	87	3.61
24	1.97	56	2.63	88	3.74
25	2.02	57	2.63	89	3.75
26	2.06	58	2.63	90	3.76
27	2.07	59	2.63	91	3.80
28	2.07	60	2.69	92	3.85
29	2.09	61	2.71	93	3.90
30	2.09	62	2.72	94	3.97
31	2.09	63	2.72	95	4.02
32	2.15	64	2.80	96	4.02

Table B8   Silver particle sizes of Ag/TiO$_2$-10MPa catalyst (Cont.)

No.	Particle sizes (nm)	No.	Particle sizes (nm)	No.	Particle sizes (nm)
97	4.07	104	4.39	111	6.54
98	4.21	105	4.56	112	7.03
99	4.23	106	4.67	113	7.36
100	4.30	107	5.24	114	7.66
101	4.30	108	5.29	115	9.75
102	4.32	109	5.32	116	9.81
103	4.32	110	5.83		

Average particle sizes = 3.1 nm

Standard deviation   = 1.5   nm
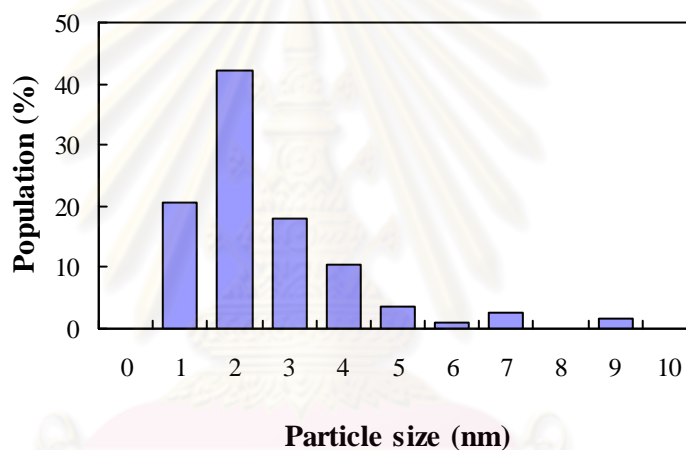
Figure B.8   Silver particle sizes distribution of Ag/TiO$_2$-10MPa catalyst

Table B9   Silver particle sizes of Ag/TiO$_2$-15MPa catalyst

No.	Particle sizes (nm)	No.	Particle sizes (nm)	No.	Particle sizes (nm)
1	1.01	10	1.63	19	2.15
2	1.10	11	1.72	20	2.15
3	1.34	12	1.72	21	2.15
4	1.50	13	1.78	22	2.16
5	1.50	14	1.84	23	2.16
6	1.53	15	1.87	24	2.16
7	1.53	16	1.93	25	2.16
8	1.59	17	1.94	26	2.16
9	1.62	18	2.00	27	2.18

Table B9   Silver particle sizes of Ag/TiO$_2$-15MPa catalyst (Cont.)

No.	Particle sizes (nm)	No.	Particle sizes (nm)	No.	Particle sizes (nm)
28	2.23	59	2.79	90	3.46
29	2.24	60	2.80	91	3.58
30	2.34	61	2.80	92	3.72
31	2.34	62	2.82	93	3.76
32	2.36	63	2.85	94	3.76
33	2.39	64	2.86	95	3.78
34	2.39	65	2.87	96	3.85
35	2.39	66	2.87	97	3.91
36	2.39	67	2.97	98	4.04
37	2.43	68	2.98	99	4.13
38	2.44	69	2.99	100	4.14
39	2.44	70	3.04	101	4.17
40	2.45	71	3.06	102	4.23
41	2.47	72	3.06	103	4.38
42	2.48	73	3.07	104	4.45
43	2.48	74	3.08	105	4.56
44	2.52	75	3.10	106	4.56
45	2.52	76	3.10	107	4.58
46	2.52	77	3.10	108	4.58
47	2.54	78	3.10	109	5.06
48	2.58	79	3.11	110	5.10
49	2.60	80	3.11	111	5.12
50	2.64	81	3.16	112	5.13
51	2.67	82	3.17	113	5.26
52	2.67	83	3.26	114	5.52
53	2.69	84	3.28	115	5.53
54	2.70	85	3.36	116	5.90
55	2.72	86	3.37	117	5.92
56	2.73	87	3.37	118	6.63
57	2.79	88	3.40		
58	2.79	89	3.43		

Average particle sizes = 3.0 nm

Standard deviation   = 1.1   nm

Figure B.9   Silver particle sizes distribution of Ag/TiO$_2$-15MPa catalyst

Table B10   Silver particle sizes of Ag/TiO$_2$-20MPa catalyst

No.	Particle sizes (nm)	No.	Particle sizes (nm)	No.	Particle sizes (nm)
1	1.18	23	1.95	45	2.24
2	1.28	24	2.02	46	2.26
3	1.37	25	2.03	47	2.26
4	1.44	26	2.07	48	2.28
5	1.48	27	2.11	49	2.34
6	1.51	28	2.15	50	2.38
7	1.52	29	2.15	51	2.38
8	1.52	30	2.15	52	2.39
9	1.52	31	2.15	53	2.43
10	1.55	32	2.15	54	2.45
11	1.64	33	2.15	55	2.45
12	1.67	34	2.17	56	2.46
13	1.69	35	2.18	57	2.46
14	1.74	36	2.18	58	2.46
15	1.76	37	2.18	59	2.46
16	1.76	38	2.19	60	2.48
17	1.76	39	2.20	61	2.48
18	1.87	40	2.20	62	2.49
19	1.90	41	2.21	63	2.51
20	1.91	42	2.22	64	2.52
21	1.93	43	2.22	65	2.52
22	1.95	44	2.22	66	2.53

Table B10 Silver particle sizes of Ag/TiO$_2$-20MPa catalyst (Cont.)

No.	Particle sizes (nm)	No.	Particle sizes (nm)	No.	Particle sizes (nm)
67	2.54	100	3.03	133	3.35
68	2.55	101	3.04	134	3.35
69	2.56	102	3.04	135	3.36
70	2.59	103	3.06	136	3.42
71	2.60	104	3.08	137	3.42
72	2.60	105	3.09	138	3.45
73	2.60	106	3.10	139	3.46
74	2.65	107	3.10	140	3.48
75	2.67	108	3.10	141	3.51
76	2.67	109	3.11	142	3.64
77	2.67	110	3.13	143	3.65
78	2.67	111	3.14	144	3.65
79	2.69	112	3.14	145	3.65
80	2.69	113	3.14	146	3.66
81	2.69	114	3.14	147	3.70
82	2.69	115	3.15	148	3.74
83	2.71	116	3.16	149	3.76
84	2.72	117	3.17	150	3.76
85	2.72	118	3.18	151	4.02
86	2.75	119	3.20	152	4.04
87	2.78	120	3.20	153	4.06
88	2.78	121	3.22	154	4.09
89	2.80	122	3.28	155	4.10
90	2.82	123	3.28	156	4.12
91	2.83	124	3.28	157	4.30
92	2.83	125	3.29	158	4.36
93	2.84	126	3.29	159	4.37
94	2.85	127	3.32	160	4.39
95	2.86	128	3.32	161	4.65
96	2.86	129	3.33	162	4.76
97	2.86	130	3.33	163	4.96
98	2.90	131	3.34	164	5.21
99	2.93	132	3.35		

Average particle sizes = 3.0 nm

Standard deviation   = 1.1   nm
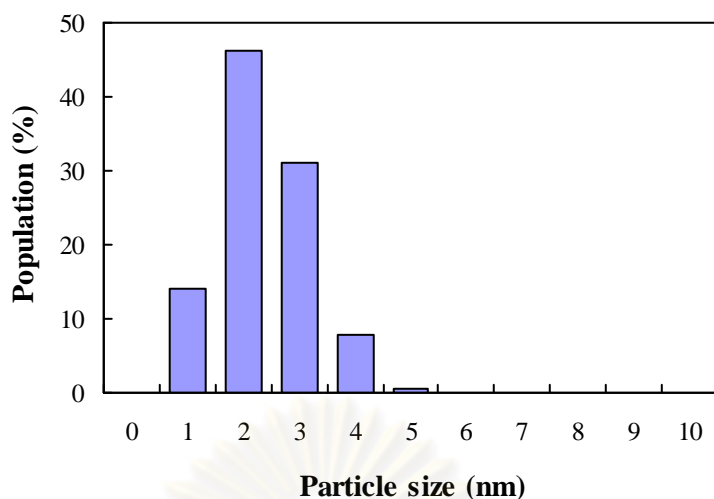
Figure B.10 Silver particle sizes distribution of Ag/TiO$_2$-20MPa catalyst

The particle sizes distributions of silver nanoparticles are shown in Table B11 to B14 for Ag/TiO$_2$-0.5h, Ag/TiO$_2$-1h, Ag/TiO$_2$-2h, and Ag/TiO$_2$-4h, respectively.

Table B11 Silver particle sizes of Ag/TiO$_2$-0.5h catalyst

No.	Particle sizes (nm)	No.	Particle sizes (nm)	No.	Particle sizes (nm)
1	1.10	19	3.71	37	4.48
2	1.87	20	3.83	38	4.67
3	2.15	21	3.86	39	4.71
4	2.16	22	3.86	40	4.76
5	2.30	23	3.93	41	4.79
6	2.33	24	4.01	42	4.79
7	2.49	25	4.07	43	4.81
8	2.91	26	4.15	44	4.92
9	2.95	27	4.18	45	5.07
10	3.20	28	4.24	46	5.09
11	3.25	29	4.25	47	5.13
12	3.33	30	4.25	48	5.17
13	3.48	31	4.29	49	5.19
14	3.53	32	4.30	50	5.26
15	3.66	33	4.39	51	5.33
16	3.69	34	4.41	52	5.40
17	3.70	35	4.43	53	5.42
18	3.70	36	4.43	54	5.47

Table B11 Silver particle sizes of Ag/TiO$_2$-0.5h catalyst (Cont.)

No.	Particle sizes (nm)	No.	Particle sizes (nm)	No.	Particle sizes (nm)
55	5.57	72	6.97	89	8.62
56	5.63	73	6.97	90	8.69
57	5.69	74	7.01	91	8.78
58	5.74	75	7.07	92	8.90
59	5.75	76	7.19	93	9.05
60	5.80	77	7.44	94	9.10
61	5.91	78	7.51	95	9.23
62	5.94	79	7.86	96	9.46
63	5.98	80	7.90	97	9.71
64	6.01	81	8.02	98	9.78
65	6.09	82	8.10	99	10.16
66	6.18	83	8.14	100	10.20
67	6.19	84	8.38	101	10.27
68	6.48	85	8.41	102	10.43
69	6.50	86	8.44	103	10.70
70	6.51	87	8.51	104	10.93
71	6.64	88	8.60		

Average particle sizes = 5.8 nm
Standard deviation   = 2.3 nm
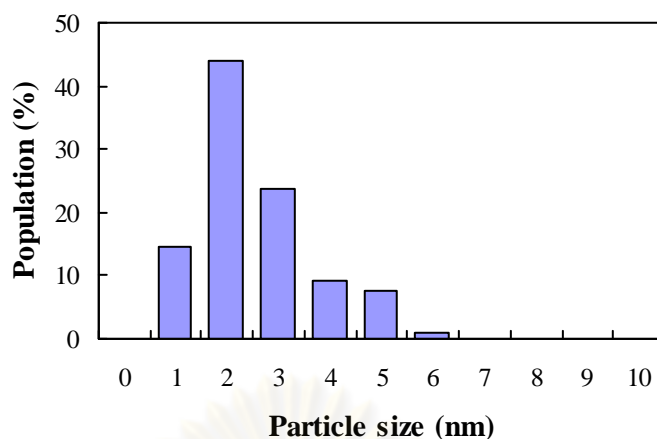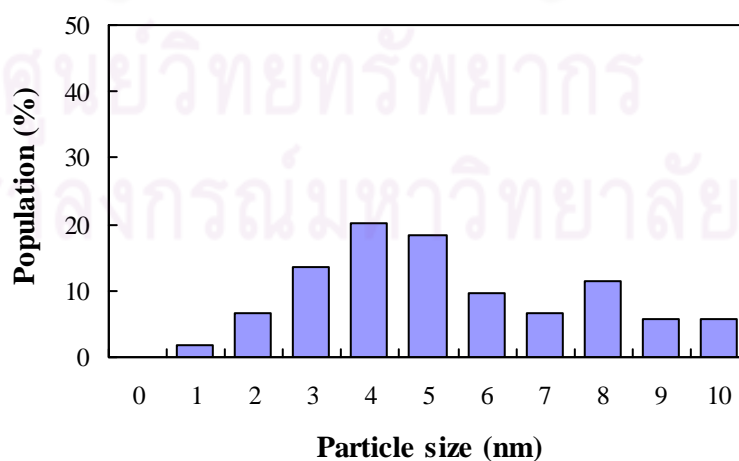

Figure B.11 Silver particle sizes distribution of Ag/TiO$_2$-0.5h catalyst

Table B12 Silver particle sizes of Ag/TiO$_2$-1h catalyst

No.	Particle sizes (nm)	No.	Particle sizes (nm)	No.	Particle sizes (nm)
1	1.18	36	2.18	71	2.60
2	1.28	37	2.18	72	2.60
3	1.37	38	2.19	73	2.60
4	1.44	39	2.20	74	2.65
5	1.48	40	2.20	75	2.67
6	1.51	41	2.21	76	2.67
7	1.52	42	2.22	77	2.67
8	1.52	43	2.22	78	2.67
9	1.52	44	2.22	79	2.69
10	1.55	45	2.24	80	2.69
11	1.64	46	2.26	81	2.69
12	1.67	47	2.26	82	2.69
13	1.69	48	2.28	83	2.71
14	1.74	49	2.34	84	2.72
15	1.76	50	2.38	85	2.72
16	1.76	51	2.38	86	2.75
17	1.76	52	2.39	87	2.78
18	1.87	53	2.43	88	2.78
19	1.90	54	2.45	89	2.80
20	1.91	55	2.45	90	2.82
21	1.93	56	2.46	91	2.83
22	1.95	57	2.46	92	2.83
23	1.95	58	2.46	93	2.84
24	2.02	59	2.46	94	2.85
25	2.03	60	2.48	95	2.86
26	2.07	61	2.48	96	2.86
27	2.11	62	2.49	97	2.86
28	2.15	63	2.51	98	2.90
29	2.15	64	2.52	99	2.93
30	2.15	65	2.52	100	3.03
31	2.15	66	2.53	101	3.04
32	2.15	67	2.54	102	3.04
33	2.15	68	2.55	103	3.06
34	2.17	69	2.56	104	3.08
35	2.18	70	2.59	105	3.09

Table B12 Silver particle sizes of Ag/TiO$_2$-1h catalyst (Cont.)

No.	Particle sizes (nm)	No.	Particle sizes (nm)	No.	Particle sizes (nm)
106	3.10	126	3.29	146	3.66
107	3.10	127	3.32	147	3.70
108	3.10	128	3.32	148	3.74
109	3.11	129	3.33	149	3.76
110	3.13	130	3.33	150	3.76
111	3.14	131	3.34	151	4.02
112	3.14	132	3.35	152	4.04
113	3.14	133	3.35	153	4.06
114	3.14	134	3.35	154	4.09
115	3.15	135	3.36	155	4.10
116	3.16	136	3.42	156	4.12
117	3.17	137	3.42	157	4.30
118	3.18	138	3.45	158	4.36
119	3.20	139	3.46	159	4.37
120	3.20	140	3.48	160	4.39
121	3.22	141	3.51	161	4.65
122	3.28	142	3.64	162	4.76
123	3.28	143	3.65	163	4.96
124	3.28	144	3.65	164	5.21
125	3.29	145	3.65		

Average particle sizes = 2.8 nm
Standard deviation   = 0.8 nm

Figure B.12   Silver particle sizes distribution of Ag/TiO$_2$-1h catalyst

Table B13 Silver particle sizes of Ag/TiO$_2$-2h catalyst

No.	Particle sizes (nm)	No.	Particle sizes (nm)	No.	Particle sizes (nm)
1	1.61	36	2.48	71	2.97
2	1.84	37	2.52	72	2.98
3	1.87	38	2.52	73	2.99
4	1.88	39	2.54	74	3.01
5	1.92	40	2.55	75	3.02
6	1.99	41	2.59	76	3.02
7	1.99	42	2.62	77	3.02
8	2.01	43	2.64	78	3.04
9	2.02	44	2.66	79	3.05
10	2.05	45	2.67	80	3.05
11	2.09	46	2.67	81	3.07
12	2.11	47	2.73	82	3.07
13	2.15	48	2.76	83	3.08
14	2.16	49	2.77	84	3.08
15	2.16	50	2.79	85	3.09
16	2.18	51	2.80	86	3.10
17	2.22	52	2.81	87	3.11
18	2.23	53	2.81	88	3.11
19	2.24	54	2.82	89	3.12
20	2.25	55	2.82	90	3.14
21	2.25	56	2.83	91	3.14
22	2.31	57	2.86	92	3.15
23	2.34	58	2.88	93	3.19
24	2.34	59	2.89	94	3.19
25	2.39	60	2.89	95	3.22
26	2.39	61	2.90	96	3.26
27	2.39	62	2.91	97	3.26
28	2.41	63	2.92	98	3.27
29	2.43	64	2.92	99	3.28
30	2.43	65	2.95	100	3.33
31	2.44	66	2.96	101	3.36
32	2.46	67	2.97	102	3.36
33	2.47	68	2.97	103	3.36
34	2.47	69	2.97	104	3.38
35	2.48	70	2.97	105	3.38

Table B13 Silver particle sizes of Ag/TiO$_2$-2h catalyst (Cont.)

No.	Particle sizes (nm)	No.	Particle sizes (nm)	No.	Particle sizes (nm)
106	3.39	141	3.89	176	4.22
107	3.40	142	3.92	177	4.23
108	3.40	143	3.92	178	4.30
109	3.44	144	3.92	179	4.30
110	3.44	145	3.93	180	4.32
111	3.45	146	3.93	181	4.32
112	3.45	147	3.93	182	4.32
113	3.45	148	3.95	183	4.34
114	3.46	149	3.95	184	4.37
115	3.47	150	3.95	185	4.37
116	3.47	151	3.96	186	4.38
117	3.48	152	3.96	187	4.39
118	3.48	153	3.97	188	4.39
119	3.49	154	3.99	189	4.39
120	3.49	155	4.00	190	4.40
121	3.55	156	4.00	191	4.42
122	3.55	157	4.02	192	4.42
123	3.56	158	4.02	193	4.42
124	3.57	159	4.04	194	4.44
125	3.57	160	4.04	195	4.48
126	3.58	161	4.04	196	4.48
127	3.58	162	4.05	197	4.50
128	3.62	163	4.05	198	4.51
129	3.65	164	4.06	199	4.51
130	3.67	165	4.07	200	4.58
131	3.68	166	4.09	201	4.58
132	3.70	167	4.10	202	4.59
133	3.71	168	4.11	203	4.60
134	3.72	169	4.11	204	4.61
135	3.76	170	4.18	205	4.64
136	3.78	171	4.19	206	4.69
137	3.80	172	4.20	207	4.69
138	3.82	173	4.20	208	4.70
139	3.83	174	4.22	209	4.70
140	3.85	175	4.22	210	4.70

Table B13 Silver particle sizes of Ag/TiO$_2$-2h catalyst (Cont.)

No.	Particle sizes (nm)	No.	Particle sizes (nm)	No.	Particle sizes (nm)
211	4.71	234	5.23	257	5.81
212	4.72	235	5.25	258	5.82
213	4.79	236	5.26	259	5.87
214	4.80	237	5.26	260	5.90
215	4.81	238	5.26	261	5.95
216	4.84	239	5.29	262	6.18
217	4.85	240	5.32	263	6.20
218	4.89	241	5.32	264	6.30
219	4.90	242	5.32	265	6.30
220	4.94	243	5.34	266	6.38
221	4.97	244	5.34	267	6.39
222	4.98	245	5.41	268	6.45
223	5.01	246	5.46	269	6.51
224	5.02	247	5.47	270	6.52
225	5.02	248	5.51	271	6.63
226	5.03	249	5.55	272	6.63
227	5.05	250	5.55	273	6.64
228	5.06	251	5.62	274	6.70
229	5.08	252	5.63	275	6.75
230	5.12	253	5.72	276	6.87
231	5.14	254	5.74	277	6.89
232	5.16	255	5.77		
233	5.21	256	5.78		

Average particle sizes = 3.9 nm
Standard deviation   = 1.2   nm
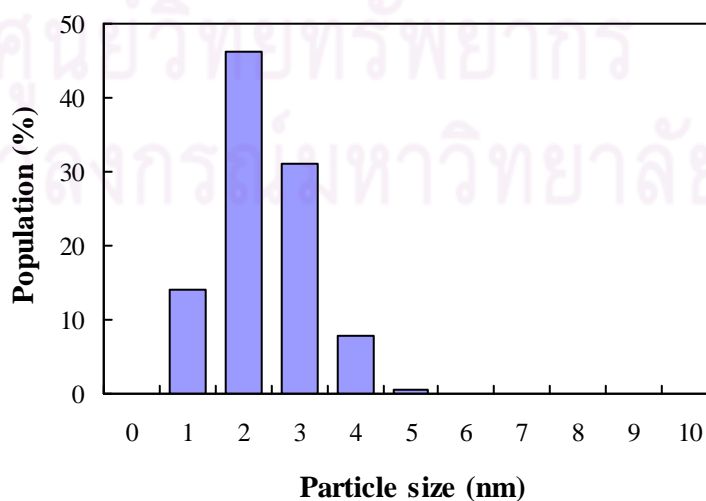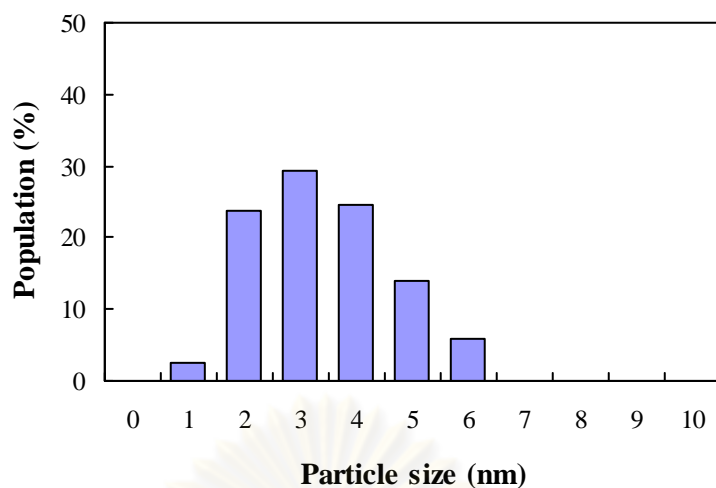
Figure B.13 Silver particle sizes distribution of Ag/TiO$_2$-2h catalyst

Table B14 Silver particle sizes of Ag/TiO$_2$-4h catalyst

No.	Particle sizes (nm)	No.	Particle sizes (nm)	No.	Particle sizes (nm)
1	1.19	23	1.94	45	2.19
2	1.28	24	1.94	46	2.19
3	1.33	25	1.94	47	2.19
4	1.49	26	1.94	48	2.23
5	1.50	27	1.94	49	2.24
6	1.55	28	1.97	50	2.24
7	1.55	29	2.07	51	2.24
8	1.59	30	2.07	52	2.26
9	1.60	31	2.07	53	2.33
10	1.60	32	2.07	54	2.35
11	1.62	33	2.07	55	2.35
12	1.73	34	2.09	56	2.35
13	1.77	35	2.16	57	2.35
14	1.78	36	2.16	58	2.36
15	1.78	37	2.16	59	2.36
16	1.81	38	2.16	60	2.38
17	1.87	39	2.16	61	2.40
18	1.88	40	2.16	62	2.41
19	1.88	41	2.18	63	2.44
20	1.88	42	2.18	64	2.46
21	1.88	43	2.18	65	2.47
22	1.92	44	2.18	66	2.48

Table B14 Silver particle sizes of Ag/TiO$_2$-4h catalyst (Cont.)

No.	Particle sizes (nm)	No.	Particle sizes (nm)	No.	Particle sizes (nm)
67	2.51	92	2.87	117	3.57
68	2.52	93	2.90	118	3.66
69	2.53	94	2.91	119	3.73
70	2.55	95	2.95	120	3.74
71	2.62	96	2.98	121	3.85
72	2.62	97	3.02	122	3.91
73	2.62	98	3.08	123	3.94
74	2.63	99	3.08	124	3.94
75	2.63	100	3.10	125	3.95
76	2.63	101	3.10	126	3.95
77	2.63	102	3.11	127	4.00
78	2.64	103	3.13	128	4.01
79	2.69	104	3.13	129	4.05
80	2.72	105	3.16	130	4.13
81	2.72	106	3.24	131	4.30
82	2.72	107	3.26	132	4.41
83	2.73	108	3.26	133	4.42
84	2.73	109	3.29	134	4.65
85	2.73	110	3.29	135	5.05
86	2.74	111	3.29	136	5.14
87	2.74	112	3.32	137	5.64
88	2.78	113	3.33	138	5.72
89	2.79	114	3.42		
90	2.86	115	3.52		
91	2.86	116	3.57		

Average particle sizes = 2.7 nm
Standard deviation   = 0.9   nm
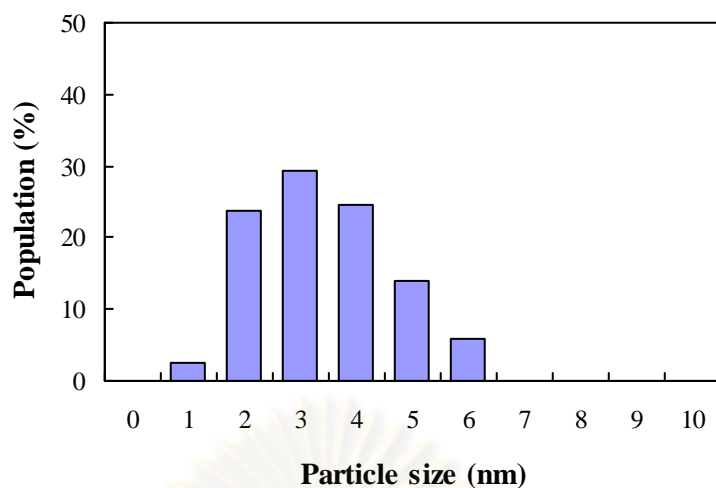
Figure B.14 Silver particle sizes distribution of Ag/TiO₂-4h catalyst

The particle sizes distributions of silver nanoparticles are shown in Table B15 to B16 for Ag/TiO₂-ST and Ag/TiO₂-P25, respectively.

Table B15 Silver particle sizes of Ag/TiO₂-ST catalyst

No.	Particle sizes (nm)	No.	Particle sizes (nm)	No.	Particle sizes (nm)
1	1.06	19	1.91	37	2.35
2	1.23	20	1.91	38	2.37
3	1.44	21	1.94	39	2.43
4	1.60	22	1.94	40	2.44
5	1.69	23	1.95	41	2.44
6	1.69	24	2.00	42	2.45
7	1.73	25	2.07	43	2.48
8	1.73	26	2.08	44	2.48
9	1.76	27	2.10	45	2.54
10	1.77	28	2.13	46	2.55
11	1.78	29	2.15	47	2.56
12	1.82	30	2.16	48	2.60
13	1.86	31	2.18	49	2.62
14	1.88	32	2.18	50	2.62
15	1.88	33	2.20	51	2.63
16	1.88	34	2.20	52	2.63
17	1.89	35	2.31	53	2.63
18	1.89	36	2.33	54	2.66

Table B15 Silver particle sizes of Ag/TiO$_2$-ST catalyst (Cont.)

No.	Particle sizes (nm)	No.	Particle sizes (nm)	No.	Particle sizes (nm)
55	2.66	88	3.05	121	3.64
56	2.70	89	3.06	122	3.67
57	2.70	90	3.08	123	3.74
58	2.72	91	3.10	124	3.74
59	2.74	92	3.10	125	3.76
60	2.74	93	3.11	126	3.76
61	2.76	94	3.11	127	3.82
62	2.79	95	3.15	128	3.83
63	2.80	96	3.21	129	3.85
64	2.83	97	3.22	130	3.87
65	2.83	98	3.23	131	3.87
66	2.85	99	3.24	132	3.87
67	2.86	100	3.24	133	3.91
68	2.89	101	3.25	134	3.93
69	2.91	102	3.29	135	4.00
70	2.91	103	3.33	136	4.10
71	2.93	104	3.38	137	4.11
72	2.93	105	3.39	138	4.31
73	2.93	106	3.40	139	4.31
74	2.93	107	3.40	140	4.33
75	2.93	108	3.44	141	4.46
76	2.94	109	3.46	142	4.56
77	2.94	110	3.46	143	4.60
78	2.94	111	3.47	144	4.66
79	2.94	112	3.48	145	4.70
80	2.94	113	3.48	146	4.70
81	2.95	114	3.53	147	4.70
82	2.95	115	3.59	148	5.02
83	2.95	116	3.59	149	5.34
84	2.98	117	3.59	150	5.54
85	3.03	118	3.59	151	5.54
86	3.05	119	3.60	152	5.65
87	3.05	120	3.60	153	5.84

Average particle sizes = 3.0 nm
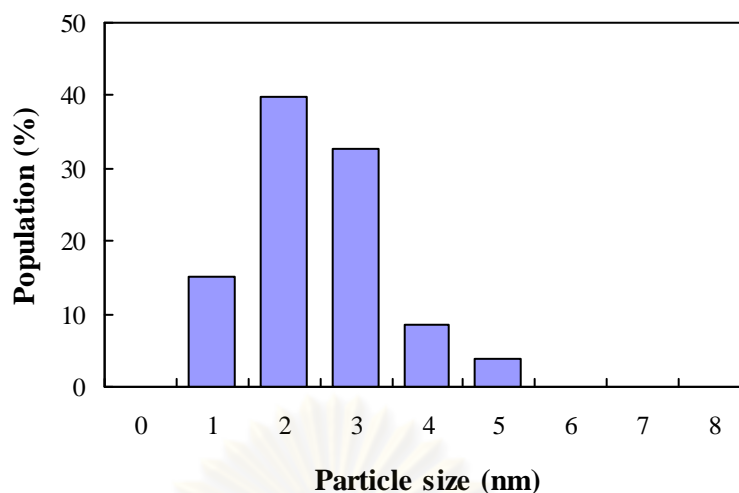Standard deviation   = 0.9   nm

Figure B.15 Silver particle sizes distribution of Ag/TiO₂-ST catalyst

Table B16 Silver particle sizes of Ag/TiO₂-P25 catalyst

No.	Particle sizes (nm)	No.	Particle sizes (nm)	No.	Particle sizes (nm)
1	1.18	23	1.95	45	2.24
2	1.28	24	2.02	46	2.26
3	1.37	25	2.03	47	2.26
4	1.44	26	2.07	48	2.28
5	1.48	27	2.11	49	2.34
6	1.51	28	2.15	50	2.38
7	1.52	29	2.15	51	2.38
8	1.52	30	2.15	52	2.39
9	1.52	31	2.15	53	2.43
10	1.55	32	2.15	54	2.45
11	1.64	33	2.15	55	2.45
12	1.67	34	2.17	56	2.46
13	1.69	35	2.18	57	2.46
14	1.74	36	2.18	58	2.46
15	1.76	37	2.18	59	2.46
16	1.76	38	2.19	60	2.48
17	1.76	39	2.20	61	2.48
18	1.87	40	2.20	62	2.49
19	1.90	41	2.21	63	2.51
20	1.91	42	2.22	64	2.52
21	1.93	43	2.22	65	2.52
22	1.95	44	2.22	66	2.53

Table B16 Silver particle sizes of Ag/TiO$_2$-P25 catalyst (Cont.)

No.	Particle sizes (nm)	No.	Particle sizes (nm)	No.	Particle sizes (nm)
67	2.54	100	3.03	133	3.35
68	2.55	101	3.04	134	3.35
69	2.56	102	3.04	135	3.36
70	2.59	103	3.06	136	3.42
71	2.60	104	3.08	137	3.42
72	2.60	105	3.09	138	3.45
73	2.60	106	3.10	139	3.46
74	2.65	107	3.10	140	3.48
75	2.67	108	3.10	141	3.51
76	2.67	109	3.11	142	3.64
77	2.67	110	3.13	143	3.65
78	2.67	111	3.14	144	3.65
79	2.69	112	3.14	145	3.65
80	2.69	113	3.14	146	3.66
81	2.69	114	3.14	147	3.70
82	2.69	115	3.15	148	3.74
83	2.71	116	3.16	149	3.76
84	2.72	117	3.17	149	3.76
85	2.72	118	3.18	150	4.02
86	2.75	119	3.20	151	4.04
87	2.78	120	3.20	152	4.06
88	2.78	121	3.22	153	4.09
89	2.80	122	3.28	154	4.10
90	2.82	123	3.28	155	4.12
91	2.83	124	3.28	156	4.30
92	2.83	125	3.29	157	4.36
93	2.84	126	3.29	158	4.37
94	2.85	127	3.32	159	4.39
95	2.86	128	3.32	160	4.65
96	2.86	129	3.33	161	4.76
97	2.86	130	3.33	162	4.96
98	2.90	131	3.34	163	5.21
99	2.93	132	3.35		

Average particle sizes = 2.8 nm
Standard deviation   = 0.8   nm
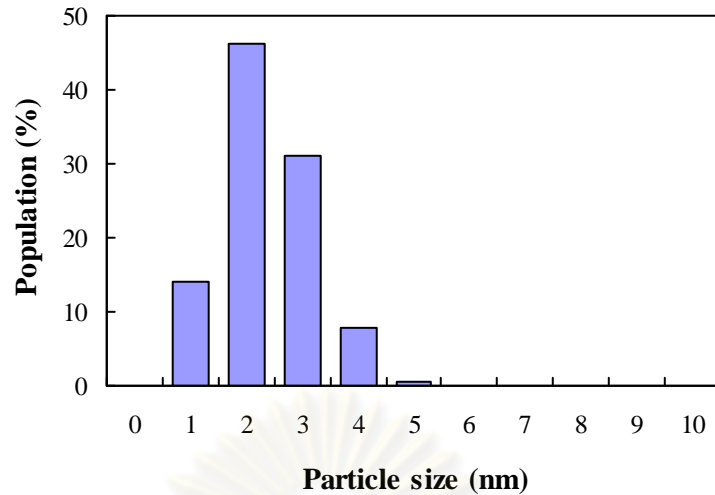
Figure B.16 Silver particle sizes distribution of Ag/TiO$_2$-P25 catalyst

Calculation of TEM results

Average particle size ($\bar{d}$)

The average particle size was calculated from the equation:

$$\bar{d} = \frac{\sum\limits_{i}^{n} d_i}{n} \tag{B1}$$

where d_i = the diameter of each particles (nm)

n = the number of appeared in the TEM images

Standard deviation (*s.d.*)

The standard deviation of particle size was calculated from the equation:

$$s.d. = \sqrt{\frac{1}{n-1} \sum\limits_{i=1}^{n} (d_i - \bar{d})^2} \tag{B2}$$

Where d_i = the diameter of each particles (nm)

$\bar{d}$ = the average particle sizes (nm)

n = the number of appeared in the TEM images

APPENDIX C

THE OPERATING CONDITIONS OF
GAS CHROMATOGRAPHY

The composition of effluent gas is analyzed by a Shimadzu gas chromatograph with a TCD. Helium was used as the carrier gas and using molecular sieves 5A column (3 m $\times$ 3 mmØ). Molecular sieves 5A were used to analyze N_2, CO, O_2, H_2 and other hydrocarbons.

Table C1 The operating condition for gas chromatograph.

Gas Chromagraph	SHIMADZU GC-8A
Detector	Thermal Conductivity Detector
Column	Molecular Sieves 5A
Carrier gas	He (99.999%)
Carrier gas flow (ml/min)	30 cc/min
Column temperature	
- initial (^{o}C)	80
- final (^{o}C)	80
Injector temperature (^{o}C)	100
Detector temperature (^{o}C)	100
Current (mA)	80

The calibration curve for calculation of composition of carbon monoxide in reactor effluent was obtained and was shown in Figure C.1. Mole of carbon monoxide as y-axis and area determined from gas chromatography as x-axis were plotted.
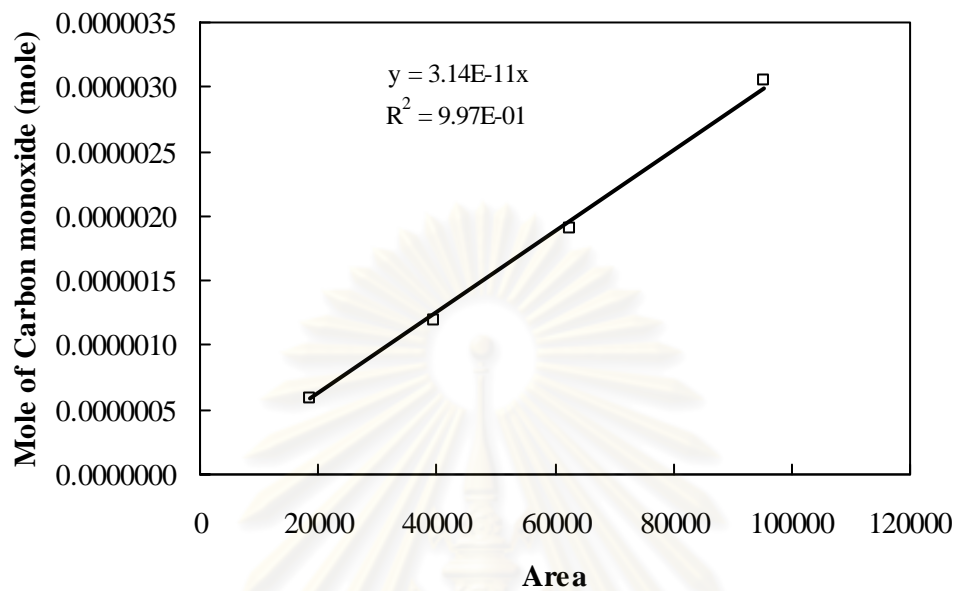

Figure C.1   The calibration curve of carbon monoxide

APPENDIX D

CALCULATION OF RESULT OF ICP-OES

Calculation of ICP-OES results

The results from ICP-OES characterization were calculated the gold and silver contents in catalysts. The example of calculation is as following:

For Au/TiO$_2$-pH6, the initial weight of catalyst was 0.0126 g and the gold concentration obtained from ICP-OES was 3.628 ppm. Therefore the gold content in the catalysts were;

The amounts of gold in the catalyst were;

In 100 g of the Au/TiO$_2$-pH6, had a gold content was ...... 2 ...... g

In 0.0126 g of the Au/TiO$_2$-pH6, had a gold content was $\dfrac{0.0126x2}{100}$ g

$$= 0.000252 \quad \text{g}$$
$$= 0.252 \quad \text{mg}$$

For digest a samples were diluted to 50 cm^3 of volume

Therefore;

The sample had a concentration were $= \dfrac{0.252x1000}{50} = 5.04$ ppm

The gold contents in the catalysts were calculated by

From the results of ICP-OES, shown the gold concentration was 3.628 ppm

Therefore;

The gold concentrations was 5.04 ppm, had a gold content was ...... 2 ...... wt%

The gold concentration was 3.628 ppm, had a gold content was $\dfrac{3.628x2}{5.04}$ wt%

$$= 1.44 \quad \text{wt\%}$$

Thus, Au/TiO$_2$-pH6 has a gold content was 1.44 wt%

APPENDIX E

LIST OF PUBLICATIONS

Manatchai Petmuang and Akawat Sirisuk. "Preparation of Ag/TiO$_2$ Catalysts via a Deposition Technique assisted by Supercritical Carbon Dioxide", 2nd SUT Graduate Conference, Suranaree University of Technology, Nakhon Ratchasima, Thailand, January 21-22, 2009.

VITA

Mr. Manatchai   Petmuang was born on November 24, 1984 in Surattani province, Thailand. He received the Bachelor Degree of Chemical Engineering from Faculty of Engineering, Srinakarinwirot University, in 2007. He continued his Master's study at Chulalongkorn University in June, 2007.